이학박사 학위논문

암 치료 효과 극대화를 위한 신규 HER2 항체-약물 결합체 개발 및 면역반응성 기전을 응용한 면역치료-방사선치료 병용요법의 항암 효능 증진

Development of a novel HER2 antibody-drug conjugate, and immune mechanism-applied immunotherapy-radiotherapy combination to improve the effect of cancer treatment

울 산 대 학 교 대 학 원

의 학 과

신 설 화

Development of a novel HER2 antibody-drug conjugate, and immune mechanism-applied immunotherapy-radiotherapy combination to improve the effect of cancer treatment

지 도 교 수　　송 시 열, 정 성 윤

이 논문을 이학박사학위 논문으로 제출함

2022년　2월

울 산 대 학 교 대 학 원

의 학 과

신 설 화

신설화의 이학박사학위 논문을 인준함

심사위원 최은경 인

심사위원 송시열 인

심사위원 정성윤 인

심사위원 정주희 인

심사위원 진형승 인

울 산 대 학 교 대 학 원

2022년 2월

Abstract

Shin, Seol Hwa

Dept. of Medical science, The Graduate School Ulsan University, Seoul 05505, Korea

PART I

An elaborate new linker system significantly enhances the efficacy of a HER2-antibody-drug conjugate against refractory HER2-positive cancers.

Despite promising efficacy in cancer cell lines and xenograft models, development of targeted anti-cancer drugs has frequently been staying in clinical trials. To improve clinical relevance of preclinical studies, patient-derived xenograft (PDX) models were generated and characterized reflecting HER2-positive gastric cancer (HER2+ GC) patients to aim successful development of targeted therapies for HER2+ GC. GC tissues from surgery of GC patients were implanted into immune-deficient mice and selected HER2+ PDXs from GC PDXs according to the histopathological diagnosis of patients. The HER2+ PDXs were verified of the patient-mimic HER2 expressing by immunohistochemistry (IHC) and explored for the feasibility by testing with Herceptin, commercialized therapeutics and novel HER2 antibody therapeutics being developed. I obtained 5 cases of HER2+ GC PDX models reflecting patient's GC tumor, consisting of 2 cases of HER2 3+ and 2 cases of HER2 2+. Novel HER2 antibody displayed improved anti-cancer efficacy in combination with Herceptin. The PDX models were successfully established to be utilized for preclinical evaluation of HER2-targeting drugs and combined therapies for GC treatment, as an ideal platform of personalized tools for precision therapy.

HER2 is amplified and overexpressed in breast and gastric cancers, and this causes poor clinical outcomes. Although T-DM1 and Enhertu have both been approved as a HER2-targeting antibody drug conjugate (ADC), the effects of these drugs are still not satisfactory to eradicate diverse tumors expressing HER2. To address this shortfall in HER2-targeted therapeutics, a novel HER2-targeting ADC composed with trastuzumab and MMAF were created an elaborate cleavable linker and manufactured, which is being investigated in a phase 1 clinical trial and is referred to as LCB-ADC in this study. LCB-ADC displayed a higher cytotoxic potency than T-DM1, and it also had a higher G2/M arrest ratio in a dose-dependent manner. In animal studies, LCB-ADC produced noticeable tumor growth inhibition compared with trastuzumab or T-DM1 in a HER2 high-expressing N87 xenograft tumor. Of particular note, LCB-ADC showed good efficacy in terms of suppressing tumor growth in a patient-derived xenograft (PDX) model of HER2-positive gastric cancer, as well as in T-DM1-resistant models such as HER2 low-expressing JIMT-1 and PDX. Collectively, the results of this research

demonstrate that LCB-ADC with elaborate linker has a higher efficacy and greater biostability than its ADC counterparts and may successfully treat cancers that are non-responsive to previous therapeutics.

PART II

Mechanistic investigation of antitumor immune responses following combined treatment with radiotherapy and immunotherapy

One of the basic mechanisms by which radiation therapy kills cancer cells is DNA damage-induced apoptosis. Radiation therapy can be curative, palliative, or serving as an adjuvant therapy after the main treatment to lower cancer risk. Recently, it has been discovered that radiation therapy shows an abscopal effect by activating target host immune cells, and not by DNA damage in cancer cells, thereby causing a general anticancer effect in addition to the localized treatment. Radiotherapy is known to affect the immune system in a variety of ways, including 1) surface MHC class I and calreticulin upregulation, and HMGB1 secretion 2) increase in the number of activated dendritic cells and antigen cross-presentation of tumors, 3) increase in tumor-infiltrating lymphocyte (TIL) density, 4) change of immune checkpoint substances, and 5) the regulation of regulatory T cells (Tregs). Radiotherapy has been shown to increase the diversity of the T-cell receptor repertoire—a protein complex found on the surface of T cells—within the tumor. Therefore, many researchers expect to further improve the anticancer effect of radiation therapy via its enhancement of the immune response. Immunotherapy has recently emerged as a promising alternative to chemotherapy, and immune checkpoint blockade (ICB) has shown impressive therapeutic response in the treatment of some solid cancers, such as lung, head, and neck cancer and metastatic malignant melanoma. This anticancer effect is mediated by immune checkpoint inhibitors, such as anti-CTLA4 and anti-PD-1, which block on the surface of T cells. The abscopal effect has been reported in patients treated with radiotherapy and ICB in clinical and preclinical studies; however, its mechanism of occurrence is still unclear. Although it is difficult to observe the effect in both clinical and preclinical studies, an optimized combination therapy comprising irradiation (IR) therapy and ICB could simultaneously reactivate exhausted T cells. In this study, tumor growth was inhibited in MC-38 allograft tumor model mice through combined treatment with IR and anti-PD-L1. Compared to that in other single treatment groups, the anti-tumor effect was enhanced in the radiation and drug-treated group in a dose-dependent manner. Moreover, all the implanted MC-38 tumor models treated with combination therapy showed a complete remission of the irradiated tumor (primary tumor). Two mice showed tumor-free as well as contralateral tumors that were not irradiated. The distribution of the immune cells at the tumor site was confirmed by testing for the levels of TILs and peripheral blood mononuclear cells (PBMC); moreover, the frequency of CD8+ T cells in the tumor was increased following combination therapy.

Taken together, these observations indicate that treating patients with a combination therapy of high-dose radiation and ICB could induce the abscopal effect of radiation therapy and enhance its antitumor

activity through its effect on the systemic immune system, which could induce a long-term immune response by increasing the levels of effector memory T cells (TEM) in the whole body.

Contents

List of tables

List of figures

List of abbreviations

Patient-derived xenograft (PDX)

Gastric cancer (GC)

Human epidermal growth factor receptor 2 (HER2)

Antibody-drug conjugate (ADC)

HER2-targeting ADC (HER2-ADC)

Drug-to-antibody ratio (DAR)

Pharmacokinetic (PK)

Cell-derived xenograft (CDX)

Subcutaneous (*s.c.*)

Intravenous (*i.v.*)

Intraperitoneal (*i.p.*)

Tumor Growth Inhibition (TGI)

Response Evaluation Criteria In Solid Tumors (RECIST)

Complete response (CR)

Partial response (PR)

Stable disease (SD)

Progressive disease (PD)

Immunohistochemistry, immunohistochemical (IHC)

Immunocytochemistry (ICC)

Phospho-histone H3 (PHH3)

Monomethyl auristatin F (MMAF)

Radiotherapy (RT)

Immunogenic cell death (ICD)

Immune checkpoint blockade (ICB)

Immune checkpoint inhibitors (ICIs)

Cytotoxic T cell lymphocytes (CTLs)

Programmed death 1 (PD-1)

Programmed death ligand 1 (PD-L1)

Cytotoxic T-Lymphocyte-Associated protein 4 (CTLA4)

Tumor infiltrating lymphocytes (TIL)

Peripheral blood mononuclear cells (PBMC)

Central memory T cells (T_{CM})

Effector memory T cells (T_{EM})

Differential expression genes (DEGs)

Tumor microenvironment (TME)

PART I. An elaborate new linker system significantly enhances the efficacy of a HER2-antibody-drug conjugate against refractory HER2-positive cancers.

PART I-1. Introduction

Conventionally, cancer cell lines and xenograft models have been used for drug screening and optimization of drug candidates for development of therapeutics. Nonetheless there have been huge efforts to develop effective treatment using those models, most novel anticancer agents have failed to reach clinical trials. According to the reports, cultured cell line and xenograft in artificial could not replace identical primary tumor microenvironment including heterogeneity (1). Consequently, investigators evaluate patient-derived xenograft (PDX) models as personalized tools, to reflect the clinical relevance in various solid tumors including breast, ovarian, pancreatic, prostate, gastric cancer (2). PDX models maintain morphology, heterogeneity, and molecular properties of primary tumors (3, 4), which permit evaluation of tumor progression and response to therapy (5-7). Herein, patient-derived xenograft (PDX) models were generated and characterized accurately reflecting HER2+ gastric cancer (GC) patient. Moreover, the value of the HER2+ GC PDXs were demonstrated as a clinically relevant tools by evaluating with traditional HER2-targeting therapy such as trastuzumab and 1A12, novel HER2 antibody (Ab) (8, 9).

Gastric cancer (GC) is the one of most frequent human malignancies and the second predominant cause of cancer-related mortality worldwide (10-13). Surgical resection is considered as the mainstay of resectable GC with possibly curable disease. However, even after curative surgery, recurrence rates are still high (13). HER2 is encoded by the proto-oncogene ERBB2, and it is a plasma membrane bound protein harboring an extracellular domain. HER2 has shown an association with tumorigenesis and cancer progression and is a particularly important prognostic indicator of invasive breast cancer. Indeed, ERBB2 gene amplification is observed in 20-25% of breast cancers and causes the overexpression of the HER2 protein (14, 15). Moreover, HER2 is overexpressed and amplified in approximately 20% of gastric cancer patients (16, 17), where it is associated with a poor prognosis and is currently recognized as a new diagnostic factor and novel therapeutic target (14, 17, 18). Accordingly, HER2 is recognized as the first target for cancer therapy and assessing the HER2 status in GC tissue has become a routine approach to these lesions (17). Trastuzumab (Herceptin), the monoclonal antibody against HER2 was shown to improve significantly the median overall survival after trastuzumab plus chemotherapy, compared to chemotherapy alone (13.8 vs. 11.1 months) in the Trastuzumab for Gastric Cancer (ToGA) trial (19-21). However, the overall tumor response rate of trastuzumab plus chemotherapy was reported to be 47% (21). For HER2-targeted therapy, diagnosis of HER2 status is required, but unfortunately HER2 scoring for diagnosis in patient is still controversial (22-24).

Antibody-drug conjugates (ADCs), the most notable anti-cancer therapeutics in terms of recent successes in the clinic, selectively deliver cytotoxic drugs to the desired tumor tissue (25, 26). Unlike chemotherapy for systemic treatment, ADC has the advantage of minimizing damage to normal cells while greatly enhancing the anticancer killing effect by targeting only cancer cells presenting the specific antigen. Because of this advantage, the development of ADCs has rapidly progressed; since Gemtuzumab ozogamicin was first approved by the US Food and Drug Administration (FDA) in 2000 (27), more than 80 clinical trials are currently underway (www.clinicaltrials.gov). To date, nine ADCs targeting different cancer cell antigens with toxins conjugated by a linker have been approved by the FDA which are Gemtuzumab ozogamicin (28), brentuximab vedotin (29), trastuzumab emtansine (30), inotuzumab ozogamicin (31), polatuzumab vedotin-piiq (32), enfortumab vedotin (33), trastuzumab deruxtecan (34), sacituzumab govitecan (35), and belantamab mafodotin (36) for leukemia, lymphoma, myeloma, breast cancer, urothelial tumors, and other cancers. Without doubt, ADCs are now firmly established as the most promising targeted anti-cancer bio-therapeutics. A variety of HER2 targeting agents have been approved by the Food and Drug Administration (FDA) in the United States, including trastuzumab, pertuzumab, lapatinib, neratinib, trastuzumab emtasine (trastuzumab-DM1; T-DM1, Kadcyla), and trastuzumab deruxtecan (fam-trastuzumab deruxtecan-nxki, Enhertu). Among these therapeutics, T-DM1, a HER2-targeting ADC (HER2-ADC) that incorporates a thioether bond to the maytansanoid derivative emtasine, has been investigated for its possible clinical application in HER2-positive metastatic breast cancer after neoadjuvant treatment with Herceptin and taxane chemotherapy (37). In the EMILIA study, T-DM1, compared to chemotherapy (lapatinib plus capecitabine), was shown to significantly improve the objective response rate (43.6% vs. 30.8%), median overall survival (30.9 vs. 25.1 month) and median progression-free survival (9.6 vs. 6.4 month) in HER2-positive advanced breast cancer patients previously treated with trastuzumab and taxane (38, 39). Additionally, the KATHERINE study reported that the number of invasive disease-free cases at 3 years was higher with T-DM1 than with trastuzumab (88.3% vs. 77.0%), and the risk of recurrence of invasive breast cancer or death was lower (by 50%) with adjuvant T-DM1 than with trastuzumab for HER2-positive early breast cancer patients with residual invasive disease after the completion of neoadjuvant therapy (40-42). Recently, Enhertu was approved in the United States for both unresectable and metastatic HER2-positive breast cancers treated with two or more anti-HER2 therapies (43). In the phase II DESTINY-Breast01 trial, Enhertu was shown to have a durable antitumor effect with an overall response rate of 60.9% (complete response 6.0%, partial response 54.9%), a median progression-free survival period of 16.4 months, and a median response duration of 14.8 months in previously treated HER2-positive breast cancer patients (44, 45). Despite its established effectiveness in HER2-positive breast cancer patients, several groups of patients, such as those with lower HER2 expression, are

initially resistant or develop resistance to T-DM1, and this drug was found to not to be superior to taxane in the GASTBY study of HER2-positive advanced gastric cancer patients (46). Hence, there is still an unmet need for effective targeting agents among low HER2-expressing breast cancers and HER2-positive gastric cancer patients and therapeutic options continue to be limited in these cases.

An ADC consists of three main structural units such as an antibody, cytotoxic agent and a linker, and all of them are important factors in the efficiency and safety of the ADC (47, 48). The suitability of using a platform technique to overcome the limitations previously observed for approved ADCs is now being investigated (49). The novel ADCs that have been proposed thus far in this regard are prepared by bonding a drug moiety with the lysine groups of an antibody, or by reducing all or part of the interchain disulfide groups of an antibody (50). These methods have some issues with regards to homogeneity, making quality control difficult (51). T-DM1 is a nonreducible thioether heterogeneous lysine conjugate of trastuzumab with a drug-to-antibody ratio (DAR) of approximately ~3.5 (37). Several latent weaknesses of T-DM1 that have been reported include a finite Cmax due to toxicities, slow internalization rate, resistance mechanisms caused by a lack of intracellular trafficking and an increased expression of the drug transporters MDR1 and MRP1, and a deficiency in payload bystander effects (52). The ultimate goal of the linker is to allow an efficient drug release to the targeted cancer cells while maintaining a stable linkage between the antibody and the drug during circulation. Since the efficacy and systemic toxicity of the antibody-drug conjugate thus depends on the stability of the linker, it plays a vital role in the safety of the ADC (53).

An advanced linker-drug technology platform was developed, that is universally applicable to manufacturing novel ADCs and was used to generate the most optimal HER2-ADC. The advantages of novel ADCs' new linker technology include: i) an accurate DAR with high homogeneity achieved *via* site-specific conjugation, due to prenylation of a CaaX body that can then be recognized by farnesyl transferase (FTase) at the end of the antibody; ii) efficient toxin release in cancer cells and increased linker stability in the bloodstream due to modified electron-donating groups in a Seattle Genetics' beta-glucuronide linker; and iii) a pharmacokinetic (PK) profile equivalent to that of an antibody.

New ADC platform was utilized to produce a novel HER2-ADC, which this research refers to as an LCB-ADC, and that was verified its efficacy and suitability in various model systems where therapeutic limitations of ADCs had been described previously. Collectively, LCB-ADCs using cleavable linker exhibited a good mode of action, biostability, and effective anticancer efficacies *in vitro* and *in vivo*. In this study, the application of our linker-drug technology enables LCB-ADCs to effectively target cancer cell types that were not responsive to previous therapeutics. LCB-ADC1 is being investigated in phase 1, a dose-escalation study in patients with HER2 expressed advanced solid tumors and local advanced or metastatic, HER2 positive breast cancer. This clinical trial was registered at clinicaltrials.gov

(NCT03944499).

PART I-2. Materials and Methods

Cell culture. Human gastric carcinoma N87 cells (ATCC no. CRL-5822, Manassas, VA) were maintained in RPMI 1640 medium (Gibco-Invitrogen, Carlsbad, CA). Human breast carcinoma JIMT-1 cells (DSMZ no. ACC 589, Inhoffenstraße, Braunschweig) were maintained in DMEM medium (Gibco-Invitrogen). Human breast adenocarcinoma MDA-MB 231-Luc-GFP cells were maintained in RPMI 1640 medium (Gibco-Invitrogen, Carlsbad, CA). Both media were supplemented with 10% fetal bovine serum (Gibco-Invitrogen) and 1% penicillin/streptomycin (Gibco-Invitrogen), and the cells were grown under a humidified atmosphere of 5% CO_2 at 37°C. The cells were tested for possible mycoplasma contamination using MycoAlert™ PLUS Mycoplasma Detection Kit (Lonza Walkersville, Inc., Walkersville, MD).

Study approval. All animal experiments were performed following a protocol approved by the Institutional Animal Care and Use Committee of the Asan Institute for Life Science (2014-12-168, 2015-12-126). All the patients provided signed informed consent. This study was approved by the Institutional Review Board (IRB) of Asan medical center (2010-0618).

Generation of gastric cancer PDX model. Five cases of gastric adenocarcinoma specimens were implanted to six-weeks-old NOD-SCID mice (Charles River Laboratories, Wilmington, MA, USA) for the first passage. To produce the gastric cancer (GC) patient-derived xenograft (PDX) models, a piece of tumor tissue in 3×3×3 mm^3 size was implanted subcutaneously (*s.c.*) into flank. After about 3 months, when the tumor size reached to 500 mm^3, the mice were anesthetized *via* an intra-peritoneal injection of a 40 mg/kg zoletil (Virbac, Virbac laboratories BP 27-06511 Carros, France) and 5 mg/kg Rumpun (Bayer, Korea, South Korea), and the tumors were surgically removed. The tumor was implanted again into male athymic nude mice (BALB/c-nude; six-weeks-old; Japan SLC, Hamamatsu, Japan) for amplification. After four consecutive passages in male athymic nude mice, the xenograft was used for examination of *in vivo* therapeutic efficacy, and full characterization including histopathological analysis, HER2 expression by IHC assays, genomic mutation detection.

***In vivo* tumor growth delay.** Cell-derived xenograft (CDX) and PDX tumor models using male athymic nude mice (BALB/c-nude (six-weeks-old); Japan SLC, Hamamatsu, Japan) were used for the examination of *in vivo* therapeutic efficacy. A suspension of 3×10^6 cells for the CDX model or a 3 x 3 x 3 mm^3 tissue block for the PDX model were implanted subcutaneously (*s.c.*) into the right hind leg of the mouse. The mice bearing xenograft tumors grown to 80 to 120 mm^3 were pair matched according

to the tumor volume into the experimental and control groups (n = 5-6/group) (54). The single or repeated dose of Herceptin (Trastuzumab, Roche, Republic of Korea), Perjeta (Pertuzumab, Roche, Republic of Korea) and 1A12, novel HER2 antibody (provided AbClon) (8, 9) were intravenously (*i.v.*) administrated through tail vein at 10 mg/kg, respectively, once a week for four weeks. T-DM1 (Kadcyla, 10172048, Roche, Basel, Switzerland), LCB-ADC1, LCB-ADC2 and LCB-ADC3 were intravenously (*i.v.*) administrated through the tail vein, and the dose was a single 2 or 5 mg/kg or repeated 5 mg/kg, once a week for 4 weeks or every other week for 4 weeks. The doses of all drugs were adjusted to the equivalent amount of the antibody. The tumor volume and body weight were monitored during whole period of experiment. Tumor volume was calculated using the formula volume = (length × width^2) × 0.5. The results were expressed as the mean ± standard deviation. Relative tumor growth inhibition was calculated as Tumor Growth Inhibition (TGI) = (Ti-T0/Ci-C0), Ti and Ci represent tumor size of treatment and control group at the end of experiments respectively; T0 and C0 represent tumor size at initiation of experiments respectively (55). An objective response was defined by Response Evaluation Criteria In Solid Tumors (RECIST) as complete response; CR (disappearance of all target lesions), partial response; PR (at least a 30% decrease in longest diameter of target lesions), stable disease; SD (neither sufficient shrinkage to qualify for PR nor sufficient increase to qualify for PD), and progressive disease; PD (at least a 20% increase in target lesions) (56).

Patients and tumor samples. All animal experiments were performed following the protocol approved by the Institutional Animal Care and Use Committee of the Asan Institute for Life Sciences. Human gastric adenocarcinoma tissues were excised from five patients during surgery. A part of fresh specimen was transferred to medium-containing antibiotics immediately after surgical resection under sterile conditions and transported to an animal facility within 2 hours for implantation into mice. The other part was frozen in liquid nitrogen or fixed in 4% formaldehyde and embedded in paraffin at 56°C for histological evaluation.

Assessment of morphology and immunophenotype. For immunohistochemical (IHC) staining of HER2, tumor tissues from the N87 CDX, JIMT-1 CDX, or PDX models were fixed with 4% paraformaldehyde, embedded in paraffin and sectioned. Immunohistochemical staining was conducted with the anti-HER2/neu (4B5) rabbit monoclonal primary antibody (#790-4493; Roche, Basel, Switzerland), and the stained sections were analyzed under a DP71 microscope (Olympus, Tokyo, Japan). The tumor tissues were counterstained with hematoxylin and eosin (H&E). The diagnosis of each case was confirmed by pathologists at Asan medical center.

Construction, expression, and purification of the Herceptin-CaaX body. Modified Herceptin antibodies were generated using standard PCR cloning protocols. Generally, Herceptin-CaaX body

plasmids were constructed by inserting a DNA sequence encoding a CaaX motif (G7CVIM) into the C-terminus of the light chain encoded in the pNATABH::Herceptin LC plasmid. HEK293 E cells were cultured in DMEM/10% FBS media on 150 mm plates (#430599; Corning, Glendale, AZ) until reaching 70~80% confluency. Then, 13 mg of DNA and 26 mg of PEI (#23966, Polysciences, Warrington, PA) were mixed at a ratio of 1:2, incubated at RT for about 20 minutes, and then added to the HEK293E cells. After 16-20 hours, the media was replaced with serum free media (No FBS DMEM (#SH30243.01; Hyclone Thermo, Marlborough, MA) and the supernatant was collected every two or three days. The supernatants were filtered through a 0.22 μm top-filter (#PR02890, Millipore, Milford, MA) and then bound to 500 ml of protein A beads (#17-1279-03; GE healthcare, Danderyd, Sweden) packed in a 5 mL column. Using a peristaltic pump, overnight binding was performed at 0.9 mL/min at 4°C. The column was washed with at least 100 mL of PBS (#70011, Gibco, Waltham, MA). Bound protein was then eluted with 0.1 M glycine-HCl (#G7126; Sigma, St. Louis, MO) into 6 fractions and neutralized with 1 M Tris (#T-1503; Sigma, St. Louis, MO) (pH 9.0). The protein was quantified and 2 or 3 fractions containing the protein were collected and concentrated with Amicon Ultra filter units (#UFC805024; Millipore). The buffer was changed about 10 times with PBS (#70011; Gibco). The protein product was confirmed to be Herceptin-HC-GCVIM or Herceptin-LC-GCVIM by western blot. To identify a protein band containing Herceptin, ImmunoPure peroxidase conjugated goat anti-human IgG Fc (#31413; Pierce, Waltham, MA) was used. Upon purification, Herceptin-CaaX was obtained from 1 L of cell culture medium. The Herceptin-CaaX body products were also analyzed with an Agilent bioanalyzer. Briefly, 8 ml of purified protein sample (approx. 1 mg/ml) was analyzed using the Agilent Protein 230 Kit (5067-1515; Agilent Technologies, Santa Clara, CA). The protein sample was then separated into 2 fractions to which 2 ml of non-reducing buffer or reducing buffer was then added. The sample was next heated at 95-100°C for 5 minutes and cooled with ice to 4°C. After a spin-down, 84 ml of deionized water was added to the sample and vortexed. Thereafter, the sample was loaded and analyzed with the kit per the manufacturer's instructions.

Prenylation. The prenylation reaction mixture was prepared with the antibodies and reacted at 30 for 12 hours. The reaction mixture was comprised of a buffer solution (50 mM Tris-HCl (pH7.4), 5 mM $MgCl_2$, 10 μM $ZnCl_2$, 5 mM DTT) containing 24 μM antibody, 200 nM FTase (#344145, Calbiochem, Milford, MA), and 1 mM LCB14-0606 (LegoChemBiosciences, Inc., US2012/0308584). After the reaction was completed, the prenylated antibody was purified with a G25 Sepharose column on an AKTA purifier (GE healthcare), which was equilibrated with PBS buffer solution. The prenylated antibody (final concentration: 12 μM) was then treated with 1 mM $CuSO_4$ and reacted at 30 for 3 hours in order to be reoxidized. After this reaction was completed, 2 mM (final concentration) EDTA was added, and the mixture was kept at 30 for 30 minutes while being gently stirred. The resultant

preparation was then purified by FPLC.

Drug conjugation. An oxime bond formation reaction mixture between the prenylated antibody and linker-toxin was prepared by mixing 100 mM Na-acetate buffer (pH 4.5, 10% DMSO), 12 μM antibody, and 360 μM linker-toxin and gently stirred at 30 . After the reaction had proceeded for 24 hours, FPLC (AKTA purifier, GE healthcare) was conducted to remove any excess amounts of small molecules used in the reaction and the protein fractions were collected to be subsequently concentrated. Depending on the type of linker-payload, the DARs of LCB-ADC1, LCB-ADC2, and LCB-ADC3 were 2, 4, and 4, respectively.

***In vivo* rat pharmacokinetics of Herceptin and LCB-ADC1.** To confirm the pharmacokinetics of Herceptin and LCB-ADC1 at the time of intravenous administration of a single dose to a rat, the following experiment was performed. Herceptin or LCB-ADC1 were intravenously administered to female rats (dose: 3.0 mg/kg) and 0.4 mL of blood was collected from the jugular vein using a 1 mL syringe (25 gauge) treated with Heparin (85 IU/mL, 35 μL) at predetermined times (3 minutes, 1 hour, 3 hours, 6 hours, 1 day, 2 days, 3 days, 4 days, 7 days, 9 days, 14 days, 17 days, 21 days, and 28 days after administration). The blood samples were placed a micro tube, treated with a roll mixer for several minutes, and then centrifuged at 14,000 rpm for 5 minutes, thereby separating the plasma. The separated plasma was put into a micro tube and stored in a deep freezer until analysis. The test materials in the plasma were measured using LC-MS. PK analysis was conducted using compartment model 2 using Phoenix™ WinNonlin® (ver. 6.3, Pharsight), and the drug-antibody ratio (DAR) was quantified by LC-MS/MS after separating the LCB-ADC1 using protein A beads.

***In vivo* monkey pharmacokinetics of Herceptin and LCB-ADC1.** To determine the pharmacokinetics of Herceptin and LCB-ADC1 in the monkey, Herceptin and LCB-ADC1 were intravenously administered into female monkeys, respectively (dose: 3.0 mg/kg). About 1.5 mL of blood was collected from the cephalic or femoral vein at predetermined times (30 minutes, 3 hours, 7 hours, 12 hours, 24 hours (2 days), 3 days, 4 days, 5 days, 6 days, 11 days, 15 days, 22 days, 29 days, and 36 days after administration), put into a tube filled with anticoagulant (EDTA-K2), stored in a wet-ice/Kryorack, and then centrifuged at 3,000 rpm for 10 minutes in a cold-storage state, thereby separating the plasma. The separated plasma was dispensed into a microtube and stored in a deep freezer until analysis. The test materials in the plasma were measured using LC-MS. PK analysis was performed with compartment model 2 using Phoenix™ WinNonlin® (ver. 6.3, Pharsight), and in order to quantify the drug-antibody ratio, free MMAF was quantified by LC-MS/MS after separating LCB-ADC1 using protein A beads and treatment with β-glucuronidase.

Cell cycle distribution. JIMT-1 and N87 cells were plated in a 60-mm tissue culture dish at a density

of 5×10^5 cells/plate and incubated overnight. Cells were treated with T-DM1 (Kadcyla, 10172048, Roche, Basel, Switzerland) or LCB-ADCs (provided by LegoChem Bioscience) at a dose of 0.25 μg/ml based on the amount of antibody for 24 and 72 hours. The cells were collected and suspended in 100% cold-ethanol for fixation, stained with propidium iodide (PI), and then the cell cycle distribution was analyzed by flow cytometry (BD FACS Cancto II).

Immunocytochemistry (ICC). N87 and JIMT-1 cells were cultured in the appropriate medium supplemented with 10% fetal bovine serum and 1% penicillin/streptomycin at 37°C under 5% CO_2. Upon confluency, the cells were detached from the flask by trypsin–EDTA, centrifuged and resuspended in media. Approximately 5×10^4 cells/ ml were then transferred onto 12 mm round coverslips in a 24-well plate and incubated for 24 hours. For assessment of microtubule interruption, they were treated with T-DM1, LCB-ADC1 or LCB-ADC2 at 0.25 μg/ml and incubated for 24 hours. Then, they were fixed with 4% formaldehyde and treated with 0.5% Triton X-100. After thorough washing with phosphate-buffered saline (PBS), the cells were incubated with anti-HER2/ErbB2 rabbit polyclonal primary antibody (#2242S; Cell Signaling, Danvers, MA), anti-α-tubulin rabbit monoclonal primary antibody (#2125S; Cell Signaling), and Alexa 594 or 488 anti-rabbit IgG (Jackson Immuno Research, West Grove, PA). The cells were incubated with Hoechst33342 (H33342; Sigma-Aldrich, St. Louis, MO) for 10 minutes at room temperature. After washing with PBS, the coverslips were mounted on slides (Vector Laboratories, Inc., Burlingame, CA). Fluorescence imaging was performed under a DP71 microscope (Olympus, Tokyo, Japan) equipped with two band-pass filters with a center wavelength.

Statistical analysis. Sample sizes were not predetermined. All data are presented as a mean ± SD (standard deviation) from at least three separate experiments. Means were compared using a one-way ANOVA test. P values were obtained by Microsoft Excel 365. P values are represented as $*P < 0.05$, $**P < 0.01$ or $***P < 0.001$, which are considered to indicate significant differences.

PART I-3. Results

1. Establishment of PDX models and phenotypic comparison.

All GC patients' samples were viable and led to growth in SCID mice after subcutaneous implantation and continued to grow in nude mice after the second generation. Five GC tissues were used for this study and assessed after H&E staining and HER2 expression. Four male patients and one female patient, aged from 50 to 79 were collated (Table 1). It was confirmed by immunohistochemical analysis that amplified tumor tissues formed in mice revealed the identical characteristics with original tumors. As shown in Figure 1, the xenograft tumor (Figure 1, right panel) had similar morphological features and HER2 expression to the original tumor (Figure 1, left panel). Two cases (11C94 and 12C63) were scored as strongly positive (3+) for HER2 staining and three cases were scored as moderately positive (2+). In addition, morphology of successive transplanted tumors tissue was identical *via* H&E staining (Figure 2) and finger printing *via* Next Generation Sequencing (NGS) shown matching rate of above 80% between original patient tissues and p5 PDX tissues (data not shown).

Table 1. Patient profiles.

No.	Case	Age	Sex	HER2 expression level in IHC	Pathology
1	11C94	50	Female	+++	TUBULAR ADENOCARCINOMA, MD
2	12C63	71	Male	+++	TUBULAR ADENOCARCINOMA, MD
3	13C127	52	Male	++	TUBULAR ADENOCARCINOMA, MD
4	14D26	72	Male	++	TUBULAR ADENOCARCINOMA, PD
5	14D27	79	Male	++	ADENOCARCINOMA, MD

MD: Moderately differentiated; PD, poorly differentiated.

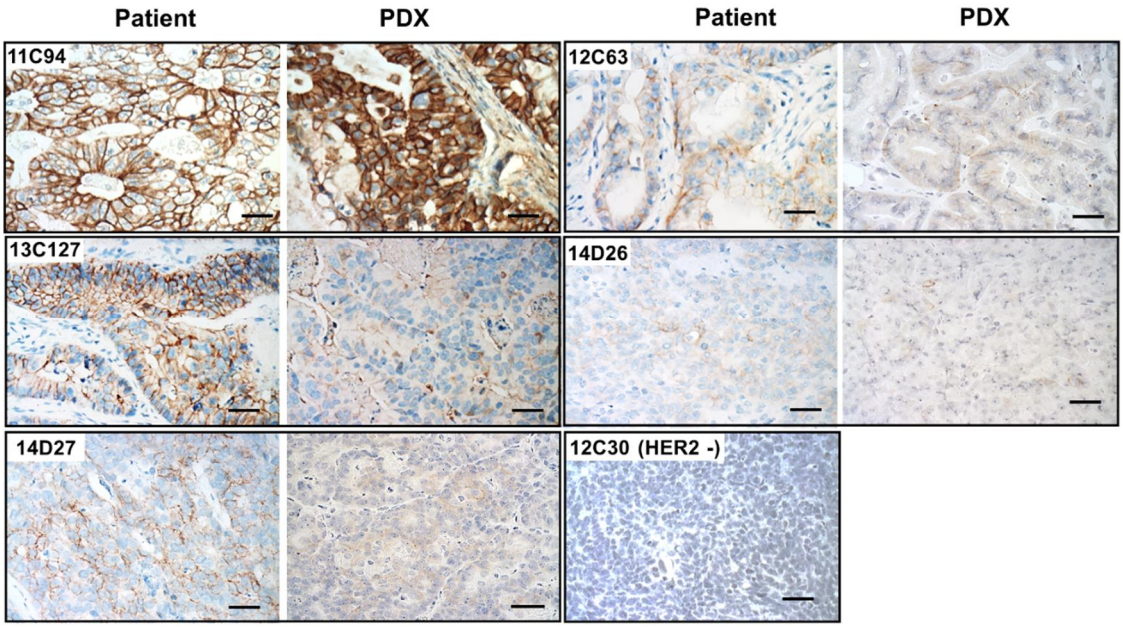

Figure. 1 Immunophenotypic comparison of patient and PDX tumors

HER2 expression was performed by immunohistochemical analysis. HER2 expression was maintained in PDX tumor compared with primary tumor from patient. DAB images of immunohistochemically stained HER2 were obtained under a microscope. Scale bar, 10 μm.

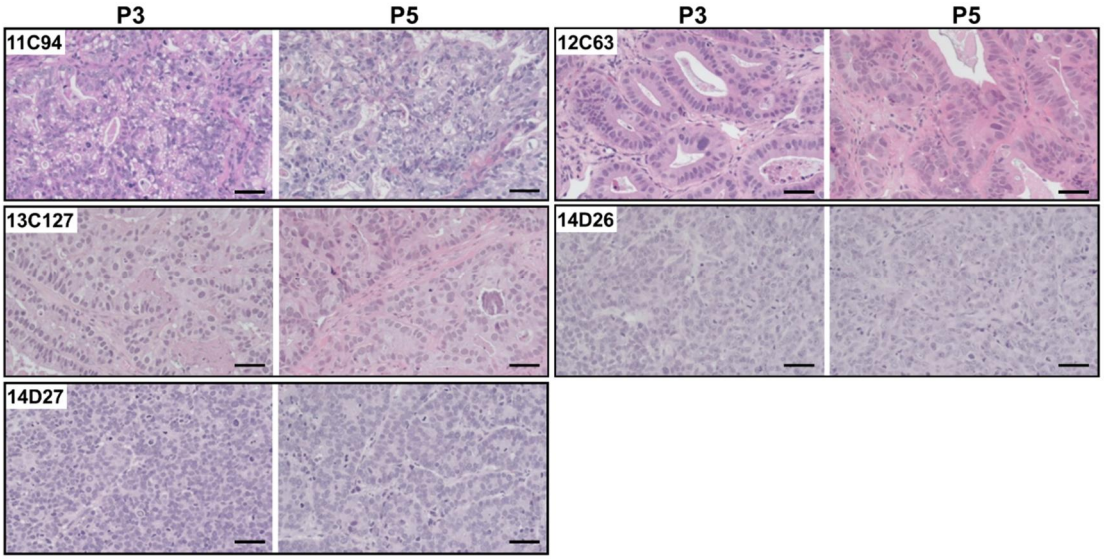

Figure 2. Histological morphology of PDX tumor between P3 and P5

Histological features were identical between P3 and P5 in PDX tumor. Histological evaluation of PDX tumor was attended by hematoxylin & eosin (H&E) and analyzed under a microscope. Scale bar, 10 μm.

2. Responses of individual GC PDX models to trastuzumab.

To assess the PDX models as personalized tool, *in vivo* anti-cancer effect of trastuzumab was evaluated in all five HER2+ GC PDX models. The mice were *i.v.* injected with trastuzumab at repeated dose of 10 mg/kg once a week for four weeks. Two GC PDX models (IHC 3+) named 11C94 and 12C63 showed highly anti-cancer effect as 99.9 and 89.9% of tumor growth inhibition (TGI), respectively, whereas three GC PDX models (IHC 2+) named 13C127, 14D26, 14D27 did not reveal any therapeutic effect as 28.5, -20.5, 12.9% of TGI at the end point, respectively (Table 2 and Figure 3). In addition, tumor volume and weight were dramatically decreased at the end point in two GC PDX models. As a result, HER2+ GC PDX according to HER2 expression was assessed with preclinical test of trastuzumab, and these results suggested that PDX model could be personalized tool for clinical relevance of novel drug candidate.

Table 2. Tumor growth inhibition (TGI) of HER2+ GC PDX models.

	TGI (%) at the end point				
Case	11C94	12C63	13C127	14D26	14D27
Herceptin	99.9	89.9	28.5	-20.5	12.9

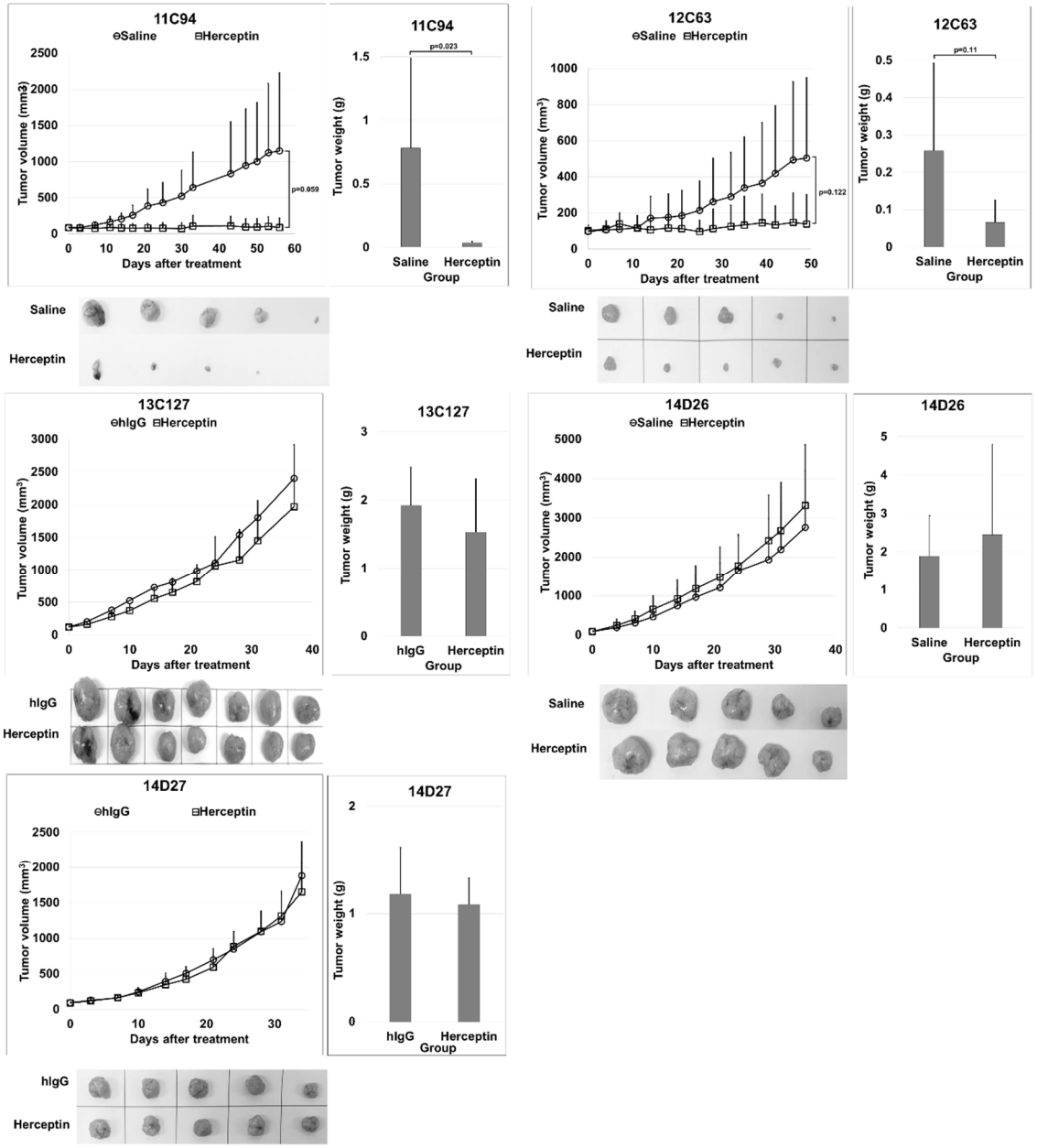

Figure 3. Trastuzumab anticancer efficacy in HER2+ GC PDX

Tumor growth delay curves. Mice bearing HER2+ GC patient's tumor of 5 cases were intravenously administrated with Herceptin at dose of 10 mg/kg once a week for four weeks. Tumor volumes and body weights were monitored during the experimental course. Tumor was removed at the end point and measured its weight. Data are represented as mean±standard deviation.

4. Evaluation of anti-cancer efficacy of new HER2 Ab in GC PDX models.

Since the feasibility of PDX models were confirmed as personalized test, *in vivo* study of therapeutic effect was next performed by 1A12, novel HER2 antibody. The 1A12 bind to sub-domain IV of HER2-ECD (extracellular domain), and it has not overlap with epitope of trastuzumab. So, the 1A12 is developed by AbClon as combination therapy with trastuzumab for GC patient (8). The mice were *i.v.* injected with trastuzumab, perjeta and 1A12 at a repeated dose of 10 mg/kg once a week for four weeks. As shown in Figure 4 and Table 3, TGI of Herceptin, Perjeta and 1A12-treated group were 80, 45, and 38%. The impact of trastuzumab plus 1A12 in 11C94, HER2+ (IHC 3+) GC PDX model was demonstrated, which remarkably increased TGI at 104% compared to conventional treatment (trastuzumab plus pertuzumab, TGI at 88%). Moreover, trastuzumab plus 1A12 resulted in CR of 60% (3/5) and PR of 40% (2/5) (Table 3). Taken together, preclinical testing of novel candidate drug could be assessed *via* HER2+ GC PDX.

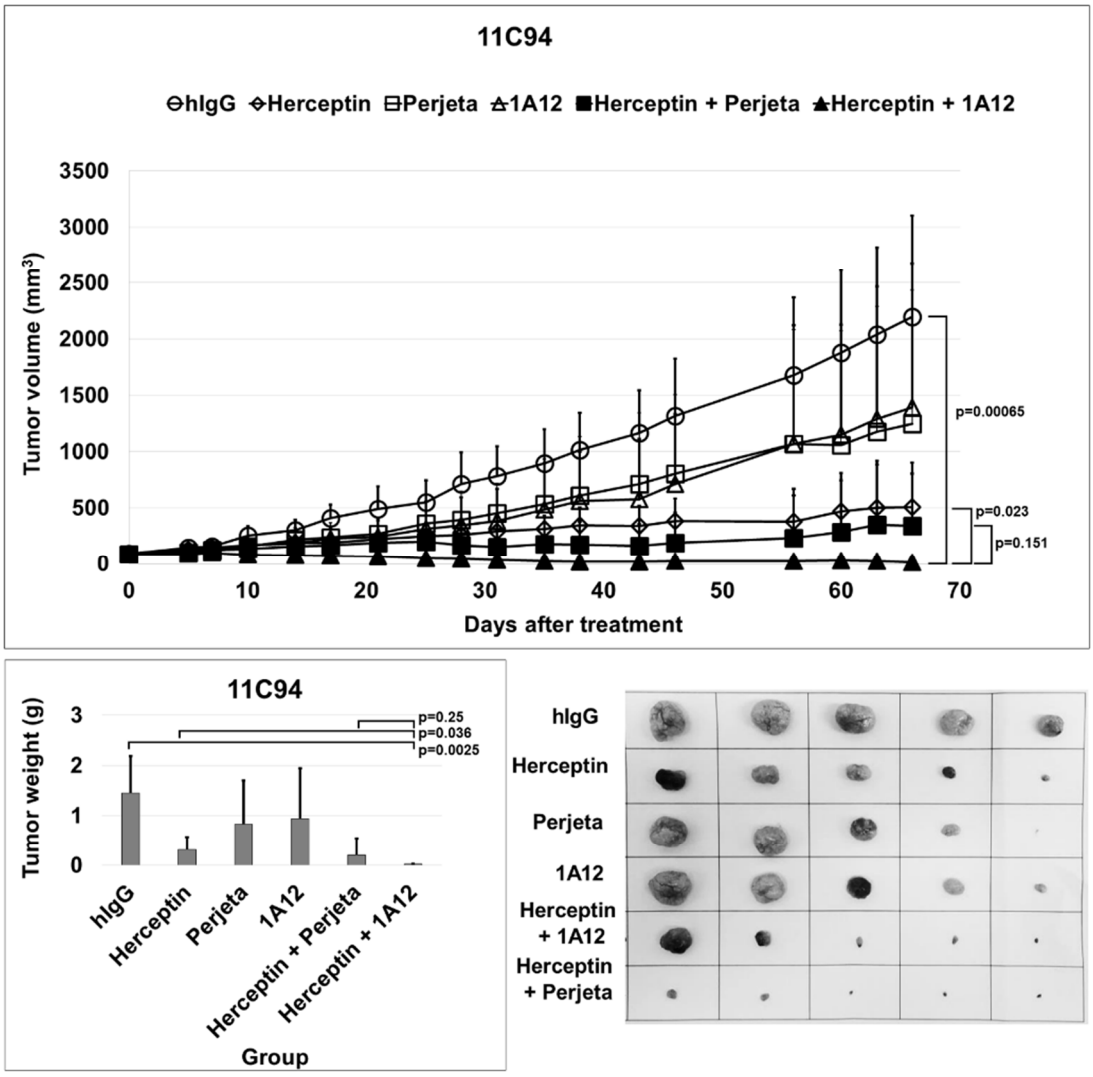

Figure 4. 1A12 anticancer efficacy in IHC 3+ case

Tumor growth delay curves. Mice bearing HER2+ (IHC 3+) GC patient's tumor was intravenously administrated with Herceptin, Perjeta and 1A12 at dose of 10 mg/kg once a week for four weeks. Tumor volumes and body weights were monitored during the experimental course. Tumor was removed at the end point and measured its weight. Data are represented as mean±standard deviation.

Table 3. Tumor growth inhibition (TGI) and RECIST in HER2+ (IHC3+) GC PDX

		[a]RECIST			
	TGI %	[b]CR	[c]PR	[d]SD	[e]PD
hIgG	-				5 (100)
Herceptin	80	1 (20)			4 (100)
Perjeta	45	1 (20)			4 (100)
1A12	38		1 (20)		4 (100)
Herceptin + Perjeta	88	2 (40)		1 (20)	2 (40)
Herceptin + 1A12	104	3 (60)	2 (40)		

a) RECIST: Response Evaluation Criteria In Solid Tumors, b) CR: Complete Response, c) PR: Partial Response, d) SD: Stable Disease, e) PD: Progressive Disease

5. LCB-ADCs are fabricated with a novel conjugation method and show an improved pharmacokinetic profile.

To achieve homogeneity of production and a smarter linker system for ADCs, a novel conjugation method was developed, and an improved linker was designed (Figure 5a and b). Additional amino acid sequences that can be recognized by farnesyl transferase (FTase) were added to the end of the antibody (light chain and/or heavy chain), termed the CaaX body. Bonding between the SH on the Cys residue of CaaX and the pyrophosphate of isoprenoid (farnesyl pyrophosphate) can then be generated by FTase (prenylation). An oxime bond is generated as a result of the subsequent reaction between the amine group of the linker-toxin and the carbonyl (ketone) group of the prenylated CaaX body. The prenylation and drug-conjugation step proceeded very efficiently with high homogeneity of the end product (Figure 5c and Table 4). To increase the linker stability, the three electron-donating groups in the Seattle Genetics beta-glucuronide linker were modified. The electron density of the phenyl ring of the self-immolative group (SIG), which is bonded to the β-glucuronide ring, is relatively high and might be susceptible to metabolism (e.g., oxidation) and therefore is possibly less stable. Through a proprietary chemical modification, we prepared a reversed amide of the self-immolative group (in relation to the directionality of the original amide), which became an electron-withdrawing group. Its electron density is decreased, and this stabilizes the linker (Figure 5d).

To review hypothesis of above-mentioned, mouse plasma stability tests were applied and observed that the modified SIG linker version is more stable in mouse plasma, which supports hypothesis of this research (Figure 6a). The HER2-targeting ADCs with the LCB type linker-toxin (LCB-ADC1 and LCB-ADC-2) maintain their stability for at least 7 days in mouse or rat plasma. When the PK profile was examined in the rat and monkey, the ADC was comparable to the original antibody (Herceptin). In addition, stable attachments of the linker toxin were observed in both species (Table 5 and Figure 6). These results demonstrated that novel HER2-ADCs (LCB-ADCs) generated this research, that were elaboratively generated for a more precise DAR, show higher stability in mouse, rat and monkey serum than conventional ADCs.

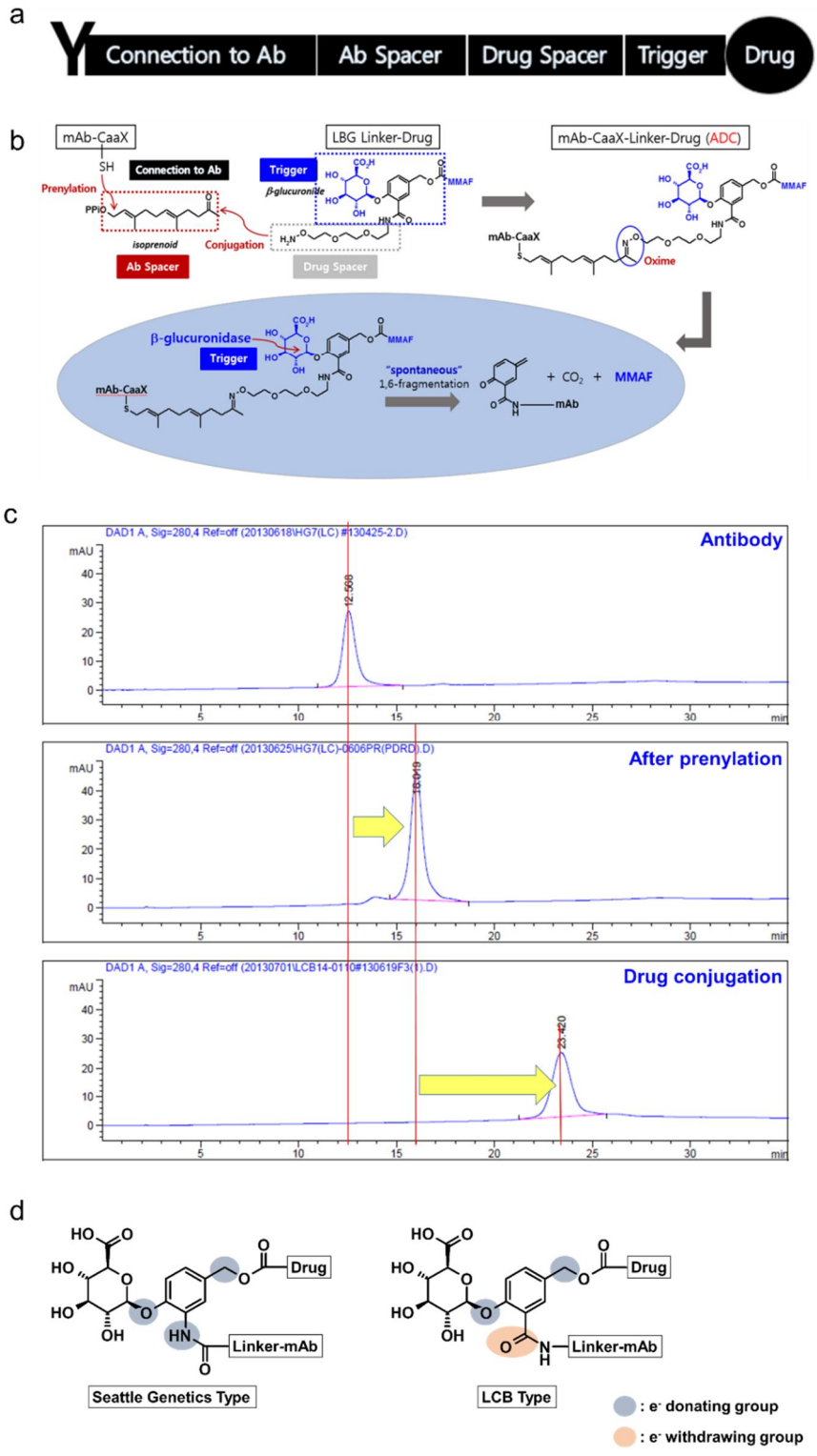

Figure 5. ADC conjugation strategy

Composition of the ADC (a). Conjugation process *in vitro* and drug release mechanism in cancer cells (b). Results of the HIC analysis with the products in each step (c). Working hypothesis of the linker stability (d).

Table 4. Compositions of LCB-ADC1, 2, and 3

ADC name	Linker type	Payload	DAR
LCB-ADC1	PEG-3	MMAF	2
LCB-ADC2	PEG-3,3,3	MMAF	4
LCB-ADC3	PEG-6,6,3	MMAF	4

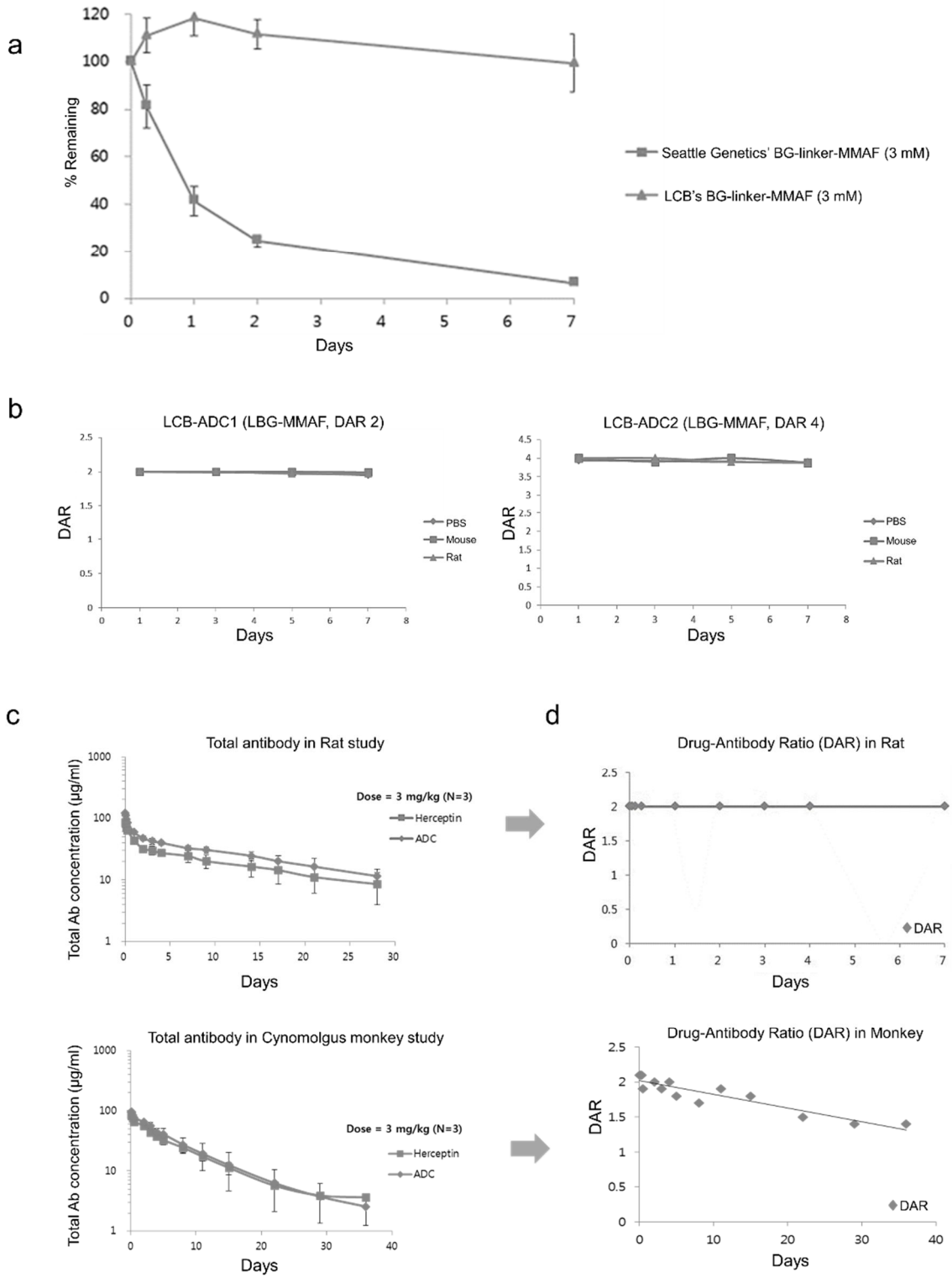

Figure 6. Stability of the linker-toxin system and PK profiles of LCB-ADC1

Comparison of linker-drug stability in mouse plasma (a). Plasma stability of ADCs in mouse or rat plasma (b). PK profiles of Herceptin and LCB-ADC1 in the rat and monkey (c). Drug-antibody ratio (DAR) calculations (d).

Table 5. The PK parameters of Herceptin and LCB-ADC1 in the rat and monkey.

	Herceptin		LCB-ADC1	
	Half-life (day)	AUC[a)] (μg×day/mL)	Half-life (day)	AUC [a)] (μg×day/mL)
Rat	13.4	689.3±21.9	12.8	965.5±33.5
Monkey	10.1	622.9±26.5	8.6	684.8±20.4

[a)] Area Under the Curve

6. LCB-ADCs showed significant anticancer effect in HER2-positive cell lines more than T-DM1.

To ensure that LCB-ADCs produces HER2-positive specific cytotoxicity, human breast cancer JIMT-1 cells (HER2-positive), MDA-MB-231 cells (HER2-negative) and human gastric cancer N87 cells (HER2-positive) were treated with LCB-ADCs, and their viabilities were assessed. Remarkable inhibitory activity to the cell growth was observed for LCB-ADCs against HER2-positive JIMT-1 and N87 treated with LCB-ADC1 at 1 μg/ml for 72 hours, with viability of 30% and 48%, respectively (Figure 7a and b). The viability of JIMT-1 and N87 treated with LCB-ADC2 at 1 μg/ml for 72 hours was 21% and 42%, respectively. The viability of JIMT-1 cells was reduced to 18% following LCB-ADC3 treatment at 1 μg/ml for 72 hours, in contrast to the viability of 107% in MDA-MB-231 cells (HER2-negative) following LCB-ADC3 treatment (Figure 7c). These results indicate that the cell growth-inhibitory activity of LCB-ADCs was remarkably enhanced by drug conjugation to the anti-HER2 antibody, and also that LCB-ADCs show target-specific growth inhibition against HER2-positive cell lines.

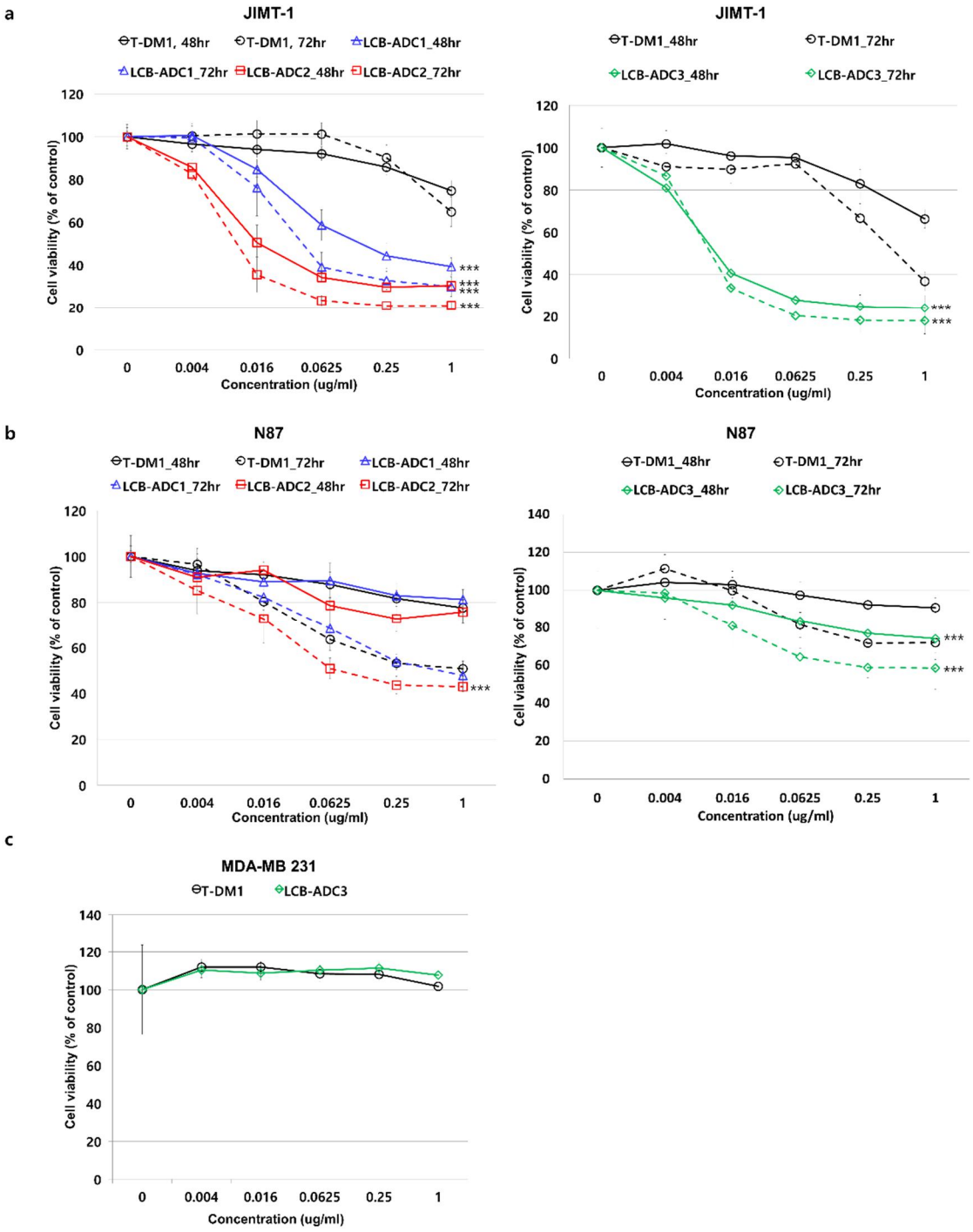

Figure 7. *In vitro* cell growth inhibitory activity in the HER2-positive cell lines

The cells JIMT-1 cells (HER2-positive) (a), N87 cells (HER2-positive) (b) and MDA-MB-231 cells (HER2-negative) (c) were treated with LCB-ADCs and T-DM1 at different concentration (0, 0.004, 0.016, 0.0625, 0.25 and 1 μg/ml) for 72 hours. Each point represents the mean and SD (n = 8). After incubation, cellular viability was measured using the cell counting kit-8. Data are presented as mean ± standard deviation. ***p<0.001 (T-DM1 vs LCB-ADC1, 2 or 3).

7. A potent pharmacologic activity of the LCB-ADCs is induced by MMAF-mediated tubulin inhibition.

Among the analogs of dolastatin, monomethyl auristatin F (MMAF) exerts known anti-neoplastic and anti-tubulin effects by inhibiting cell division *via* the disruption of tubulin polymerization. MMAF was used as the toxic component of our LCB-ADCs as it was designed to be much more active when delivered into cells with an antibody. It harbors a binding site in its C-terminal carboxyl group for a dipeptide linker attachment to enzymes capable of catalyzing drug release, and it can modulate the efficacy, potency, and tolerability of the drug. To evaluate the effect of novel LCB-ADCs on the cell cycle distribution caused by the payload tubulin inhibitors, human breast cancer JIMT-1 and human gastric cancer N87 cells were treated and then analyzed by flow cytometry (Figure 8). Trastuzumab emtansine (T-DM1 or Kadcyla, Genentech), that pairs trastuzumab (Herceptin, Genentech) with the microtubule inhibitor DM1 containing a non-reducible thioether linker (57), and was approved in 2013 as a second-line treatment for HER2-positive metastatic breast cancer, was used as the reference ADC for comparison (39). HER2 expression in the JIMT-1 and N87 cells was first evaluated by immunocytochemistry (Figure 8a). LCB-ADC1, 2, and 3 induced G2/M phase arrest to 47.7%, 63.8% and 68.5% of the cell populations after 24 hours in the HER2 low expressing JIMT-1, cells, respectively, and they maintained this arrest for up to 72 hours unlike the control or T-DM1 treated cells (Figure 8b). In contrast, the N87 high expressing HER2 cells showed a similar induction of G2/M phase arrest by all three LCB-ADC drugs and by T-DM1 (Figure 8c). T-DM1 did not induce G2/M phase arrest in the JIMT-1 cells until 72 hours post-treatment, and this was identical to the control. This is consistent with previous evidence that T-DM1 is effective only in cells expressing high levels of HER2 (46). Moreover, while T-DM1 showed different effects in the two cell lines I tested, LCB-ADCs showed similarly potent effects in all of the cells regardless of their HER2 expression level (Figure 8b). Furthermore, LCB-ADC2 and LCB-ADC3, both having a DAR of 4, showed a greater effect on G2/M phase arrest than LCB-ADC1 in JIMT-1 cells. This suggested that a higher HER2 expression level allows for a higher accessibility of the HER2-ADCs, leading to a more readily disrupted cell cycle regardless of the DAR homogeneity. In cells where access to HER2-ADCs is low due to low HER2 expression, the homogeneity of the ADC and the effective delivery of the payload drug will be crucial. The LCB-ADCs disrupted tubulin polymerization in the JIMT-1 cell line within 24 hours, whereas all of the drugs in the experiment including T-DM1 could exert this effect in the N87 cells. Abnormal tubulin polymerization induced by the payload drugs of the ADCs was visualized by tubulin staining (Figure 9, red arrow), and the resulting mitotic arrest and eventual death of the cells was captured using live cell imaging.

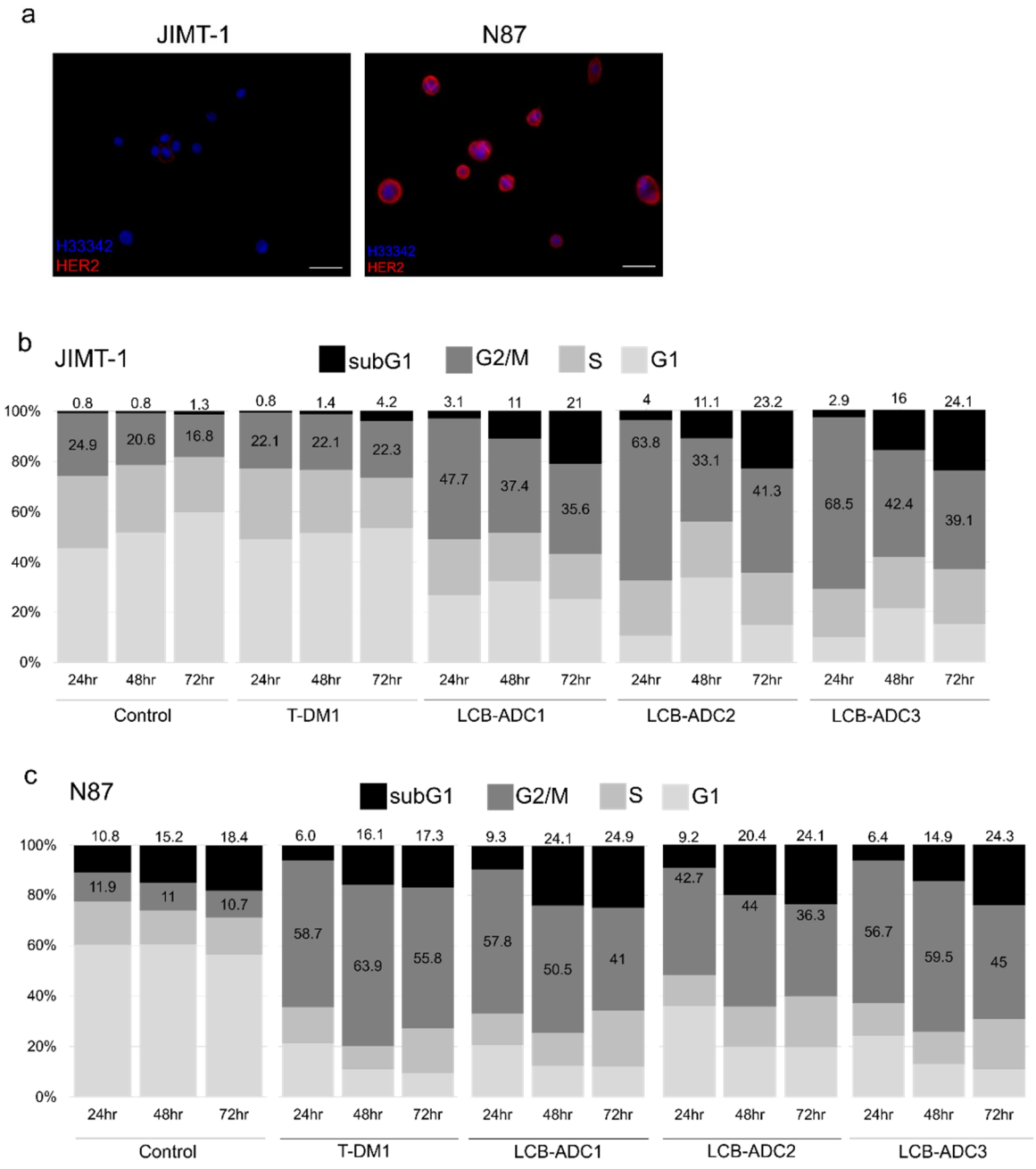

Figure 8. HER2 expression and cell cycle distribution in JIMT-1 and N87 cells

HER2 expression in JIMT-1 and N87 cells stained *via* ICC (red, Alexa 594-stained HER2; blue, Hoechst-stained nuclei, scale bar; 10 μm) (a). Cell cycle distribution in JIMT-1 (b) and N87 cells (c) treated with T-DM1, LCB-ADC1 or LCB-ADC2 at 0.25 μg/ml for 72 h. Cells stained with propidium iodide (PI) were analyzed by flow cytometry.

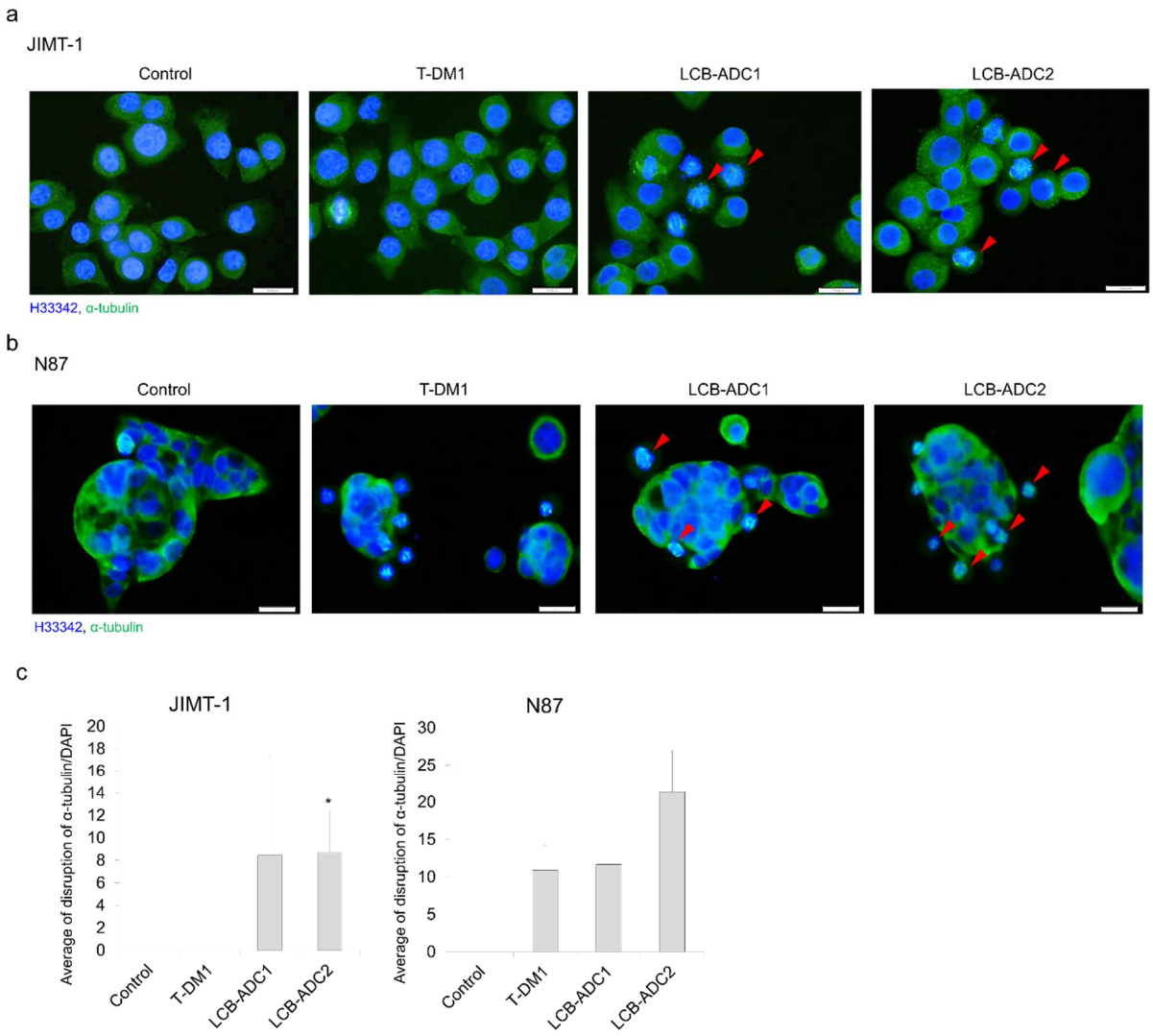

Figure 9. *In vitro* microtubule interruption by LCB-ADCs

JIMT-1 (a) and N87 cells (b) were treated with T-DM1, LCB-ADC1 or LCB-ADC2 at 0.06 μg/ml for 16 h or 24 h and stained with anti-α-tubulin (blue, Hoechst-stained nuclei; green, Alexa 488-stained α-tubulin, scale bar; 10 μm). c) Ratio of tubulin disrupted cell per DAPI stained cells (n=3). Data values are a mean ± standard deviation. *$p<0.05$ (T-DM1 vs LCB-ADC2).

8. LCB-ADCs effectively target HER2-positive xenograft tumors that are resistant to T-DM1.

In vivo experiments were conducted and found that T-DM1 displayed a moderate effect in an N87 xenograft tumor-bearing mouse model, but not in the counterpart JIMT-1 model, likely due to the different HER2 expression levels (Figure 10a and b). In contrast to T-DM1, the LCB-ADCs showed potent *in vivo* efficacy in both the JIMT-1 and N87 xenograft models, as well as a DAR-dependency between LCB-ADC1 and LCB-ADC2. In the JIMT-1 model, tumor growth was 96% inhibited by LCB-ADC1, 115% by LCB-ADC2, and tumor-free complete remission (CR) was observed in 3 out of 5 mice in the LCB-ADC2-treated group at the end point of the experiment (Figure 10a). In the N87 model, tumor growth was inhibited by 48%, 67%, and 101% by T-DM1, LCB-ADC1, LCB-ADC2, respectively, and 1 out of 5 mice were tumor-free in the LCB-ADC2-treated group at the end point (Figure 10b). Moreover, repeated treatments with LCB-ADC1 produced very effective tumor growth inhibition, with tumor-free CR observed in 7 out of 8 animals at the end point (Figure 10d).

T-DM1 showed intermediate efficacy in the high HER2-expressing N87 tumor model but had no effect in the low expressing JIMT-1 model, which had comparable tumor growth to the control group (Figure 10). These results indicated that while LCB-ADCs have very potent antitumor efficacy against low expressing HER2 lesions that are resistant to T-DM1, they are also more effective than T-DM1 against high expressing HER2 tumors.

To determine whether developed linker-drug technology may be clinically applicable and thus potentially address one of the most critical limitations of existing HER2-ADCs, the *in vivo* efficacy of LCB-ADCs were evaluated in patient-derived xenograft (PDX) tumor models, which were considered to be the most relevant model for patients (58). PDX models prepared with human GC tissues in which HER2 expression was relatively high (HER2 +++ GC PDX) or low (HER2 ++ GC PDX) (59) were treated with T-DM1 or LCB-ADCs (Figure 6a, b). In the HER2 +++ model, tumor growth was inhibited by 103%, 99%, and 111% by T-DM1, LCB-ADC1, and LCB-ADC2, respectively, and 2 out of 5 mice were tumor-free in the LCB-ADC2-treated group at day 38 (Figure 11a). In the HER2 ++ GC PDX model, tumor growth was inhibited by 66% using repeated LCB-ADC1 treatments at 5 mg/kg, 107% by repeated treatments with LCB-ADC3 at 5 mg/kg, and tumor-free complete remission (CR) was observed in all mice in the LCB-ADC3-treated group at the end point (Figure 11b). In addition, repeated doses of LCB-ADC3 at 2 mg/kg produced sufficient tumor growth inhibition (107%), with tumor-free CR observed in 4 out of 8 animals at the end point (Figure 11b). In the HER2 +++ GC PDX model, T-DM1 showed a potent therapeutic efficacy as expected. However, the LCB-ADCs displayed an equally potent efficacy to T-DM1 in this model with one treatment (Figure 11a), but it showed a more prolonged efficacy than T-DM1 over a repeated course (Figure 11a). Although T-DM1 has been successfully translated to the clinic for HER2-positive cancer patients, its lack of efficacy in tumor cells expressing

relatively low HER2 levels is an important unmet clinical need (46). T-DM1 did not have any effect in the HER2 ++ GC PDX model but the LCB-ADCs still showed dramatic therapeutic efficacy in these mice. LCB-ADC1 inhibited the growth of the tumors by 66% and LCB-ADC3, after pegylation of LCB-ADC2 in order to test a clinically suitable candidate, produced completely tumor-free mice in all cases, which was confirmed by measurement of the tumor weights in each group and by macrography (Figure 11). LCB-ADC3 was further examined to see if it was still effective at a lower dosage or as a single treatment in the HER2 ++ GC PDX model. A lower dose of LCB-ADC3 displayed a strong therapeutic efficacy whereby up to 3 out of 5 mice became tumor-free following repeated treatments at a lower concentration of this drug and there was a greatly increased survival rate (Figure 13). Moreover, LCB-ADC3 showed sufficient antitumor potency with a tumor inhibition rate of 106% and complete remission (CR) in all HER2 ++ GC PDX mice after only a single treatment (Figure 12b). These results clearly demonstrated that the HER2-targeting LCB-ADCs produced by developed linker-drug technology in this research are clinically applicable and address some of the significant shortfalls with current HER2-targeting therapeutics.

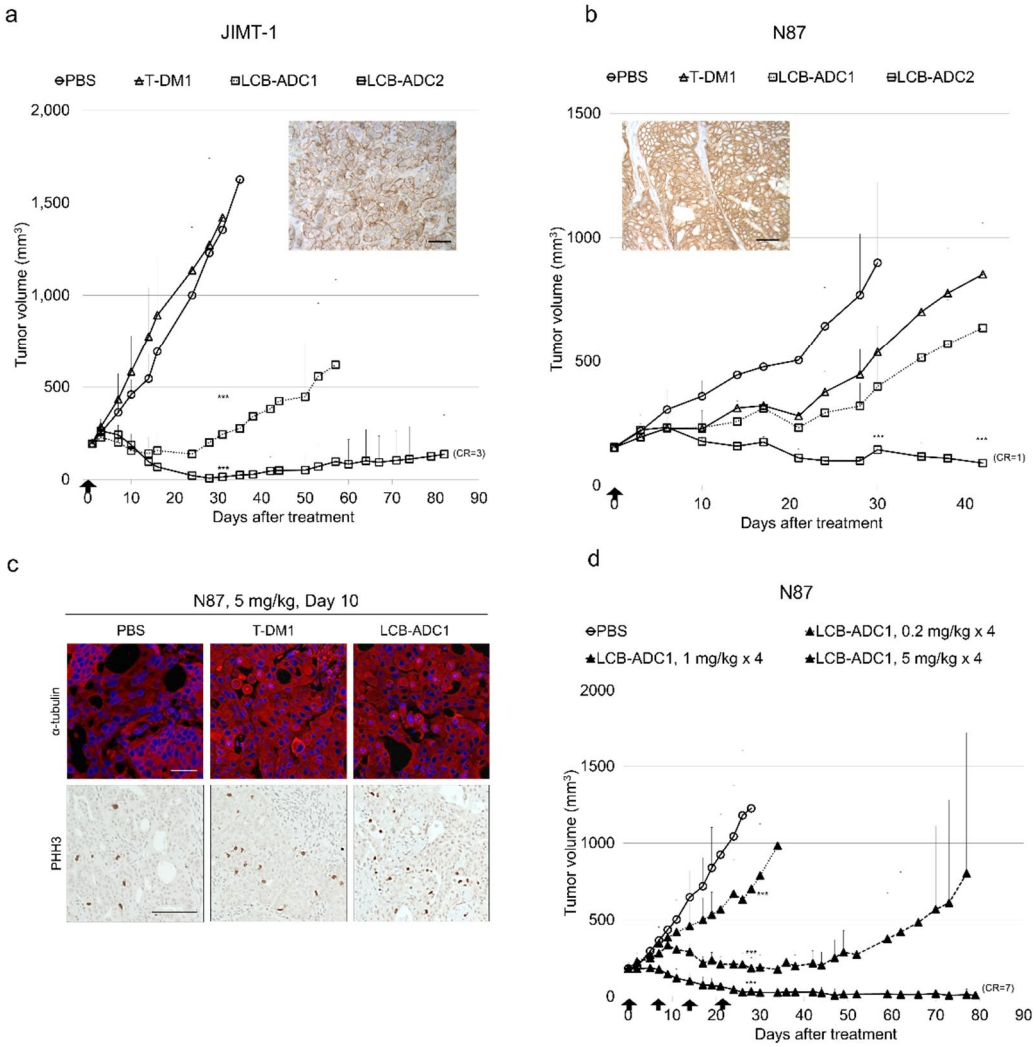

Figure 10. Therapeutic efficacy of LCB-ADCs in HER2-positive CDX models

Effect of LCB-ADC1, LCB-ADC2, T-DM1 in JIMT-1 cells (a). Drugs were *i.v.* injected at 2 mg/kg once (↑), n=5. Data values are the mean ± standard deviation. ***p<0.001 (T-DM1 vs LCB-ADC1 or 2). Effect of LCB-ADC1, LCB-ADC2, T-DM1 in N87 cells (b). Drugs were *i.v.* injected at 2 mg/kg once (↑), n=5. Data values are the mean ± standard deviation. ***p<0.001 (T-DM1 vs LCB-ADC 2). HER2 expression in tumor tissue was detected by IHC (brown, DAB-stained HER2; blue, hematoxylin-stained nuclei, Scale bar; 10 μm). *In vivo* microtubule interruption and mitotic arrest by LCB-ADC1 (c). Mice bearing N87 tumors were *i.v.* administered with T-DM1, LCB-ADC1 at 5 mg/kg once. After 10 days, the tumors were isolated, fixed and stained with anti-α-tubulin (upper, blue, Hoechst-stained nuclei; red, Alexa 594-stained α-tubulin, scale bar; 10 μm) or anti-phosphohistone H3 (PHH3) (lower, blue, hematoxylin-stained nuclei; brown, DAB-stained PHH3, scale bar; 100 μm). Effect of LCB-ADC1 in N87 cells (d). Drugs were *i.v.* injected at 0.2, 1 or 5 mg/kg, once a week for 4 weeks (↑), n=8. Data values are the mean ± standard deviation. ***p<0.001 (T-DM1 vs LCB-ADC1).

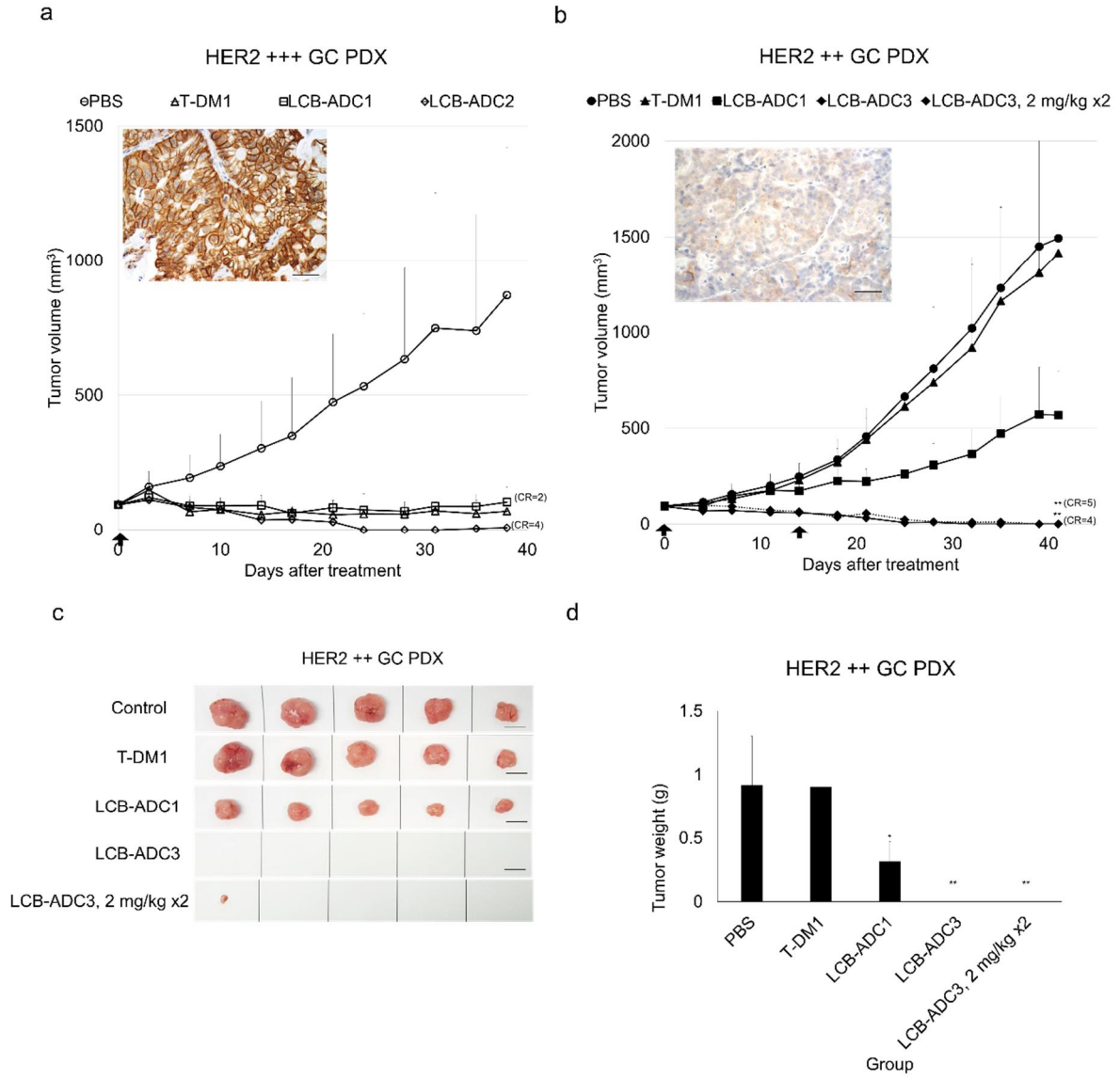

Figure 11. Therapeutic efficacy of LCB-ADCs in HER2-positive GC PDX models

Effect of LCB-ADC1, LCB-ADC2, T-DM1 in a HER2 +++ GC PDX model (a). The drugs were *i.v.* injected at 5 mg/kg once (↑), n=5. Effect of LCB-ADC1, LCB-ADC3, T-DM1 in a HER2 ++ GC PDX model (b). Drugs were *i.v.* injected at 5 mg/kg twice (↑), n=5. Data values are a mean ± standard deviation. **p<0.01 (T-DM1 vs LCB-ADC3, single or repeated treatment). HER2 expression in tumor tissues was detected by IHC (brown, DAB-stained HER2; blue, hematoxylin-stained nuclei, Scale bar; 10 μm). Mice bearing HER2 ++ GC patient-derived tumors were *i.v.* administered with LCB-ADC1, LCB-ADC3 or T-DM1 at 5 mg/kg, every other week for 4 weeks, n=5 (c and d). At the end of the experiment, tumors were isolated, photographed (scale bar; 1 cm) (c) and weighed (d). Data values are mean ± standard deviation. *p<0.05 (T-DM1 vs LCB-ADC1), **p<0.01 (T-DM1 vs LCB-ADC3).

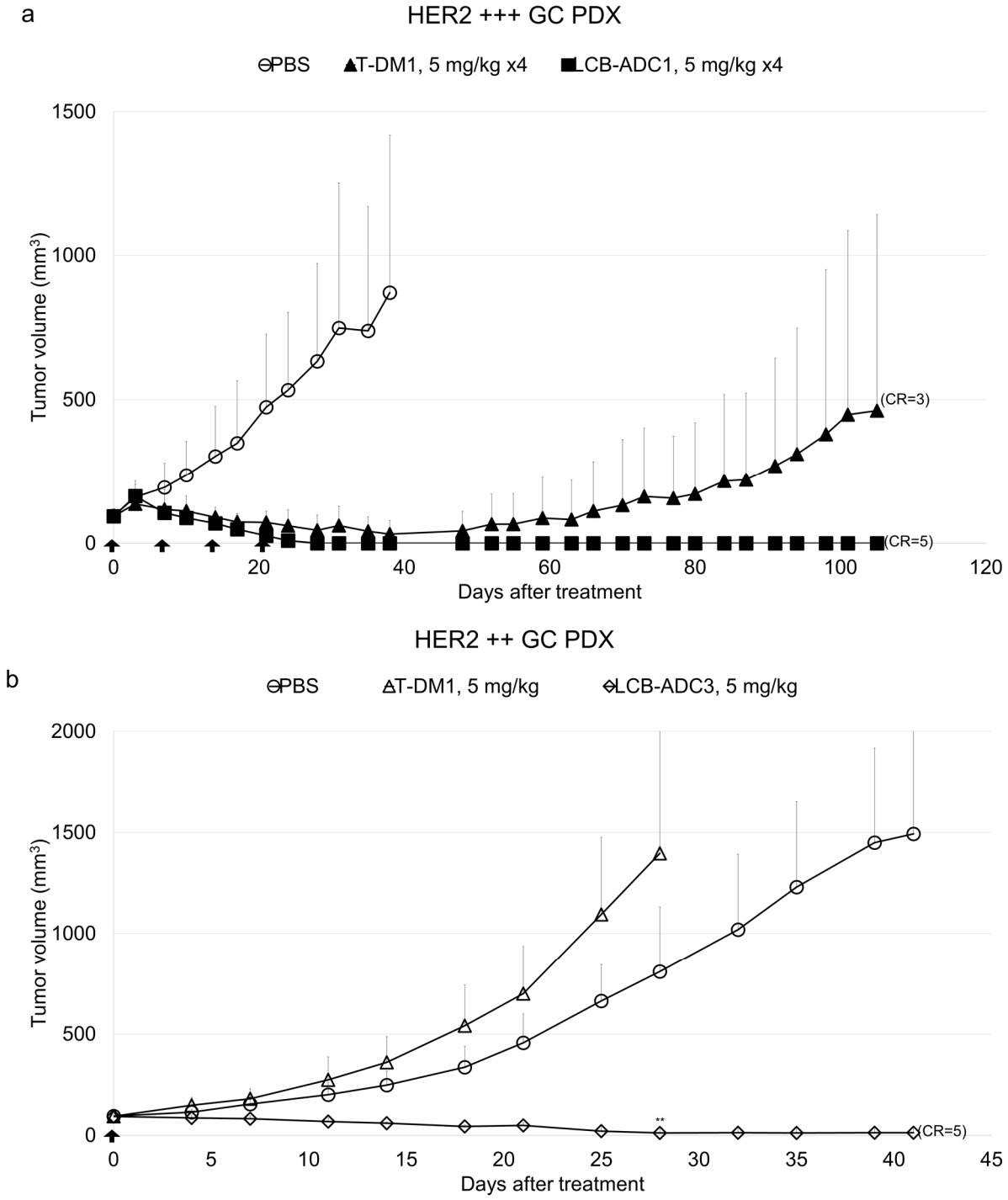

Figure 12. *In vivo* efficacy of LCB-ADCs and T-DM1 in the HER2-positive GC PDX model

Mice bearing HER2 +++ GC patient-derived tumors were *i.v.* administered with LCB-ADC1 or T-DM1 at 5 mg/kg, weekly for 4 weeks (↑) (a). Data are presented as the mean ± standard deviation. Effect of LCB-ADC3, T-DM1 in a HER2 ++ GC PDX model (b). Drugs were *i.v.* injected at 5 mg/kg once (↑). Data values are presented as the mean ± standard deviation. **p<0.01 (T-DM1 vs LCB-ADC3).

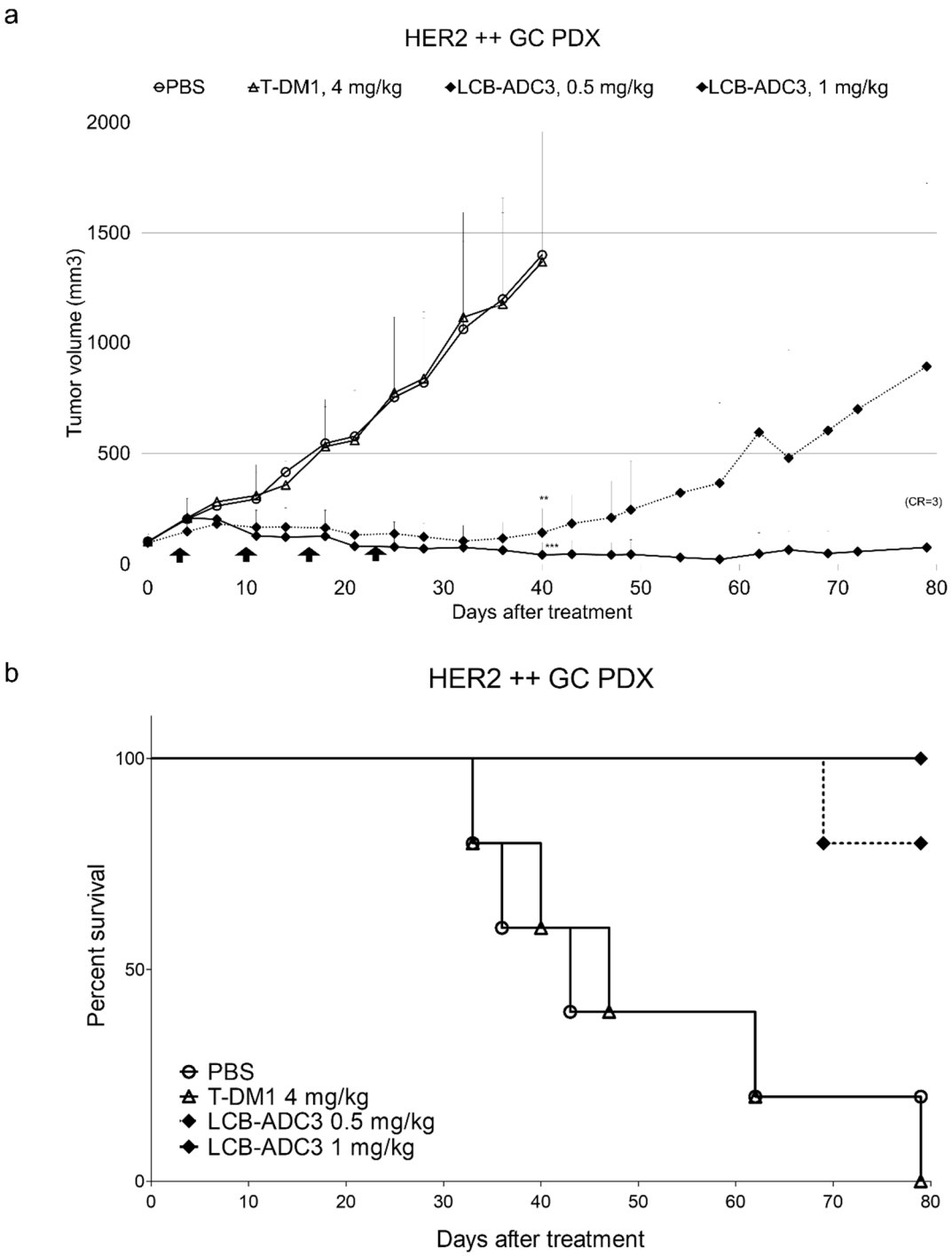

Figure 13. *In vivo* efficacy of LCB-ADC3 at a low dose in a HER2 ++ GC PDX model

Tumor growth delay curves (a) and survival rate when the tumor volume reached 1500 mm^3 (b). Mice bearing patient-derived tumors were *i.v.* administered LCB-ADC3 (0.5 mg/kg or 1 mg/kg) or T-DM1 (4 mg/kg), weekly for 4 weeks (↑), n=5. Data values are the mean ± standard deviation. **p<0.01 (T-DM1 vs LCB-ADC3, 0.05 mg/kg), ***p<0.001 (T-DM1 vs LCB-ADC3, 1 mg/kg).

9. LCB-ADCs evokes mitotic arrest in HER2-overexpressing and -low expressing CDX and PDX models.

Cells under mitotic arrest with abnormal tubulin polymerization and the presentation of phospho-histone H3 (PHH3) induced by the intracellular influx of the payload drug were observed in the N87 tumor tissues of HER2-ADC treated mice, and this effect was more significantly augmented by LCB-ADC1 than by T-DM1 (Figure 10c). When N87 xenograft mice were periodically treated with LCB-ADC1 with a DAR of 2, sufficient inhibition was achieved at a lower dose of 1 mg/kg, and dose-dependency was verified (Figure 10d). Cells arrested in mitosis (expressing PHH3) due to HER2-ADC exposure were observed in these PDX models (Figure 15). Considerable changes of body weight were not observed in this experiment, indicating that no mice suffered from severe toxicity (Figure 15). These results further indicated that LCB-ADCs displayed an efficient anti-cancer effect in HER2-expressing tumors even at a low level of HER2, and strongly suggest that the intended advantages of LCB-ADCs, such as increased linker stability in the bloodstream, an accurate DAR and reliable homogeneity, and an improved PK profile can be observed in xenograft tumor models.

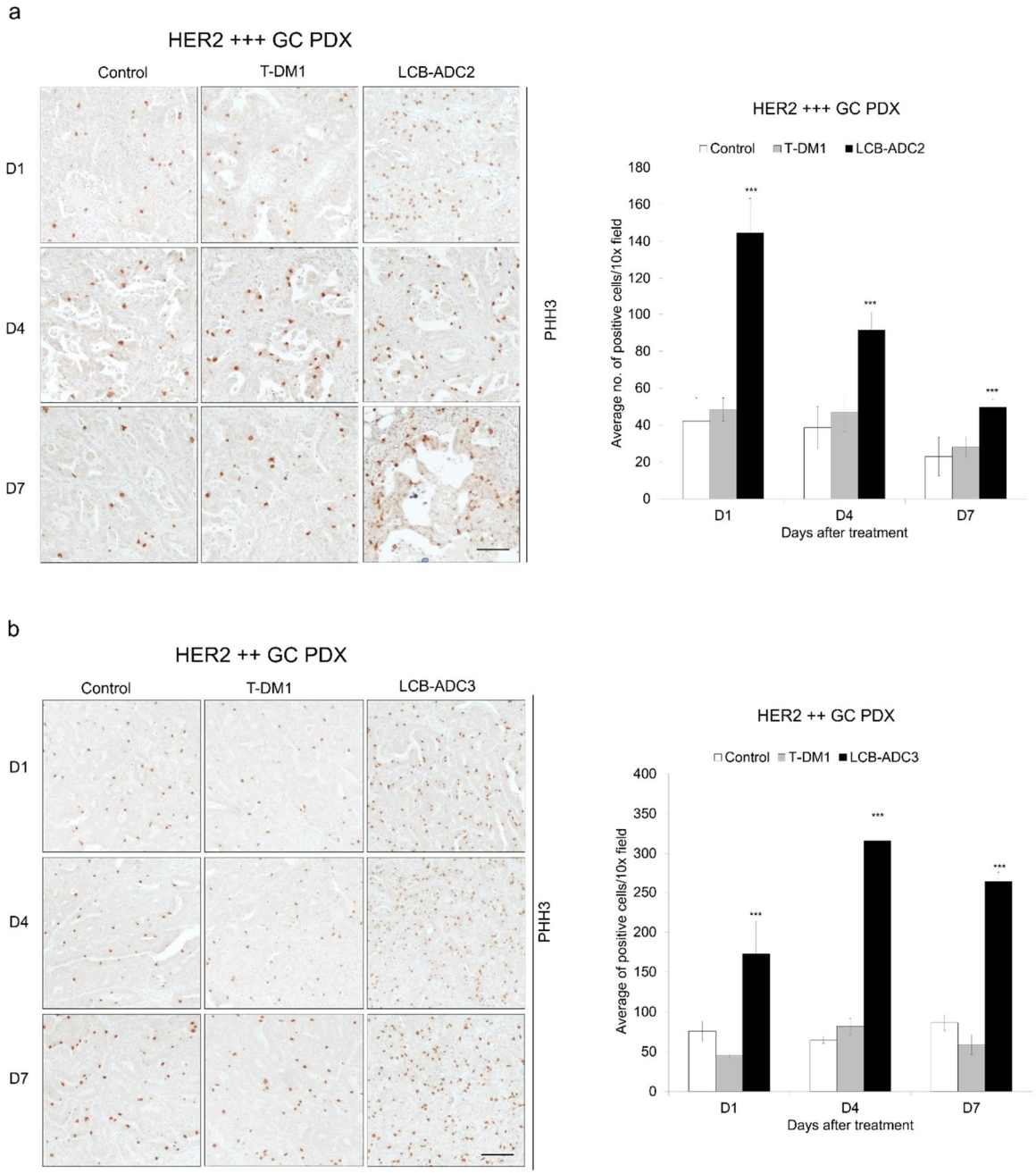

Figure 14. Mitotic arrest of HER2-positive GC PDX tumor tissue

Mice bearing HER2-positive PDX tumors were *i.v.* administered with LCB-ADC2 (a), LCB-ADC3 (b) or T-DM1 at 5 mg/kg once, n=5. After 1, 4, and 7 days, the tumors were isolated, fixed and stained with anti-phosphohistone H3 (PHH3) (blue, hematoxylin-stained nuclei; brown, DAB-stained PHH3, scale bar, 100 μm). Data values are a mean ± standard deviation. ***$p<0.001$ (T-DM1 vs LCB-ADC2 or 3).

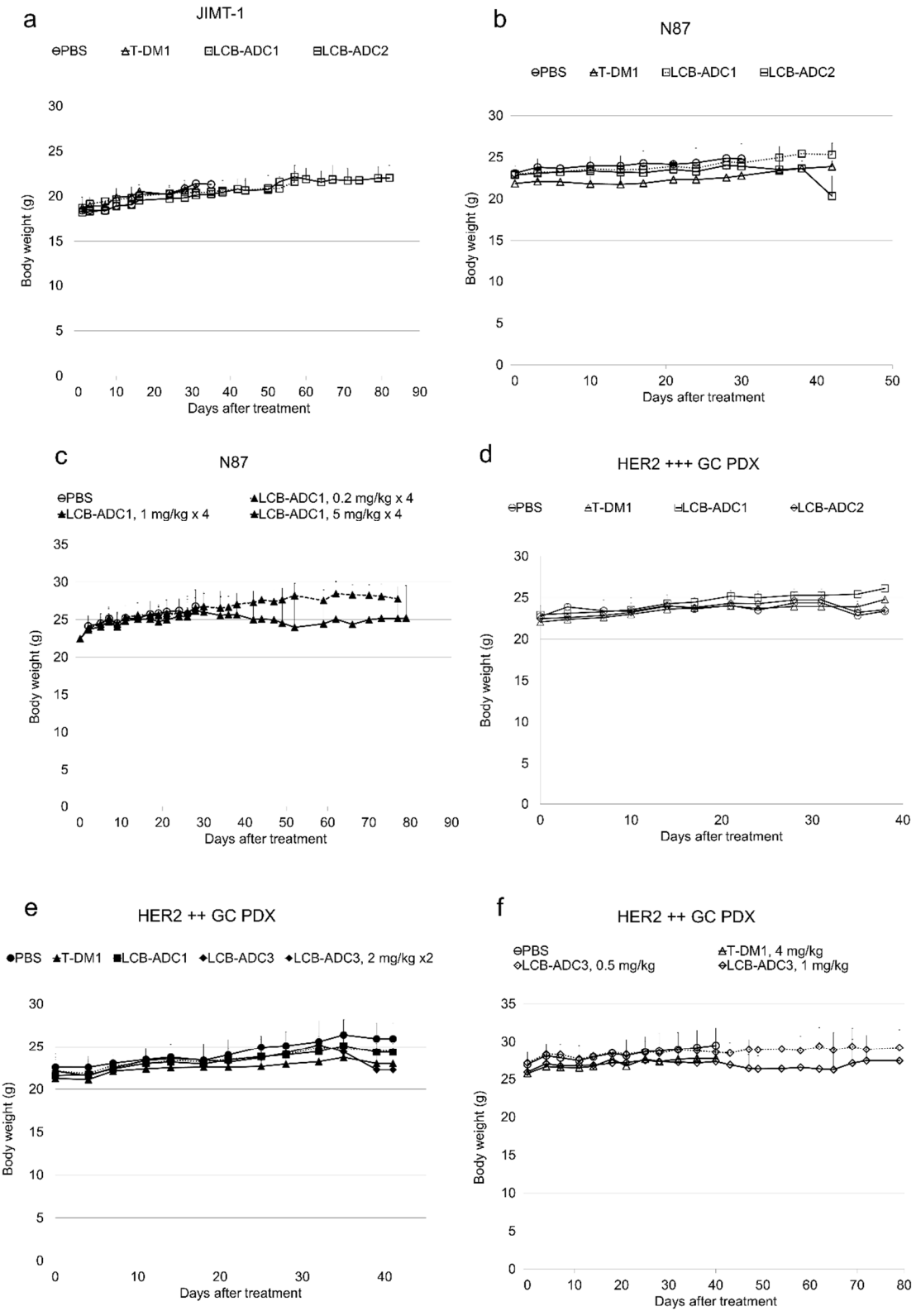

Figure 15. Body weight of mice in the HER2 positive CDX and PDX models corresponding to (a) figure 9a, (b) figure 9b, (c) figure 9d, (d) figure 10a, (e) figure 10b, and (f) figure 12.

PART I-4. Discussion

Recently, researchers have been developing PDX tumor models in variable cancer types because novel drug candidates proved of its efficacy in cancer cell line-based xenograft tumor models have been failed in clinical trials (1, 3, 4). In the present study, HER2+ GC PDX tumor models were established using gastric cancer tissues derived directly from patient and confirmed histological identity between original tumor of patient and PDX tumor tissue. Clinically, HER2+ GC occurs approximately 20%, and patients are diagnosed *via* histological methods (16, 17). The intensity of HER2 overexpression in GCs is typically scored using IHC staining (3+ or 2+) and fluorescence in situ hybridization (FISH) (21). Most HER2-targeting therapies are given to histologically HER2-positive patients (IHC3+ or IHC2+/FISH-positive cases), but HER2 scoring as a diagnostic process in these patients is still controversial (22, 23). The HER2 status guidelines were announced following the results of the Trastuzumab for Gastric Cancer (ToGA trial), which showed that this drug significantly increased the survival time of patients when administered in combination with 5-fluorouracil or capecitabine and cisplatin, and this status has since become an important predictor of treatment outcomes for breast as well as stomach cancer (20, 21). Based on these findings, a combination of trastuzumab with other chemotherapeutics in patients with HER2 positive GC has become the primary standard therapy. Despite the availability of various HER2-targeting agents such as trastuzumab, pertuzumab, lapatinib, and T-DM1, which have been approved for treating patients with HER2-positive tumors worldwide, the trastuzumab monoclonal antibody against the HER2 protein is the only targeted treatment used for patients with HER2-positive GC (21). All the established cases showed growth in athymic mice and maintenance of histological feature was confirmed by homology comparison. HER2 expression was analogous in PDX tumor with original tumors, also morphological feature was remained between generated PDX tumors. Furthermore, HER2-targeting therapy was evaluated in established HER2+ GC PDX model that result in difference of tumor growth inhibition according to HER2 scoring. Especially, HER2+ (IHC 3+) cases were revealed remarkable antitumor effect as low T/C value (Figure 3). In addition, *in vivo* efficacy of novel HER2 antibody, 1A12 was assessed in HER2+ (IHC 3+), and that demonstrated dramatic tumor growth inhibition as CR with PR of 100 % ($p=0.023$, Herceptin vs. Herceptin plus 1A12) (Figure 4 and Table 3). Taken together, results in this research suggest that HER2+ GC PDX could be a personalized tool and could improve preclinical testing for successful clinical trials of novel drug candidate. In order to the exacting obstacle caused by lack of appropriate model for new drug development, PDX models have been generated reflecting the patient's tumor microenvironment

and examined with the conventional treatments and novel drug candidate, demonstrating the potential of PDX models for the development of personalized treatment. I strongly expect that the PDX models should be effectively utilized to predict responsiveness of anti-cancer agents for precision medicine, ultimately leading to improved patient survival rates.

ADCs have been continuously investigated as a significant breakthrough technology for targeted therapeutics against various cancers, with 9 such drugs having current approval for clinical use and more than 40 kinds of ADCs currently in clinical trials (60). The most interesting ADC to emerge has been T-DM1 (Kadcyla) that consists of a HER2 antibody (trastuzumab) conjugated with DM1 that has been approved by the US FDA as a treatment for breast cancer (37). Despite the development of T-DM1 for cancers that are resistant to trastuzumab, many patients treated with this drug ultimately progress to late-stage disease, and some HER2-positive patients have no or a low response (61). In the previous TDM4450g trial, 46% of metastatic breast cancers did not respond to T-DM1.[40] Moreover, T-DM1 was found not to improve the objective response in the EMILIA trial in a second-line setting among patients treated with trastuzumab and taxane, i.e. in 228 (66%) of the 397 subjects (39). Furthermore, the recent GASTBY study has reported that T-DM1 was not superior to taxane in HER2-positive advanced GC patients receiving previous HER2-targeting therapy, in which the median overall survival was 7.9 months with T-DM1 and 8.6 months with taxane (46). Although Enhertu was recently approved by the FDA for treating HER2-positive breast cancers, about 40% of metastatic breast cancer cases showed a low or zero response to this ADC in the phase II DESTINY-Breast01 trial (43). In addition, although Enhertu is comprised of a maleimide tetrapeptide-based cleavable linker and has a higher DAR of ~ 8 (62), it is a less elaborate molecule but similar to T-DM1. In contrast, LCB-ADCs harbor a cleavable linker and have a precise DAR. An expected feature of LCB-ADCs are fewer adverse effects because LCB-ADCs did not show severe weight change, and this technology thus represents a promising new ADC-platform for a variety of targets.

Retrospective analyses of two phase II trials of T-DM1 have indicated that lower response rates were achieved in patients with lower HER2 levels (62, 63), suggesting that the actual HER2 expression level is critical for this drug to work, even in the subset of cancers that are judged to be HER2-positive. The major limitations of T-DM1 are thought to be the inexact DAR control and its non-cleavable linker (37). This prompted us to search for methods that would enhance the linker stability and produce harmonious fabrication (Figure 5). I expected that breast and gastric cancers that would not respond to T-DM1 could be targeted successfully with better next-generation anti-HER2 ADCs and found this to be the case with LCB-ADCs of this research. These novel agents displayed overwhelming efficacy in both *in vitro* and *in vivo* systems, including in the T-DM1-none-responsive breast cancer line JIMT-1, GC line N87, and in gastric PDX models with low HER2 expression (HER2++) (Figure 8, 10, 11, 12 and 13). Substantial

G2/M arrest and rapid cell death was caused in all cases by the effective actions of MMAF, as observed *via* live imaging (data not shown) and histologically increased PHH3 levels (Figure 10 and 14). Of note in particular, complete remission was observed in our xenograft models following LCB-ADC treatments, i.e., the N87, JIMT-1 and HER2++ PDX models that were not responsive to the established ADC, T-DM1.

In contrast with T-DM1, LCB-ADCs contain a cleavable linker that is designed to facilitate a higher efficacy through various mechanisms, including the bystander effect (63), and they were constructed to achieve a consistent DAR of 2 or 4, that is, stable in plasma and thus significantly lengthening the half-life of the drug (Figure 6). I observed that LCB-ADCs had a significantly improved antitumor efficacy in both HER2 overexpressing and low-expressing cases. As another example, lysine-MCC-DM1, which is formed by the proteolytic degradation of T-DM1 in the lysosomes, also cannot cross the cell membrane and T-DM1, and therefore cannot induce a bystander effect (40). Both DM1 and the auristatins are highly cytotoxic payloads and cause cell death by inhibiting tubulin polymerization (63). Antibody-dependent cellular cytotoxicity (ADCC) likely contributes substantially to the efficacy of trastuzumab and T-DM1 *in vivo* (21, 52). The HT-19 antibody component of XMT-1522 may also evoke ADCC (22).

In conclusion, I here describe a novel and highly effective linker-drug technology that can be adopted as a platform technology for a broad range of ADCs and has the potential to greatly enhance their efficacy against a wide range of cancer targets. In this research, LCB-ADCs targeting HER2 show a stronger inhibitory effect against breast and GC cells than T-DM1, including those that are sensitive to T-DM1. In addition, these novel agents show significant efficacy against GC cells with primary or acquired resistance to T-DM1 *in vitro*, and against T-DM1–resistant breast cancer and GC xenografts *in vivo*. A full clinical evaluation of LCB-ADCs in patients with HER2-positive breast or gastric cancer is warranted.

PART II. Mechanistic investigation of antitumor immune responses following combined treatment with radiotherapy and immunotherapy

PART II-1. Introduction

Radiotherapy (RT) is one of the most effective treatments against various types of solid tumors in approximately 50% of the patients suffering from cancer (64). The antitumor effect of RT involves the induction of double-stranded DNA breaks, which leads to tumor cell death *via* apoptosis, necrosis, autophagy, mitotic catastrophe, or replicative senescence (65). Conventionally radiation therapy was used to treat a relatively wide range of patients compared to present RT due to its limitations in the planning and irradiation part of the treatment technology (66), and it also was recognized that it suppressed the immune system of the patients (67). However, due to the recent development of sophisticated IR technologies, such as stereotactic radiosurgery (SRS) and stereotactic body radiotherapy (SBRT), radiation exposure can be minimized in normal tissues (68). Additionally, with the implementation of image-guided radiotherapy (IGRT) and intensity-modulated radiotherapy (IMRT), the need for additional radiation therapy has greatly diminished, which has enabled a reduction in the overall number of complications (69, 70). These therapeutic strategies can reduce the side effects of RT by minimizing radiation exposure on the surrounding healthy tissues by accurately applying it within a few millimeters of the tumor (71, 72). More recently, RT has been shown to have immunological effects, such as immunogenic cell death (ICD), enhanced antigen presentation, and cytotoxic T cell activation (73). Clinical and preclinical studies have reported that the immunological role of RT affects the treatment of distant metastasis. This phenomenon is called the “abscopal effect,” a term first introduced by Mole in 1953 (74, 75). This also suggests that radiation therapy is closely related to the immune responses induced during cancer treatment (76). Despite continuous efforts to increase the anticancer efficacy of RT, it is still significantly limited due to its unavoidable toxicity to normal tissues, and thus is mainly utilized for the treatment of localized tumors. Therefore, a combination of RT with other therapies, such as immune checkpoint blockade (ICB) is proposed to enhance the immune-modulating effect of RT (77, 78).

The immune system in the human body can be classified into innate and adaptive immunity (79). Innate immunity is responsible for primary immunity, and includes cells, such as dendritic cells, macrophages, and natural killer cells, which can be subepithelial or submucosal (80, 81). Adaptive immunity is responsible for secondary immunity. Immunotherapy interventions, such as adoptive T cell transfer (82), dendritic cell vaccines (83), peptide vaccines (84), use of oncolytic viruses (85), cytokine therapies (86), and use of monoclonal antibodies (87) have made remarkable progress in the field of oncology. Among them, preclinical and clinical studies on ICB are being conducted most actively, as it

represents one of the breakthrough treatments in clinical oncology. Recently, US Food and Drug Administration (FDA) has approved various immune checkpoint inhibitors (ICIs) for the treatment of metastatic malignant melanoma, and lung, head, and neck cancer. Programmed death 1 (PD-1) and programmed death ligand 1 (PD-L1) play key roles in the immunosuppressive pathway in the tumor microenvironment by inducing T cell exhaustion. Therefore, the PD-1/PD-L1 axis has been characterized as a promising inhibitory target for immune activation through the modulation of effector T cell function (88, 89). Recently, the therapeutic interaction between effector T cells and radiation therapy has been shown to affect the effect of ICB. (82). Despite the emerging success of ICB, its response rate is still low because of poor immunogenicity, e.g., only lymphocyte-excluded cold tumors are susceptible to ICB action as opposed to lymphocyte-infiltrated hot tumors (90, 91). The low response rate of ICB therapy can be overcome by combining it with other immunotherapies, such as anti-cytotoxic T-lymphocyte-associated protein 4 (CTLA4) therapy, or RT (92, 93). Although the combination of immunotherapy and traditional therapies, such as RT or chemotherapy have shown exciting results in clinical and basic research, patients eventually suffer from relapse and durable responses are rare. Moreover, the mechanisms underlying the effects of such a combination therapy are still poorly understood.

Hence, in this study, I investigated immune modulation, including that of lymphocyte-infiltrated hot tumors, activation of T cells, and the local upregulation of the PD-L1/PD-1 axis following IR therapy to potentially determine a strategy to improve therapeutic outcomes and enhance the abscopal effect of the combined radiotherapy–immunotherapy.

PART II-2. Materials and Methods

Cell culture. Murine colon adenocarcinoma MC-38 cells (Kerafast no. ENH204-FP, Boston, MA) were maintained in DMEM medium (Gibco-Invitrogen, Carlsbad, CA). Murine colorectal carcinoma cells (ATCC no. CRL-2638, Manassas, VA) were maintained in RPMI-1640 medium (Gibco-Invitrogen, Carlsbad, CA). Murine melanoma B16-F10 cells (ATCC no. CRL-6475, Manassas, VA) were maintained in DMEM medium (Gibco-Invitrogen, Carlsbad, CA). Murine Lewis Lung Carcinoma LLC1 cells (ATCC no. CRL-1642, Manassas, VA) were maintained in DMEM medium (Gibco-Invitrogen, Carlsbad, CA).

***In vivo* tumor growth delay.** MC-38 and B16-F10 cells were implanted subcutaneously (*s.c.*) to right or both hind leg of C57BL/6J mice (male, six-weeks-old, Japan SLC, Hamamatsu, Japan). CT-26 cells were implanted subcutaneously (*s.c.*) to right or both hind leg of BALB/c mice (male, six-weeks-old, Japan SLC, Hamamatsu, Japan). B16-F10 cells were implanted subcutaneously (*s.c.*) to right hind leg of C57BL/6J mice (male, six-weeks-old, Japan SLC, Hamamatsu, Japan). LLC1 cells were implanted subcutaneously (*s.c.*) to right hind leg of BALB/c mice (male, six-weeks-old, Japan SLC, Hamamatsu, Japan). The mice bearing xenograft tumors grown to 80 to 120 mm^3 were pair matched according to the tumor volume into the experimental and control groups (n = 3-6/group). anti–PD-L1 (clone 10F.9G2; Bio-XCell) was intraperitoneal (*i.p.*) administrated to mice, and dose was a single 5 or 10 mg/kg after irradiated single 5-25 Gy. The doses of all drugs were adjusted to the equivalent amount of the antibody. The tumor volumes were calculated using the formula volume = (length × $width^2$) × 0.5. The results are expressed as a mean ± standard deviation.

Flow cytometry. Flow cytometry analysis was performed on freshly isolated blood and single cells from tumors. Mice were anesthetized and blood was collected *via* cardiac puncture in K_2EDTA tube. Tumors were excised and collected in ice-cold DMEM media with 10% FBS. Single-cell suspensions of these organs were obtained using a gentleMACS dissociator (Miltenyi Biotec B.V.) and filtered through a 70 μm pore cell strainer. Then, 3×10^6 cells were transferred to a round-bottom tube where staining was performed while kept on ice. Cells were stained with LIVE/DEAD Fixable Aqua Dead Cell Stain kit (L/D Aqua, Life Technologies) according to manufacturer's instructions, washed with staining buffer (PBS, 2% FBS and 2 mM EDTA), incubated with anti-CD16/32 (2.4G2, BD Biosciences) to block Fc receptors (FcRs) and stained with the following surface marker antibodies for flow cytometry analysis: anti-CD45-BV510 (clone 30-F11), anti-CD3-FITC (145-2C11), anti-CD4-PerCP-

Cy™5.5 (RM4-5), anti-CD8-BV421 (53–6.7), anti-CD44-BV785 (IM7), anti-CD62L-APC-Cy™7 (MEL-14) (all from Biolegend). Fluorescence compensation was defined using single stained cells. Data were acquired using 13-color panels with a CytoFLEX (Beckman Coulter). Data were analyzed with FlowJo V.10.8.0 software.

Nanostring. The Nanostring (NanoString Technologies, Inc., Seattle, WA, USA) procedure was performed to target 561 different Mouse Immunology panel (XT-CSO-MIM1-12, nCounter Mouse Immunology kit V1CSO). Briefly, 250-1500 ng of ribonucleic acid (RNA) was hybridized to the capture probe set at 65 °C for 16–24 h using a thermocycler. Samples were inserted into the nCounter Prep Station to remove excess probes, purify, and immobilize the sample on the internal surface of a sample cartridge for 3 h. Finally, the sample cartridge was transferred to the nCounter Digital Analyzer, where color codes were counted and tabulated for each target molecule. The data counted by the digital analyzer is read as a Reporter Code Count (RCC) file. RCC file contains not only positive and negative counts but also in other words, it is data that counts the number of genes corresponding to a code set. The expression number for the base sequence of the probe part was analyzed using nSolver Analysis Software.

Statistical analysis. Sample sizes were not predetermined. All data are presented as a mean ± SD (standard deviation) from at least three separate experiments. Means were compared using a one-way ANOVA test. P values were obtained by Microsoft Excel 365. P values are represented as *$P < 0.05$, **$P < 0.01$ or ***$P < 0.001$, which are considered to indicate significant differences.

PART II-3. Results

1. Combination therapy with IR and ICB enhanced tumor growth inhibition.

In various syngeneic models, the tumor growth inhibition efficacy of IR and ICIs was assessed in four allograft mouse models (Figure 16). The percentages of tumor growth inhibition (TGI) observed after combination therapy were 101.6%, 102.1%, 22.4%, and 92.4% in MC-38 model mice on day 17 (Figure 16a), CT-26 mice on day 12 (Figure 16b), the LLC1 model on day 13 (Figure 16c), and the B16-F10 model on day 7 (Figure 16d), respectively. The MC- 38 and CT-26 mice showed the most remarkable antitumor effect after undergoing combination therapy. The TGI observed after ICB therapy alone was 66.6%, 5.4%, 6.6%, and 8.7% in the MC-38 model on day 17, the B16-F10 model on day 7, the CT-26 model on day 12, and the LLC1 model on day 13, respectively. The MC-38 model showed the highest response to the ICB, and the B16-F10 and LLC-1 models showed similar growth compared to that observed in the isotype-treated group. Moreover, in the MC-38 model, the highest inhibition was observed when the tumor size was greatly reduced. These results demonstrated that combination therapy could enhance the anti-tumor effect in different syngeneic models.

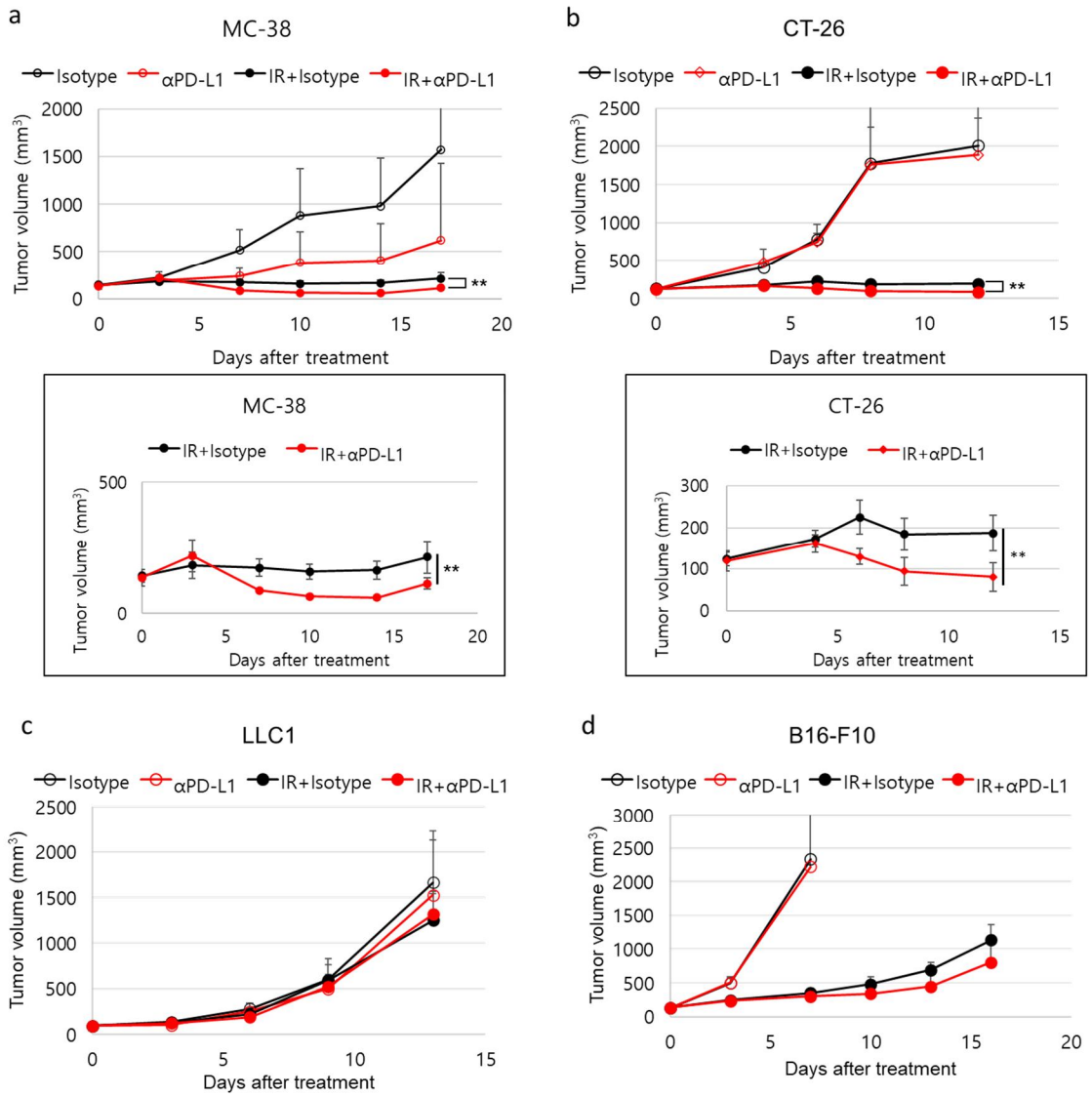

Figure 16. *In vivo* tumor growth inhibition efficacy by combination therapy in syngeneic models

Tumor growth delay curve in MC-38, CT-26, LLC1 and B16-F10. Mice bearing MC-38 tumor were *i.p.* administrated with anti-PD-L1 at a concentration of 5 mg/kg after irradiated with 5 Gy (a, n=5). Data values are the mean ± standard deviation. **p<0.01 (IR+Isotype vs IR+anti-PD-L1). Mice bearing CT-26 tumor were *i.p.* administrated with anti-PD-L1 at a concentration of 5 mg/kg after irradiated with 20 Gy (b, n=5). Data values are the mean ± standard deviation. **p<0.01 (IR+Isotype vs IR+anti-PD-L1). Mice bearing LLC1 tumor were *i.p.* administrated with anti-PD-L1 at a concentration of 5 mg/kg after irradiated with 5 Gy (c, n=5). Mice bearing B16-F10 tumor were *i.p.* administrated with anti-PD-L1 at a concentration of 5 mg/kg after irradiated with 12 Gy (d, n=5). Data are represented as mean ± standard deviation. Means were compared using a one-way ANOVA test. P values were obtained by Microsoft Excel 365.

2. Combination therapy with IR and ICB can induce memory immune response.

To confirm the enhancement of the anticancer efficacy by combination therapy and whether it accompanies an immune response, a tumor re-challenge experiment was performed in the MC-38 model. As shown in Figure 17, TGI was the highest at 107% after treatment with IR and anti-PD-L1. These tumors were harvested and complete remission (CR) was observed in the primary tumors of three mice (Figure 17d). To evaluate the induction of memory immune responses in the mice following combination therapy, cells from the MC-38 model were re-implanted into the contralateral hind leg of the primary tumor, which was not transplanted with a tumor. The results of this re-challenge experiment showed no growth of the re-implanted tumors in cells treated with IR and anti-PD-L1; thus, indicating CR (Figure 17b). Moreover, considerable changes in body weight were not observed, indicating that no mice suffered from severe toxicity (Figure 17c). These results suggest that combination therapy could enhance the anticancer effect of RT and induce memory immune responses.

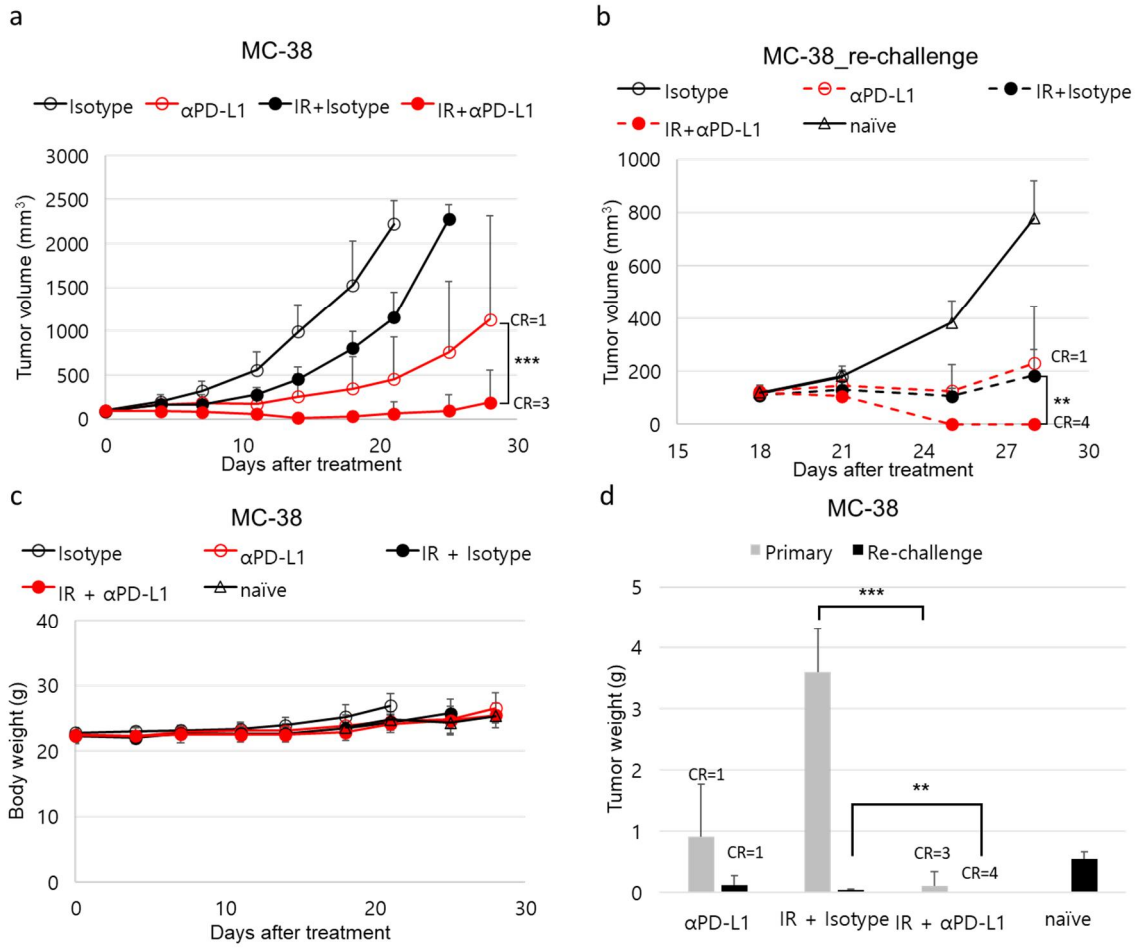

Figure 17. *In vivo* re-challenge experiment of combination therapy in MC-38 syngeneic model

Tumor growth delay curve, re-challenge tumor growth curve and body weight in MC-38. Mice bearing MC-38 tumor were *i.p.* administrated with anti-PD-L1 at a concentration of 5 mg/kg after irradiated with 5 Gy (a, n=5). Data values are the mean ± standard deviation. ***p<0.001 (anti-PD-L1 vs IR+anti-PD-L1). Re-implantation of MC-38 cells was *s.c.* injected on contralateral hind leg at day 18 (b, n=5). Data values are the mean ± standard deviation. **p<0.01 (IR+Isotype vs IR+anti-PD-L1). Change in body weight of mice (c). After mice were sacrificed and tumor weight was measured at the end point (d). Data are represented as mean ± standard deviation. **p<0.01 (IR+Isotype vs IR+anti-PD-L1 in re-challenged tumors). ***p<0.01 (IR+Isotype vs IR+anti-PD-L1 in primary tumors).

3. Combination therapy with high dose-IR and ICB can induce the abscopal effect of RT.

According to previous experiments, systemic immunity is involved in combination therapy as is evident from the results of the re-challenge experiment undertaken using the MC-38 model, and it was expected that this could induce an abscopal effect. The effect could not be observed under an identical regimen in the re-challenge experiment carried out with an MC-38 model implanted with tumor cells into both hind legs. Therefore, the process was changed by increasing the radiation and anti-PD-L1 dose. Consequently, following a combination therapy with high-dose IR (25 Gy) and anti-PD-L1, tumor growth was found to be inhibited—and the survival rate had increased—not only in the irradiated primary tumor (right) (Figure 18a), but also in the contralateral secondary tumor (left), which was never irradiated (Figure 18b). Moreover, the combination therapy with high-dose IR and ICB showed in strong therapeutic efficacy whereby all primary tumor-harboring mice and 2 out of 5 secondary tumor-harboring mice became tumor-free (Figure 18e and f), resulting in a greatly enhanced survival rate (Figure 18d). Considerable changes in body weight were not observed in this experiment (Figure 18c). These results clearly demonstrated that the combination therapy with high-dose IR and anti-PD-L1 could induce an abscopal effect.

a

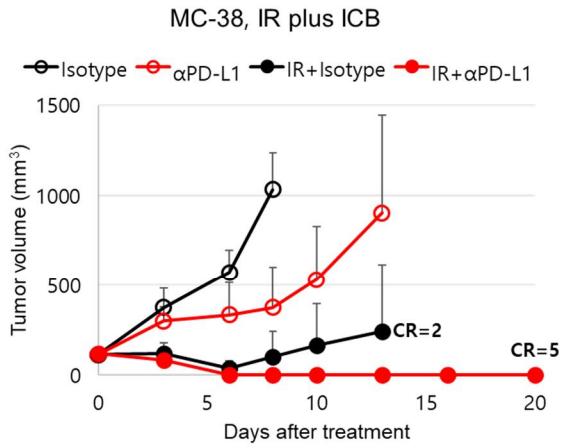
MC-38, IR plus ICB
Isotype
αPD-L1
IR+Isotype
IR+αPD-L1
Tumor volume (mm3)
1500
1000
500
0
CR=2
CR=5
0
5
10
15
20
Days after treatment

b

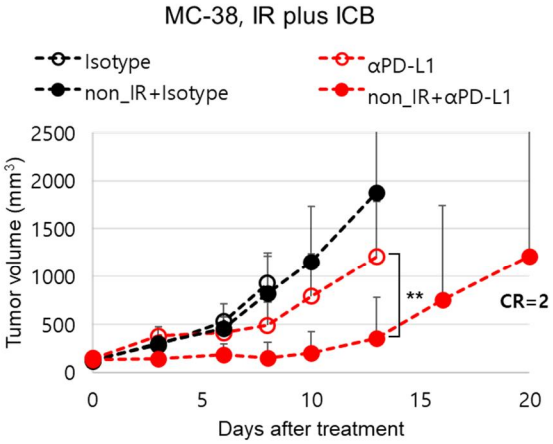
MC-38, IR plus ICB
Isotype
αPD-L1
non_IR+Isotype
non_IR+αPD-L1
Tumor volume (mm3)
2500
2000
1500
1000
500
0
**
CR=2
0
5
10
15
20
Days after treatment

c

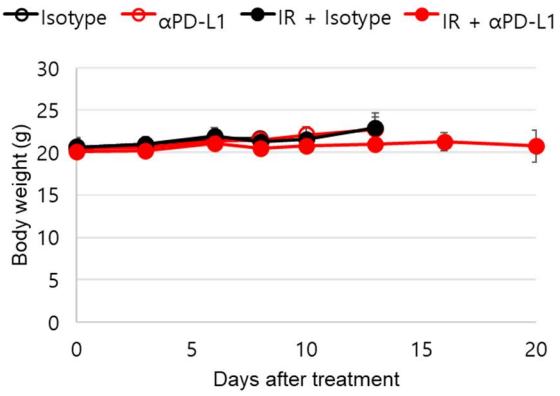
MC-38, IR plus ICB
Isotype
αPD-L1
IR + Isotype
IR + αPD-L1
Body weight (g)
30
25
20
15
10
5
0
0
5
10
15
20
Days after treatment

d

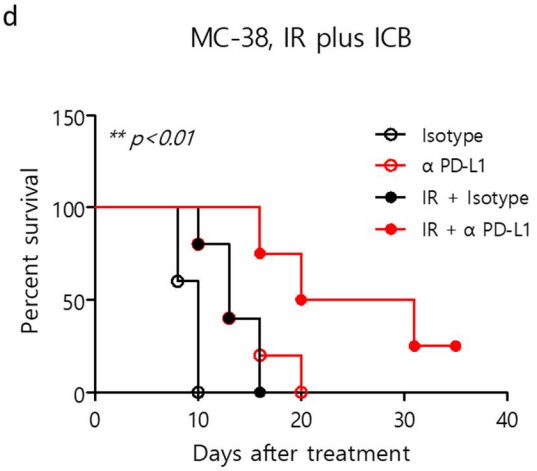
MC-38, IR plus ICB
** p<0.01
Isotype
α PD-L1
IR + Isotype
IR + α PD-L1
Percent survival
150
100
50
0
0
10
20
30
40
Days after treatment

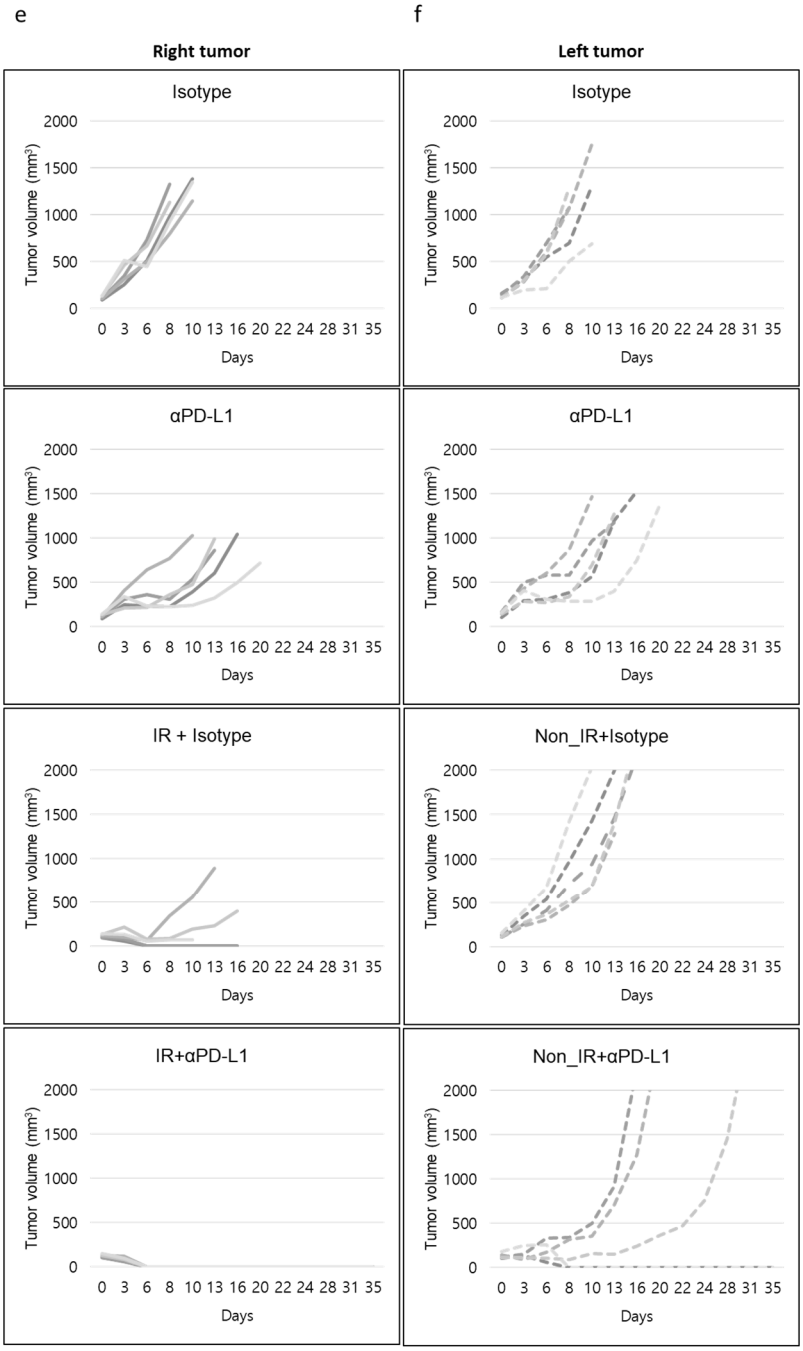

Figure 18. Induction of abscopal effect by combination therapy in MC-38 syngeneic model

Primary (a) or secondary (b) tumor growth delay curve, body weight and survival curve in MC-38. Mice bearing MC-38 tumor were *i.p.* administrated with anti-PD-L1 at a concentration of 10 mg/kg after irradiated with 25 Gy (a, n=5). Data are represented as mean ± standard deviation. **p<0.01 (anti-PD-L1 vs IR+anti-PD-L1 in secondary tumors). Change in body weight of mice (c). survival rate curve (d), **p<0.01. Individual tumor growth curve each mouse in primary tumor (right tumor, e) and secondary tumor (left tumor, f). Data are represented as mean ± standard deviation.

4. Combination therapy with IR and ICB recruits tumor-infiltrating lymphocytes (TILs) and affects the systemic immune response.

In vivo studies, combination therapy was found to improve the anticancer efficacy and the abscopal effect of RT, which is presumed to be associated with the immune response. To assess the distribution of immune cells expected to be involved in the underlying mechanism of this effect, TILs and peripheral blood mononuclear cells (PBMC) of MC-38 model mice were analyzed. Among the TILs, the cytotoxic T cells (CD8+ cells) showed an increase in number in the combination therapy group compared with its number in the IR group on day 7, and this increase then initiated TGI (Figure 19b). Among the PBMCs, the number of effector memory T cells (TEM, CD8+CD44+CD62L-) was also significantly increased in the combination therapy group compared to that in the IR group (Figure 20b). Thus, it could be concluded that CD8+ T cells are involved in inducing the abscopal effect. Further, it is noteworthy that memory T cells play an important role in the systemic immune response induced after RT.

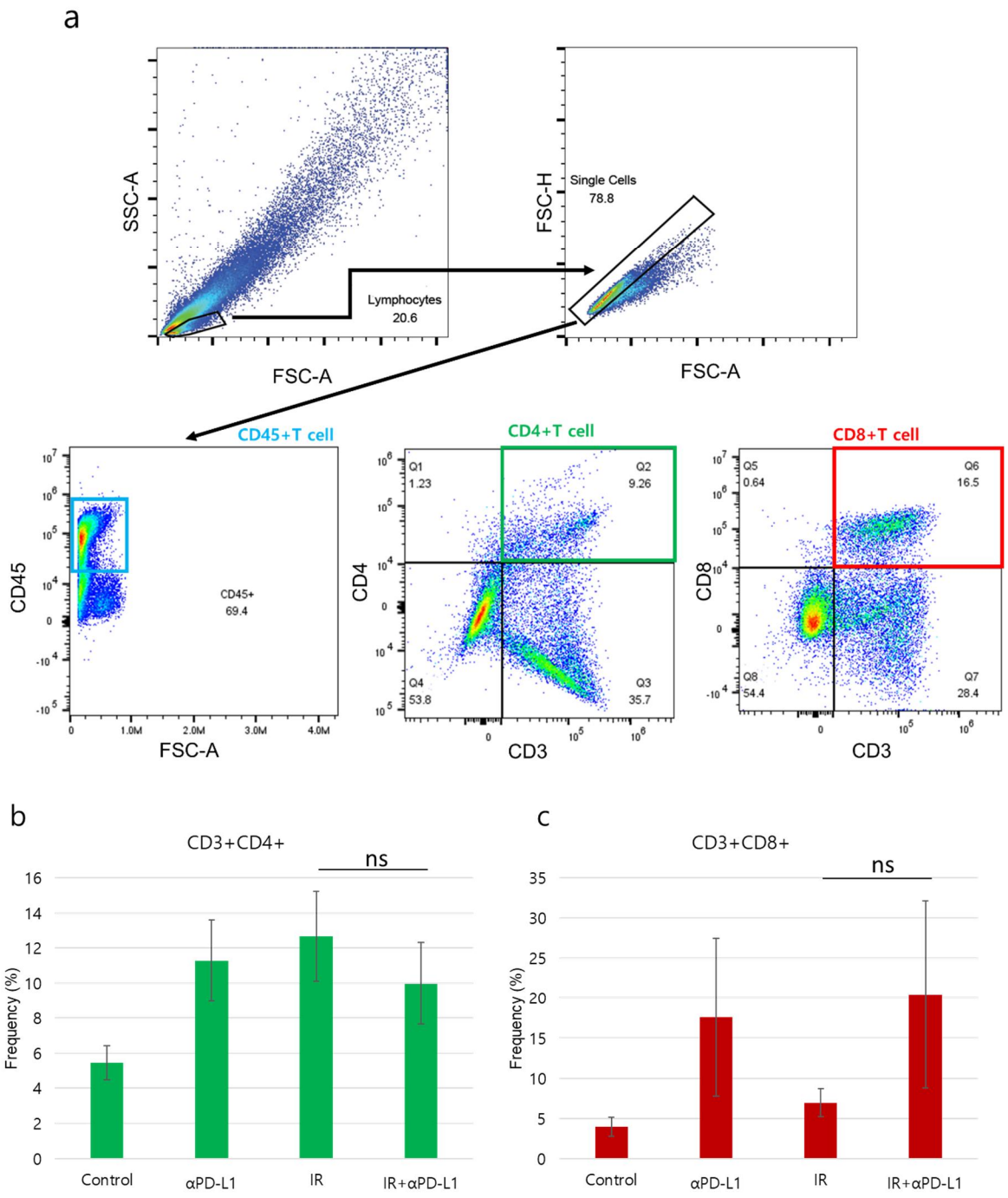

Figure 19. Increase of CD8+ T cells in tumor-infiltrating lymphocyte after radiation plus ICB

The Flow cytometric gating strategy to analyze lymphocyte subsets in tumor-infiltrating lymphocyte (a). Frequency of CD3+CD4+ T cells analyzed by flow cytometry after treatment of irradiation plus ICB on day 7 (n=3) (b). Frequency of CD3+CD8+ T cells analyzed by flow cytometry after treatment of irradiation plus ICB on day 7 (n=3) (c). Data are represented as mean ± standard deviation.

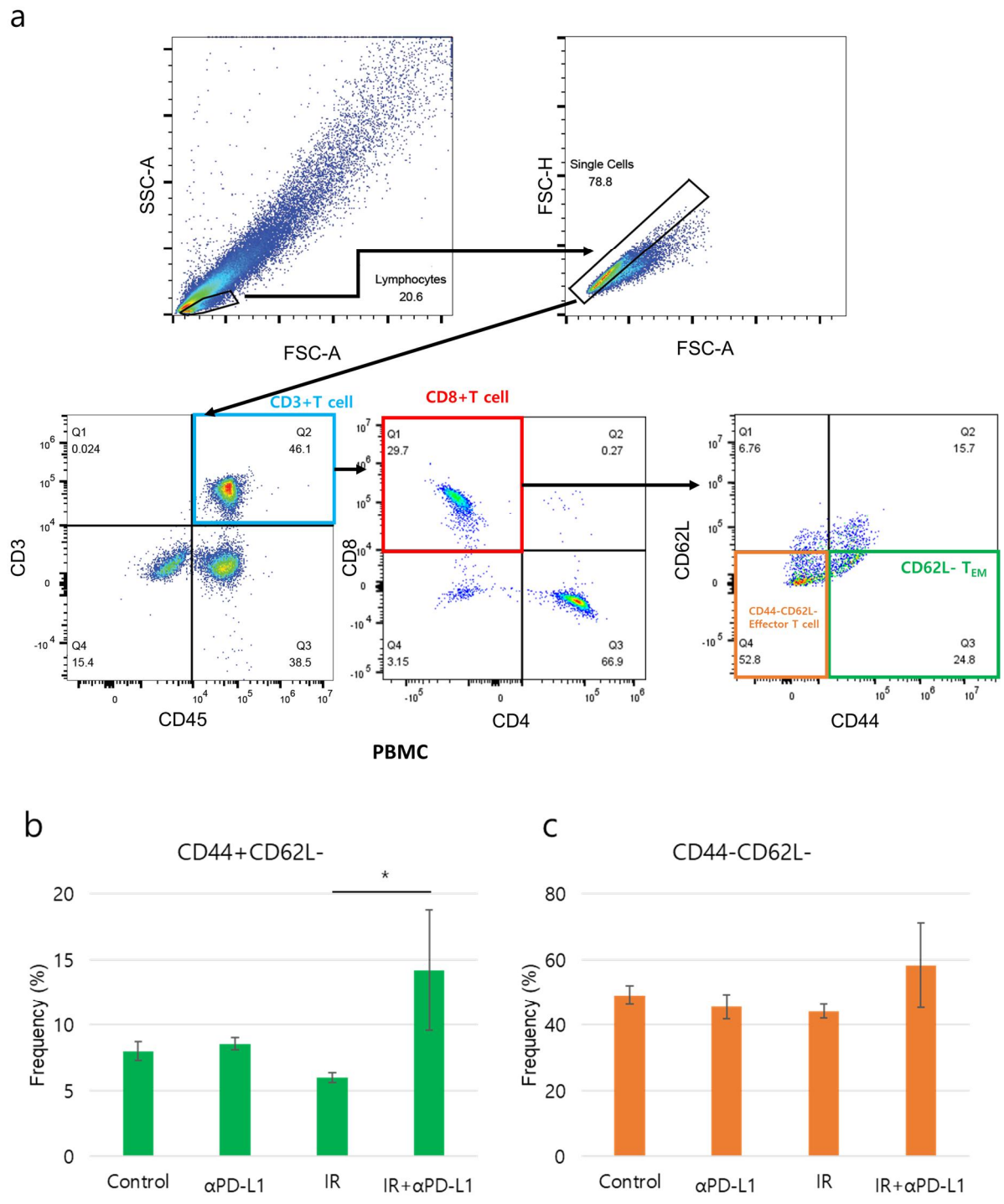

Figure 20. Increase of effector memory T cells (T_{EM}) in PBMC after irradiation plus ICB

The Flow cytometric gating strategy to analyze lymphocyte subsets in PBMC (a). Frequency of effector memory T cells analyzed by flow cytometry after radiation plus ICB on day 7 (b). Frequency of effector T cells analyzed by flow cytometry after radiation plus ICB on day 7 (c). Data are represented as mean ± standard deviation. *$p<0.05$ (IR+Isotype vs IR+anti-PD-L1).

5. Analysis of gene expression related to the immune mechanisms involved in the abscopal effect of RT

The NanoString nCounter Analysis System was used to screen genes involved in the abscopal effect of combination therapy. A target gene is detected using a probe written specifically for it, and the oligo end of each probe was labeled in a barcode format for 4 types of fluorescence, and each barcode was synthesized to generate a specific signal. A total of 561 genes were compared, and it was confirmed that the expression of 267 genes in the irradiated tumors and 91 genes in the non-irradiated tumors of combination therapy group differed by more than 2-fold compared to that of those in the control, irradiation, and anti-PD-L1 groups. A total of 4 genes in the irradiated tumors and 15 genes in non-irradiated tumors showed overlapping expression between the monotherapy and combination therapy (G1;Isotype vs. G4;IR+anti-PD-L1, G2;anti-PD-L1 vs. G4;IR+anti-PD-L1, G3;IR vs. G4;IR+anti-PD-L1) groups, and each comparison was confirmed as shown in Figure 23. The top 20 mRNA hits in IR or non-IR tumors treated with combination therapy that showed the highest fold change and significance are shown in Tables 6 and 7. *Cd74*, *Cul9*, and *H2-Ab1* were the three most affected genes in the irradiated tumors of G4 compared with those of G3, whereas *Il7r*, *Sh2d1a*, and *Bst1* were the three most expressed genes in the non-irradiated tumors of G4 compared with those of G3. Additionally, lots of genes in top 20 of all compare were involved lymphocyte activation. In Figure 22, Venn diagrams show the number of genes and their intersection at the level of RNA expression. In the diagram for G4 vs. G1 and G4 vs. G2, 11 common genes were found to be upregulated in the right tumor (IR) sets. However, only 4 common genes between G4 vs. G1 and G4 vs. G2 were downregulated in the right tumor. There was only 1 common gene between G4 vs. G1 and G4 vs. G3 in the list of the upregulated genes in the right tumor, whereas the intersections with G4 vs. G3 and other groups in the set of downregulated genes in the right tumor did not yield any common genes. In the upregulated gene list of the left tumor (non-irradiated) for G4 vs. G1, G4 vs. G2, and G4 vs. G3, only 1 gene was found to be common, whereas 19 genes were commonly expressed between G4 vs. G1 and G4 vs. G3.

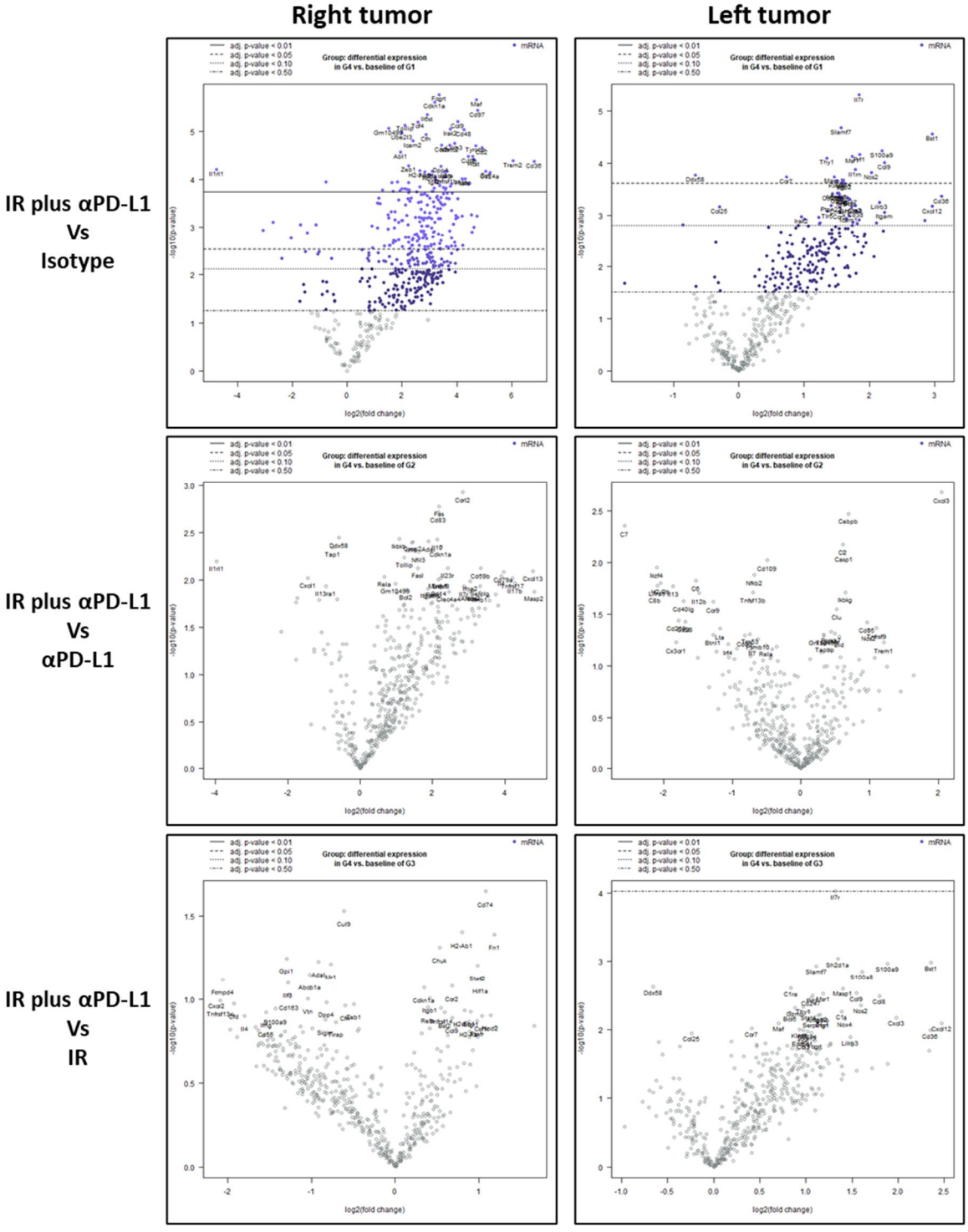

Figure 21. Change of mRNA expression in abscopal effect models

Differential expression genes (DEGs) volcano plot of each comparison between groups on nCounter Mouse Immunology genes panel (n=3). Right tumor was irradiated tumors, and left tumor was non-irradiated tumors.

Table 6. The list of top 20 in differential expression genes (DEGs) of irradiated tumor

IR					
G4 vs. G1	Log2 fold change	**G4 vs. G2**	Log2 fold change	**G4 vs. G3**	Log2 fold change
Fcgrt	3.36	Ccrl2	2.84	Cd74	1.08
Maf	4.71	Fas	2.19	Cul9	-0.612
Cdkn1a	3.19	Cd83	2.16	H2-Ab1	0.799
Cd97	4.76	Ddx58	-0.577	Fn1	1.19
Il6st	2.92	Ikbkb	1.09	Chuk	0.531
Ccl9	4.04	Il10	2.13	Gpi1	-1.3
Tcf4	2.58	Adal	1.9	Adal	-0.92
Tollip	2.11	Casp2	1.46	Mr1	-0.768
Gm10499	1.52	Il15	1.42	Stat2	0.985
Irak2	3.75	Cdkn1a	2.24	Abcb1a	-1.02
Cd48	4.25	Tap1	-0.753	Hif1a	1.02
Ube2l3	2	Nfil3	1.62	Frmpd4	-2.06
Cfh	2.88	Tollip	1.22	Ilf3	-1.28
Icam2	2.39	Il1rl1	-3.98	Ccr2	0.682
Lilrb3	3.91	Il23r	2.43	Cdkn1a	0.349
Ccr2	3.44	Fasl	1.6	Cxcr2	-2.14
Nfatc2	3.73	Cd59b	3.33	Cd163	-1.27
Tyrobp	4.69	Cxcl13	4.78	Itgb1	0.414
Cd2	4.91	Cd79a	3.97	Vtn	-1.04
Abl1	1.95	Il4	3.91	Tnfrsf13c	-2.09

Table 7. The list of top 20 in differential expression genes (DEGs) of non-irradiated tumor

Non-IR					
G4 vs. G1	Log2 fold change	**G4 vs. G2**	Log2 fold change	**G4 vs. G3**	Log2 fold change
Il7r	1.84	Cxcl3	2.04	Il7r	1.32
Slamf7	1.57	Cebpb	0.689	Sh2d1a	1.35
Bst1	2.96	C7	-2.57	Bst1	2.36
S100a9	2.19	C2	0.611	S100a9	1.89
Prf1	1.85	Casp1	0.626	Slamf7	1.11
Msr1	1.74	Cd109	-0.491	S100a8	1.61
Thy1	1.35	Ikzf4	-2.1	Ddx58	-0.659
Ccl9	2.23	Nfkb2	-0.685	C1ra	0.837
Il1rn	1.78	C6	-1.53	Masp1	1.4
Nos2	2.03	H2-Ob	-2.04	Ccl9	1.55
Ddx58	-0.66	Lilra5	-2.09	Msr1	1.19
Masp1	1.46	Il13	-1.86	Prf1	1.07
Ccr7	0.735	C8b	-2.12	Ccl8	1.8
Stat4	1.6	Ikbkg	0.646	Cd247	1.06
Klrd1	1.5	Tnfsf13b	-0.7	Nos2	1.6
Irf8	1.58	Il12b	-1.48	Thy1	0.97
Itgb2	1.61	Cd40lg	-1.71	Gzmb	0.885
Fcgr1	1.53	Ccr9	-1.28	C1s	1.39
Arhgdib	1.51	Clu	0.521	Stat4	1.03
Cd274	1.43	Cd209g	-1.78	Bcl6	0.832

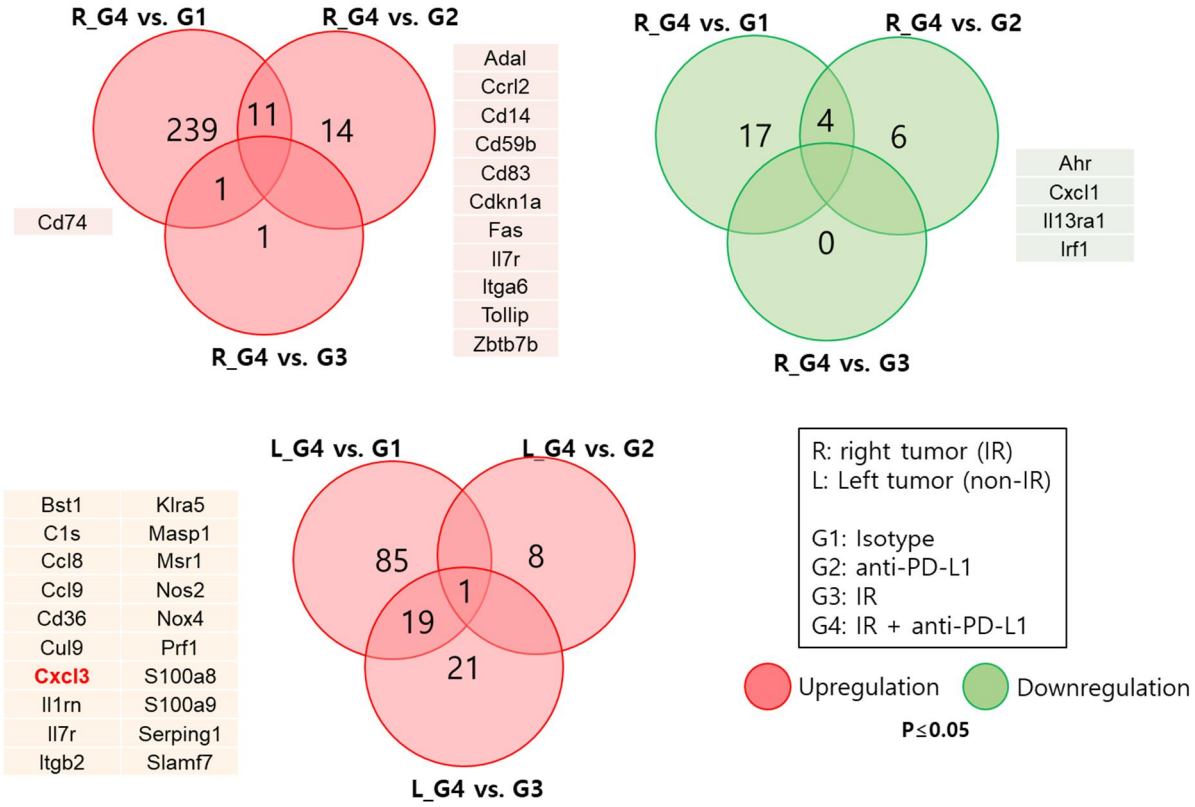

Figure 22. Venn diagram showing the number of up-regulated (red) or down-regulated (green) genes that overlapped of DEGs in the four groups (G1; Isotype, G2; anti-PD-L1, G3; IR, G4; IR+anti-PD-L1) by NanoString.

PART II-4. Discussions

RT is one of the cornerstone treatment modalities used across a spectrum of tumor types. It is also the most used cancer treatment strategy, with approximately 50% of the patients with solid tumors receiving curative or palliative irradiation as part of their treatment (94). RT induces single- and double-stranded DNA breaks, which leads to apoptosis (95). In addition, it affects various processes in the tumor microenvironment (TME) (96, 97), including vascular depletion (98, 99), endothelial cell death, stromal fibrosis (100), degree of oxygenation (101) and the immune function (102, 103). With respect to its effect on the immune function, RT enhances innate and adaptive antitumor immunity and modulates several components of the immune response through various processes, such as i) the exposure of neo-antigen (104); ii) promotion of secreted proinflammatory cytokines, such as IL1 and IL6 (105, 106); iii) enhanced expression of damage-associated molecular patterns, including calreticulin, high mobility group box 1 (HMGB1), and ATP (107); iv) increased expression of MHC-I on tumor cells (108); v) activation of the stimulator of interferon genes (STING) pathway leading to type-I interferon (IFN) secretion (109, 110). Type-I IFNs can induce PD-L1 expression, which has been proposed to limit local immunity and promote tumor relapse (102, 110). PD-L1 expression in the tumor microenvironment provides an opportunity for therapeutic intervention using regulators, such as anti-PD-L1 and anti-PD-1. In clinical trials, PD-L1 or PD-1 antibodies can elicit favorable responses in approximately 25% of the patients depending on the tumor type. Moreover, the presence of PD-L1 is a prognostic biomarker for predicting treatment success (111, 112).

Immunotherapy has emerged as a promising cancer treatment strategy, which directly stimulates the immune system to induce immune cells and attack cancer cells, unlike conventional anticancer drugs that target the tumor alone (113). Immune anticancer therapy is classified into immune checkpoint inhibitor therapy (114), immune cell therapy (115), anticancer vaccines (116), and immune virus therapeutics (117). Cancer cells have different properties compared to those of normal cells, with the differing constituents being known as tumor-specific antigens. Immune cells, such as T cells specifically detect these antigens and initiate the targeted removal of cancer cells (118). However, when the balance between the proliferating cancer cells and the counter-acting immune system is disrupted, cancer cells begin to show an increase in proliferation. In this process, cancer cells evade detection by the immune system to avoid the attack by T cells (immune evasion) (119). This is called an immune checkpoint (checkpoint), which is regulated by immune checkpoint receptors, such as PD-1, PD-L1, and CTLA-4. Immune checkpoint inhibitors prevent the binding of PD-L1 and PD-1, thereby maintaining the immune function of T cells (120). There are 3 immune checkpoint inhibitors that neutralize PD-1: Keytruda

(pembrolizumab) (121), Opdivo (nivolizumab) (122) and Libtayo (cemiplimab) (123). Immune checkpoint inhibitors that neutralize PD-L1 and restore the antitumor activity of T cells include Tecentriq (atezolizumab) (124), Imfinzi (duvalumab) (125) and Bavencio (avelumab) (126). Yervoy (ipilimumab) is another immune checkpoint inhibitor which inhibits the immune evasion capacity of cancer cells by targeting CTLA-4 (127). Despite the conceivable advantages associated with immunotherapy using checkpoint inhibitors, there are demerits of using them for cancer treatment (128). To overcome some of these inherent limitations of this type of immunotherapy, several research studies are currently investigating how combination therapies with checkpoint inhibitors and other forms of antineoplastic treatment may benefit patients for the years to come (129-131).

Here, I investigated the anticancer efficacy of a combination therapy using irradiation and anti-PD-L1 in various syngeneic models (MC-38, CT-26, LLC1, B16-F10; Figure 16). The MC-38 and CT-26 models showed a synergistic effect displaying complete response (CR) by combination therapy compared with the observations in the groups receiving individual treatment. Moreover, MC-38 cells did not grow after the re-challenge implantation in CR mice of the MC-38 syngeneic model that were subjected to combination therapy (Figure 17). Furthermore, I observed an increased frequency of CD8+ T cells in the TIL population of MC-38 tumors on day 7 following the combination treatment (Figure. 19). In addition, the high-dose irradiation (25 Gy) plus anti-PD-L1 combination treatment induced an abscopal effect in the MC-38 syngeneic model, which showed CR in both the primary tumor (irradiated) and the secondary tumor (non-irradiated) (Figure 18). Combination therapy showed an increase in the frequency of effector memory T cells (TEM) among the PBMCs on day 7 (Figure 20). Based on these results, I confirmed that the irradiation and anti-PD-L1 combination treatment resulted in an enhancement of the anti-tumor immune response and the anticancer effect. Among the various immune cell populations, the CD8+ T cells that were recruited to the tumors were the cells primarily involved in executing this anticancer effect. This effect also alerted the systemic immune response; memory T cells were found to play an important role in the activation of the systemic immunity and thereby, in inducing the abscopal effect.

In conclusion, the RT and ICB therapy used in combination show a synergistic action, resulting in enhanced anticancer effect compared to that obtained with each individual therapy and largely overcome the limitation of localized RT. Thus, this investigation suggests that combination therapy with radiation and immunotherapy is a promising new treatment strategy for enhancing the anticancer efficacy of the treatment through the induction the abscopal effect.

References

1. Daniel VC, Marchionni L, Hierman JS, Rhodes JT, Devereux WL, Rudin CM, Yung R, Parmigiani G, Dorsch M, Peacock CD, Watkins DN. A primary xenograft model of small-cell lung cancer reveals irreversible changes in gene expression imposed by culture in vitro. Cancer Res. 2009;69(8):3364-3373.

2. RA VANN, Thomas T, Krook M, Chukkapalli S, Hoenerhoff MJ, Dillman JR, Lawlor ER, Opipari VP, Newman EA. Tissue-directed Implantation Using Ultrasound Visualization for Development of Biologically Relevant Metastatic Tumor Xenografts. In Vivo. 2017;31(5):779-791.

3. Tentler JJ, Tan AC, Weekes CD, Jimeno A, Leong S, Pitts TM, Arcaroli JJ, Messersmith WA, Eckhardt SG. Patient-derived tumour xenografts as models for oncology drug development. Nat Rev Clin Oncol. 2012;9(6):338-350.

4. Siolas D, Hannon GJ. Patient-derived tumor xenografts: transforming clinical samples into mouse models. Cancer Res. 2013;73(17):5315-5319.

5. Scott CL, Becker MA, Haluska P, Samimi G. Patient-derived xenograft models to improve targeted therapy in epithelial ovarian cancer treatment. Front Oncol. 2013;3:295.

6. Whittle JR, Lewis MT, Lindeman GJ, Visvader JE. Patient-derived xenograft models of breast cancer and their predictive power. Breast Cancer Res. 2015;17:17.

7. Landis MD, Lehmann BD, Pietenpol JA, Chang JC. Patient-derived breast tumor xenografts facilitating personalized cancer therapy. Breast Cancer Res. 2013;15(1):201.

8. Ko BK, Choi S, Cui LG, Lee YH, Hwang IS, Kim KT, Shim H, Lee JS. Affinity Maturation of Monoclonal Antibody 1E11 by Targeted Randomization in CDR3 Regions Optimizes Therapeutic Antibody Targeting of HER2-Positive Gastric Cancer. PLoS One. 2015;10(7):e0134600.

9. Ko BK, Lee SY, Lee YH, Hwang IS, Persson H, Rockberg J, Borrebaeck C, Park D, Kim KT, Uhlen M, Lee JS. Combination of novel HER2-targeting antibody 1E11 with trastuzumab shows synergistic antitumor activity in HER2-positive gastric cancer. Mol Oncol. 2015;9(2):398-408.

10. Kelley JR, Duggan JM. Gastric cancer epidemiology and risk factors. J Clin Epidemiol.

2003;56(1):1-9.
11. Power DG, Kelsen DP, Shah MA. Advanced gastric cancer--slow but steady progress. Cancer Treat Rev. 2010;36(5):384-392.
12. Leung WK, Wu MS, Kakugawa Y, Kim JJ, Yeoh KG, Goh KL, Wu KC, Wu DC, Sollano J, Kachintorn U, Gotoda T, Lin JT, You WC, Ng EK, Sung JJ, Asia Pacific Working Group on Gastric C. Screening for gastric cancer in Asia: current evidence and practice. Lancet Oncol. 2008;9(3):279-287.
13. Kamangar F, Dores GM, Anderson WF. Patterns of cancer incidence, mortality, and prevalence across five continents: defining priorities to reduce cancer disparities in different geographic regions of the world. J Clin Oncol. 2006;24(14):2137-2150.
14. Watanabe J, Ito Y, Saeki T, Masuda N, Takano T, Takao S, Nakagami K, Tsugawa K, Nakagawa S, Kanatani K, Nakayama T. Safety Evaluation of Trastuzumab Emtansine in Japanese Patients with HER2-Positive Advanced Breast Cancer. In Vivo. 2017;31(3):493-500.
15. Cimpean AM, Tarlui V, Cumpanas AA, Bolintineanu S, Cumpanas A, Raica M. Critical Overview of HER2 Assessement in Bladder Cancer: What Is Missing for a Better Therapeutic Approach? Anticancer Res. 2017;37(9):4935-4942.
16. Tanner M, Hollmen M, Junttila TT, Kapanen AI, Tommola S, Soini Y, Helin H, Salo J, Joensuu H, Sihvo E, Elenius K, Isola J. Amplification of HER-2 in gastric carcinoma: association with Topoisomerase IIalpha gene amplification, intestinal type, poor prognosis and sensitivity to trastuzumab. Ann Oncol. 2005;16(2):273-278.
17. Gravalos C, Jimeno A. HER2 in gastric cancer: a new prognostic factor and a novel therapeutic target. Ann Oncol. 2008;19(9):1523-1529.
18. Yonemura Y, Ninomiya I, Yamaguchi A, Fushida S, Kimura H, Ohoyama S, Miyazaki I, Endou Y, Tanaka M, Sasaki T. Evaluation of immunoreactivity for erbB-2 protein as a marker of poor short term prognosis in gastric cancer. Cancer Res. 1991;51(3):1034-1038.
19. Liu Y, Ling Y, Qi Q, Zhu M, Wan M, Zhang Y, Zhang C. Trastuzumab increases the sensitivity of HER2-amplified human gastric cancer cells to oxaliplatin and cisplatin by affecting the expression of telomere-associated proteins. Oncol Lett. 2015;9(2):999-1005.
20. Van Cutsem E, Bang YJ, Feng-Yi F, Xu JM, Lee KW, Jiao SC, Chong JL, Lopez-Sanchez RI, Price T, Gladkov O, Stoss O, Hill J, Ng V, Lehle M, Thomas M, Kiermaier A, Ruschoff J. HER2 screening data from ToGA: targeting HER2 in gastric and gastroesophageal junction

cancer. Gastric Cancer. 2015;18(3):476-484.
21. Bang YJ, Van Cutsem E, Feyereislova A, Chung HC, Shen L, Sawaki A, Lordick F, Ohtsu A, Omuro Y, Satoh T, Aprile G, Kulikov E, Hill J, Lehle M, Ruschoff J, Kang YK, To GATI. Trastuzumab in combination with chemotherapy versus chemotherapy alone for treatment of HER2-positive advanced gastric or gastro-oesophageal junction cancer (ToGA): a phase 3, open-label, randomised controlled trial. Lancet. 2010;376(9742):687-697.
22. Stahl P, Seeschaaf C, Lebok P, Kutup A, Bockhorn M, Izbicki JR, Bokemeyer C, Simon R, Sauter G, Marx AH. Heterogeneity of amplification of HER2, EGFR, CCND1 and MYC in gastric cancer. BMC Gastroenterol. 2015;15:7.
23. Kelly CM, Janjigian YY. The genomics and therapeutics of HER2-positive gastric cancer-from trastuzumab and beyond. J Gastrointest Oncol. 2016;7(5):750-762.
24. Larsen SA, Meldgaard T, Fridriksdottir AJ, Lykkemark S, Poulsen PC, Overgaard LF, Petersen HB, Petersen OW, Kristensen P. Raising an Antibody Specific to Breast Cancer Subpopulations Using Phage Display on Tissue Sections. Cancer Genomics Proteomics. 2016;13(1):21-30.
25. Alley SC, Okeley NM, Senter PD. Antibody-drug conjugates: targeted drug delivery for cancer. Curr Opin Chem Biol. 2010;14(4):529-537.
26. Diamantis N, Banerji U. Antibody-drug conjugates--an emerging class of cancer treatment. Br J Cancer. 2016;114(4):362-367.
27. Miller JL. FDA approves antibody-directed cytotoxic agent for acute myeloid leukemia. Am J Health Syst Pharm. 2000;57(13):1202, 1204.
28. Fostvedt LK, Hibma JE, Masters JC, Vandendries E, Ruiz-Garcia A. Pharmacokinetic/Pharmacodynamic Modeling to Support the Re-approval of Gemtuzumab Ozogamicin. Clin Pharmacol Ther. 2019;106(5):1006-1017.
29. Berger GK, McBride A, Lawson S, Royball K, Yun S, Gee K, Bin Riaz I, Saleh AA, Puvvada S, Anwer F. Brentuximab vedotin for treatment of non-Hodgkin lymphomas: A systematic review. Crit Rev Oncol Hematol. 2017;109:42-50.
30. Amiri-Kordestani L, Blumenthal GM, Xu QC, Zhang L, Tang SW, Ha L, Weinberg WC, Chi B, Candau-Chacon R, Hughes P, Russell AM, Miksinski SP, Chen XH, McGuinn WD, Palmby T, Schrieber SJ, Liu Q, Wang J, Song P, Mehrotra N, Skarupa L, Clouse K, Al-Hakim A, Sridhara R, Ibrahim A, Justice R, Pazdur R, Cortazar P. FDA approval: ado-trastuzumab

emtansine for the treatment of patients with HER2-positive metastatic breast cancer. Clin Cancer Res. 2014;20(17):4436-4441.
31. Lamb YN. Inotuzumab Ozogamicin: First Global Approval. Drugs. 2017;77(14):1603-1610.
32. Deeks ED. Polatuzumab Vedotin: First Global Approval. Drugs. 2019;79(13):1467-1475.
33. Chang E, Weinstock C, Zhang L, Charlab R, Dorff SE, Gong Y, Hsu V, Li F, Ricks TK, Song P, Tang S, Waldron PE, Yu J, Zahalka E, Goldberg KB, Pazdur R, Theoret MR, Ibrahim A, Beaver JA. FDA Approval Summary: Enfortumab Vedotin for Locally Advanced or Metastatic Urothelial Carcinoma. Clin Cancer Res. 2021;27(4):922-927.
34. Bartsch R. Trastuzumab-deruxtecan: an investigational agent for the treatment of HER2-positive breast cancer. Expert Opin Investig Drugs. 2020;29(9):901-910.
35. Wahby S, Fashoyin-Aje L, Osgood CL, Cheng J, Fiero MH, Zhang L, Tang S, Hamed SS, Song P, Charlab R, Dorff SE, Ricks TK, Barnett-Ringgold K, Dinin J, Goldberg KB, Theoret MR, Pazdur R, Amiri-Kordestani L, Beaver JA. FDA Approval Summary: Accelerated Approval of Sacituzumab Govitecan-hziy for Third-line Treatment of Metastatic Triple-negative Breast Cancer. Clin Cancer Res. 2021;27(7):1850-1854.
36. Markham A. Belantamab Mafodotin: First Approval. Drugs. 2020;80(15):1607-1613.
37. Lewis Phillips GD, Li G, Dugger DL, Crocker LM, Parsons KL, Mai E, Blattler WA, Lambert JM, Chari RV, Lutz RJ, Wong WL, Jacobson FS, Koeppen H, Schwall RH, Kenkare-Mitra SR, Spencer SD, Sliwkowski MX. Targeting HER2-positive breast cancer with trastuzumab-DM1, an antibody-cytotoxic drug conjugate. Cancer Res. 2008;68(22):9280-9290.
38. Dieras V, Miles D, Verma S, Pegram M, Welslau M, Baselga J, Krop IE, Blackwell K, Hoersch S, Xu J, Green M, Gianni L. Trastuzumab emtansine versus capecitabine plus lapatinib in patients with previously treated HER2-positive advanced breast cancer (EMILIA): a descriptive analysis of final overall survival results from a randomised, open-label, phase 3 trial. Lancet Oncol. 2017;18(6):732-742.
39. Verma S, Miles D, Gianni L, Krop IE, Welslau M, Baselga J, Pegram M, Oh DY, Dieras V, Guardino E, Fang L, Lu MW, Olsen S, Blackwell K, Group ES. Trastuzumab emtansine for HER2-positive advanced breast cancer. N Engl J Med. 2012;367(19):1783-1791.
40. von Minckwitz G, Huang CS, Mano MS, Loibl S, Mamounas EP, Untch M, Wolmark N, Rastogi P, Schneeweiss A, Redondo A, Fischer HH, Jacot W, Conlin AK, Arce-Salinas C,

Wapnir IL, Jackisch C, DiGiovanna MP, Fasching PA, Crown JP, Wulfing P, Shao Z, Rota Caremoli E, Wu H, Lam LH, Tesarowski D, Smitt M, Douthwaite H, Singel SM, Geyer CE, Jr., Investigators K. Trastuzumab Emtansine for Residual Invasive HER2-Positive Breast Cancer. N Engl J Med. 2019;380(7):617-628.

41. Pegram MD, Miles D, Tsui CK, Zong Y. HER2-Overexpressing/Amplified Breast Cancer as a Testing Ground for Antibody-Drug Conjugate Drug Development in Solid Tumors. Clin Cancer Res. 2020;26(4):775-786.

42. Wu J, Kong R, Tian S, Li H, Wu K, Kong L. Can trastuzumab emtansine be replaced by additional chemotherapy plus targeted therapy for HER2-overexpressing breast cancer patients with residual disease after neoadjuvant chemotherapy? Chin J Cancer Res. 2019;31(6):878-891.

43. Keam SJ. Trastuzumab Deruxtecan: First Approval. Drugs. 2020;80(5):501-508.

44. Shitara K, Bang YJ, Iwasa S, Sugimoto N, Ryu MH, Sakai D, Chung HC, Kawakami H, Yabusaki H, Lee J, Saito K, Kawaguchi Y, Kamio T, Kojima A, Sugihara M, Yamaguchi K, Investigators DE-G. Trastuzumab Deruxtecan in Previously Treated HER2-Positive Gastric Cancer. N Engl J Med. 2020;382(25):2419-2430.

45. Shitara K, Iwata H, Takahashi S, Tamura K, Park H, Modi S, Tsurutani J, Kadowaki S, Yamaguchi K, Iwasa S, Saito K, Fujisaki Y, Sugihara M, Shahidi J, Doi T. Trastuzumab deruxtecan (DS-8201a) in patients with advanced HER2-positive gastric cancer: a dose-expansion, phase 1 study. Lancet Oncol. 2019;20(6):827-836.

46. Thuss-Patience PC, Shah MA, Ohtsu A, Van Cutsem E, Ajani JA, Castro H, Mansoor W, Chung HC, Bodoky G, Shitara K, Phillips GDL, van der Horst T, Harle-Yge ML, Althaus BL, Kang YK. Trastuzumab emtansine versus taxane use for previously treated HER2-positive locally advanced or metastatic gastric or gastro-oesophageal junction adenocarcinoma (GATSBY): an international randomised, open-label, adaptive, phase 2/3 study. Lancet Oncol. 2017;18(5):640-653.

47. Ducry L, Stump B. Antibody-drug conjugates: linking cytotoxic payloads to monoclonal antibodies. Bioconjug Chem. 2010;21(1):5-13.

48. Bouchard H, Viskov C, Garcia-Echeverria C. Antibody-drug conjugates-a new wave of cancer drugs. Bioorg Med Chem Lett. 2014;24(23):5357-5363.

49. Barok M, Joensuu H, Isola J. Trastuzumab emtansine: mechanisms of action and drug

resistance. Breast Cancer Res. 2014;16(2):209.
50. Parslow AC, Parakh S, Lee FT, Gan HK, Scott AM. Antibody-Drug Conjugates for Cancer Therapy. Biomedicines. 2016;4(3).
51. Lambert JM, Morris CQ. Antibody-Drug Conjugates (ADCs) for Personalized Treatment of Solid Tumors: A Review. Adv Ther. 2017;34(5):1015-1035.
52. Collins DM, Bossenmaier B, Kollmorgen G, Niederfellner G. Acquired Resistance to Antibody-Drug Conjugates. Cancers (Basel). 2019;11(3).
53. Beck A, Haeuw JF, Wurch T, Goetsch L, Bailly C, Corvaia N. The next generation of antibody-drug conjugates comes of age. Discov Med. 2010;10(53):329-339.
54. Park HL, Kim KY, Park JS, Shin JE, Kim HR, Yang B, Kim JY, Shim JY, Shin EA, Noh SM. Clinicopathological Analysis of Ultrasound-guided Vacuum-assisted Breast Biopsy for the Diagnosis and Treatment of Breast Disease. Anticancer Res. 2018;38(4):2455-2462.
55. Garrido-Laguna I, Uson M, Rajeshkumar NV, Tan AC, de Oliveira E, Karikari C, Villaroel MC, Salomon A, Taylor G, Sharma R, Hruban RH, Maitra A, Laheru D, Rubio-Viqueira B, Jimeno A, Hidalgo M. Tumor engraftment in nude mice and enrichment in stroma- related gene pathways predict poor survival and resistance to gemcitabine in patients with pancreatic cancer. Clin Cancer Res. 2011;17(17):5793-5800.
56. Amendt C, Staub E, Friese-Hamim M, Storkel S, Stroh C. Association of EGFR expression level and cetuximab activity in patient-derived xenograft models of human non-small cell lung cancer. Clin Cancer Res. 2014;20(17):4478-4487.
57. Tai W, Mahato R, Cheng K. The role of HER2 in cancer therapy and targeted drug delivery. J Control Release. 2010;146(3):264-275.
58. Byrne AT, Alferez DG, Amant F, Annibali D, Arribas J, Biankin AV, Bruna A, Budinska E, Caldas C, Chang DK, Clarke RB, Clevers H, Coukos G, Dangles-Marie V, Eckhardt SG, Gonzalez-Suarez E, Hermans E, Hidalgo M, Jarzabek MA, de Jong S, Jonkers J, Kemper K, Lanfrancone L, Maelandsmo GM, Marangoni E, Marine JC, Medico E, Norum JH, Palmer HG, Peeper DS, Pelicci PG, Piris-Gimenez A, Roman-Roman S, Rueda OM, Seoane J, Serra V, Soucek L, Vanhecke D, Villanueva A, Vinolo E, Bertotti A, Trusolino L. Interrogating open issues in cancer precision medicine with patient-derived xenografts. Nat Rev Cancer. 2017;17(4):254-268.
59. Shin SH, Park SS, Ju EJ, Park J, Ko EJ, Hwang JJ, Suh YA, Jang SJ, Lee JS, Ko BK, Kim

KT, Lee JS, Song SY, Jeong SY, Choi EK. Establishment of a Patient-derived Xenograft for Development of Personalized HER2-targeting Therapy in Gastric Cancer. Anticancer Res. 2018;38(1):287-293.

60. Thomas A, Teicher BA, Hassan R. Antibody-drug conjugates for cancer therapy. Lancet Oncol. 2016;17(6):e254-e262.

61. Barok M, Tanner M, Koninki K, Isola J. Trastuzumab-DM1 causes tumour growth inhibition by mitotic catastrophe in trastuzumab-resistant breast cancer cells in vivo. Breast Cancer Res. 2011;13(2):R46.

62. Ogitani Y, Aida T, Hagihara K, Yamaguchi J, Ishii C, Harada N, Soma M, Okamoto H, Oitate M, Arakawa S, Hirai T, Atsumi R, Nakada T, Hayakawa I, Abe Y, Agatsuma T. DS-8201a, A Novel HER2-Targeting ADC with a Novel DNA Topoisomerase I Inhibitor, Demonstrates a Promising Antitumor Efficacy with Differentiation from T-DM1. Clin Cancer Res. 2016;22(20):5097-5108.

63. Kovtun YV, Goldmacher VS. Cell killing by antibody-drug conjugates. Cancer Lett. 2007;255(2):232-240.

64. Harrington KJ, Billingham LJ, Brunner TB, Burnet NG, Chan CS, Hoskin P, Mackay RI, Maughan TS, Macdougall J, McKenna WG, Nutting CM, Oliver A, Plummer R, Stratford IJ, Illidge T. Guidelines for preclinical and early phase clinical assessment of novel radiosensitisers. Br J Cancer. 2011;105(5):628-639.

65. Liauw SL, Connell PP, Weichselbaum RR. New paradigms and future challenges in radiation oncology: an update of biological targets and technology. Sci Transl Med. 2013;5(173):173sr172.

66. Foote RL, Stafford SL, Petersen IA, Pulido JS, Clarke MJ, Schild SE, Garces YI, Olivier KR, Miller RC, Haddock MG, Yan E, Laack NN, Arndt CA, Buskirk SJ, Miller VL, Brent CR, Kruse JJ, Ezzell GA, Herman MG, Gunderson LL, Erlichman C, Diasio RB. The clinical case for proton beam therapy. Radiat Oncol. 2012;7:174.

67. Order SE. The effects of therapeutic irradiation on lymphocytes and immunity. Cancer. 1977;39(2 Suppl):737-743.

68. Ngwa W, Irabor OC, Schoenfeld JD, Hesser J, Demaria S, Formenti SC. Using immunotherapy to boost the abscopal effect. Nat Rev Cancer. 2018;18(5):313-322.

69. Jaffray D, Kupelian P, Djemil T, Macklis RM. Review of image-guided radiation therapy.

Expert Rev Anticancer Ther. 2007;7(1):89-103.
70. Staffurth J, Radiotherapy Development B. A review of the clinical evidence for intensity-modulated radiotherapy. Clin Oncol (R Coll Radiol). 2010;22(8):643-657.
71. Chang JY, Zhang X, Wang X, Kang Y, Riley B, Bilton S, Mohan R, Komaki R, Cox JD. Significant reduction of normal tissue dose by proton radiotherapy compared with three-dimensional conformal or intensity-modulated radiation therapy in Stage I or Stage III non-small-cell lung cancer. Int J Radiat Oncol Biol Phys. 2006;65(4):1087-1096.
72. Baumann M, Krause M, Overgaard J, Debus J, Bentzen SM, Daartz J, Richter C, Zips D, Bortfeld T. Radiation oncology in the era of precision medicine. Nat Rev Cancer. 2016;16(4):234-249.
73. Kroemer G, Galluzzi L, Kepp O, Zitvogel L. Immunogenic cell death in cancer therapy. Annu Rev Immunol. 2013;31:51-72.
74. Mole RH. Whole body irradiation; radiobiology or medicine? Br J Radiol. 1953;26(305):234-241.
75. Ashrafizadeh M, Farhood B, Eleojo Musa A, Taeb S, Rezaeyan A, Najafi M. Abscopal effect in radioimmunotherapy. Int Immunopharmacol. 2020;85:106663.
76. Postow MA, Callahan MK, Barker CA, Yamada Y, Yuan J, Kitano S, Mu Z, Rasalan T, Adamow M, Ritter E, Sedrak C, Jungbluth AA, Chua R, Yang AS, Roman RA, Rosner S, Benson B, Allison JP, Lesokhin AM, Gnjatic S, Wolchok JD. Immunologic correlates of the abscopal effect in a patient with melanoma. N Engl J Med. 2012;366(10):925-931.
77. Kang J, Demaria S, Formenti S. Current clinical trials testing the combination of immunotherapy with radiotherapy. J Immunother Cancer. 2016;4:51.
78. Dewan MZ, Galloway AE, Kawashima N, Dewyngaert JK, Babb JS, Formenti SC, Demaria S. Fractionated but not single-dose radiotherapy induces an immune-mediated abscopal effect when combined with anti-CTLA-4 antibody. Clin Cancer Res. 2009;15(17):5379-5388.
79. Lehrnbecher T, Koehl U, Wittekindt B, Bochennek K, Tramsen L, Klingebiel T, Chanock SJ. Changes in host defence induced by malignancies and antineoplastic treatment: implication for immunotherapeutic strategies. Lancet Oncol. 2008;9(3):269-278.
80. Spranger S, Bao R, Gajewski TF. Melanoma-intrinsic beta-catenin signalling prevents anti-tumour immunity. Nature. 2015;523(7559):231-235.
81. Derer A, Spiljar M, Baumler M, Hecht M, Fietkau R, Frey B, Gaipl US. Chemoradiation

Increases PD-L1 Expression in Certain Melanoma and Glioblastoma Cells. Front Immunol. 2016;7:610.
82. Wang Z, Wu Z, Liu Y, Han W. New development in CAR-T cell therapy. J Hematol Oncol. 2017;10(1):53.
83. Santos PM, Butterfield LH. Dendritic Cell-Based Cancer Vaccines. J Immunol. 2018;200(2):443-449.
84. Cerezo D, Pena MJ, Mijares M, Martinez G, Blanca I, De Sanctis JB. Peptide vaccines for cancer therapy. Recent Pat Inflamm Allergy Drug Discov. 2015;9(1):38-45.
85. Kaufman HL, Kohlhapp FJ, Zloza A. Oncolytic viruses: a new class of immunotherapy drugs. Nat Rev Drug Discov. 2015;14(9):642-662.
86. Ohno M, Natsume A, Wakabayashi T. Cytokine therapy. Adv Exp Med Biol. 2012;746:86-94.
87. Petitprez F, Meylan M, de Reynies A, Sautes-Fridman C, Fridman WH. The Tumor Microenvironment in the Response to Immune Checkpoint Blockade Therapies. Front Immunol. 2020;11:784.
88. Liang SC, Latchman YE, Buhlmann JE, Tomczak MF, Horwitz BH, Freeman GJ, Sharpe AH. Regulation of PD-1, PD-L1, and PD-L2 expression during normal and autoimmune responses. Eur J Immunol. 2003;33(10):2706-2716.
89. Dong H, Strome SE, Salomao DR, Tamura H, Hirano F, Flies DB, Roche PC, Lu J, Zhu G, Tamada K, Lennon VA, Celis E, Chen L. Tumor-associated B7-H1 promotes T-cell apoptosis: a potential mechanism of immune evasion. Nat Med. 2002;8(8):793-800.
90. Sharma P, Hu-Lieskovan S, Wargo JA, Ribas A. Primary, Adaptive, and Acquired Resistance to Cancer Immunotherapy. Cell. 2017;168(4):707-723.
91. Herbst RS, Soria JC, Kowanetz M, Fine GD, Hamid O, Gordon MS, Sosman JA, McDermott DF, Powderly JD, Gettinger SN, Kohrt HE, Horn L, Lawrence DP, Rost S, Leabman M, Xiao Y, Mokatrin A, Koeppen H, Hegde PS, Mellman I, Chen DS, Hodi FS. Predictive correlates of response to the anti-PD-L1 antibody MPDL3280A in cancer patients. Nature. 2014;515(7528):563-567.
92. Rudqvist NP, Pilones KA, Lhuillier C, Wennerberg E, Sidhom JW, Emerson RO, Robins HS, Schneck J, Formenti SC, Demaria S. Radiotherapy and CTLA-4 Blockade Shape the TCR Repertoire of Tumor-Infiltrating T Cells. Cancer Immunol Res. 2018;6(2):139-150.

93. Postow MA, Callahan MK, Wolchok JD. Immune Checkpoint Blockade in Cancer Therapy. J Clin Oncol. 2015;33(17):1974-1982.
94. Orth M, Lauber K, Niyazi M, Friedl AA, Li M, Maihofer C, Schuttrumpf L, Ernst A, Niemoller OM, Belka C. Current concepts in clinical radiation oncology. Radiat Environ Biophys. 2014;53(1):1-29.
95. Galluzzi L, Maiuri MC, Vitale I, Zischka H, Castedo M, Zitvogel L, Kroemer G. Cell death modalities: classification and pathophysiological implications. Cell Death Differ. 2007;14(7):1237-1243.
96. Bernstein MB, Krishnan S, Hodge JW, Chang JY. Immunotherapy and stereotactic ablative radiotherapy (ISABR): a curative approach? Nat Rev Clin Oncol. 2016;13(8):516-524.
97. Chajon E, Castelli J, Marsiglia H, De Crevoisier R. The synergistic effect of radiotherapy and immunotherapy: A promising but not simple partnership. Crit Rev Oncol Hematol. 2017;111:124-132.
98. Barker HE, Paget JT, Khan AA, Harrington KJ. The tumour microenvironment after radiotherapy: mechanisms of resistance and recurrence. Nat Rev Cancer. 2015;15(7):409-425.
99. Paris F, Fuks Z, Kang A, Capodieci P, Juan G, Ehleiter D, Haimovitz-Friedman A, Cordon-Cardo C, Kolesnick R. Endothelial apoptosis as the primary lesion initiating intestinal radiation damage in mice. Science. 2001;293(5528):293-297.
100. Yarnold J, Brotons MC. Pathogenetic mechanisms in radiation fibrosis. Radiother Oncol. 2010;97(1):149-161.
101. Chin MS, Freniere BB, Bonney CF, Lancerotto L, Saleeby JH, Lo YC, Orgill DP, Fitzgerald TJ, Lalikos JF. Skin perfusion and oxygenation changes in radiation fibrosis. Plast Reconstr Surg. 2013;131(4):707-716.
102. Burnette BC, Liang H, Lee Y, Chlewicki L, Khodarev NN, Weichselbaum RR, Fu YX, Auh SL. The efficacy of radiotherapy relies upon induction of type i interferon-dependent innate and adaptive immunity. Cancer Res. 2011;71(7):2488-2496.
103. Lee Y, Auh SL, Wang Y, Burnette B, Wang Y, Meng Y, Beckett M, Sharma R, Chin R, Tu T, Weichselbaum RR, Fu YX. Therapeutic effects of ablative radiation on local tumor require CD8+ T cells: changing strategies for cancer treatment. Blood. 2009;114(3):589-595.
104. Deng L, Liang H, Xu M, Yang X, Burnette B, Arina A, Li XD, Mauceri H, Beckett M, Darga T, Huang X, Gajewski TF, Chen ZJ, Fu YX, Weichselbaum RR. STING-Dependent

Cytosolic DNA Sensing Promotes Radiation-Induced Type I Interferon-Dependent Antitumor Immunity in Immunogenic Tumors. Immunity. 2014;41(5):843-852.
105. Kaminski JM, Shinohara E, Summers JB, Niermann KJ, Morimoto A, Brousal J. The controversial abscopal effect. Cancer Treat Rev. 2005;31(3):159-172.
106. Haikerwal SJ, Hagekyriakou J, MacManus M, Martin OA, Haynes NM. Building immunity to cancer with radiation therapy. Cancer Lett. 2015;368(2):198-208.
107. Grass GD, Krishna N, Kim S. The immune mechanisms of abscopal effect in radiation therapy. Curr Probl Cancer. 2016;40(1):10-24.
108. Reits EA, Hodge JW, Herberts CA, Groothuis TA, Chakraborty M, Wansley EK, Camphausen K, Luiten RM, de Ru AH, Neijssen J, Griekspoor A, Mesman E, Verreck FA, Spits H, Schlom J, van Veelen P, Neefjes JJ. Radiation modulates the peptide repertoire, enhances MHC class I expression, and induces successful antitumor immunotherapy. J Exp Med. 2006;203(5):1259-1271.
109. Zhang P, Su DM, Liang M, Fu J. Chemopreventive agents induce programmed death-1-ligand 1 (PD-L1) surface expression in breast cancer cells and promote PD-L1-mediated T cell apoptosis. Mol Immunol. 2008;45(5):1470-1476.
110. Corso CD, Ali AN, Diaz R. Radiation-induced tumor neoantigens: imaging and therapeutic implications. Am J Cancer Res. 2011;1(3):390-412.
111. Brahmer JR, Tykodi SS, Chow LQ, Hwu WJ, Topalian SL, Hwu P, Drake CG, Camacho LH, Kauh J, Odunsi K, Pitot HC, Hamid O, Bhatia S, Martins R, Eaton K, Chen S, Salay TM, Alaparthy S, Grosso JF, Korman AJ, Parker SM, Agrawal S, Goldberg SM, Pardoll DM, Gupta A, Wigginton JM. Safety and activity of anti-PD-L1 antibody in patients with advanced cancer. N Engl J Med. 2012;366(26):2455-2465.
112. Topalian SL, Hodi FS, Brahmer JR, Gettinger SN, Smith DC, McDermott DF, Powderly JD, Carvajal RD, Sosman JA, Atkins MB, Leming PD, Spigel DR, Antonia SJ, Horn L, Drake CG, Pardoll DM, Chen L, Sharfman WH, Anders RA, Taube JM, McMiller TL, Xu H, Korman AJ, Jure-Kunkel M, Agrawal S, McDonald D, Kollia GD, Gupta A, Wigginton JM, Sznol M. Safety, activity, and immune correlates of anti-PD-1 antibody in cancer. N Engl J Med. 2012;366(26):2443-2454.
113. Yang Y. Cancer immunotherapy: harnessing the immune system to battle cancer. J Clin Invest. 2015;125(9):3335-3337.

114. de Miguel M, Calvo E. Clinical Challenges of Immune Checkpoint Inhibitors. Cancer Cell. 2020;38(3):326-333.
115. Oved JH, Barrett DM, Teachey DT. Cellular therapy: Immune-related complications. Immunol Rev. 2019;290(1):114-126.
116. Tartour E. [Anti-cancer vaccines: What future in anti-cancer immunotherapy strategies?]. Biol Aujourdhui. 2018;212(3-4):69-76.
117. Raja J, Ludwig JM, Gettinger SN, Schalper KA, Kim HS. Oncolytic virus immunotherapy: future prospects for oncology. J Immunother Cancer. 2018;6(1):140.
118. Baxevanis CN, Perez SA, Papamichail M. Cancer immunotherapy. Crit Rev Clin Lab Sci. 2009;46(4):167-189.
119. Sanmamed MF, Pastor F, Rodriguez A, Perez-Gracia JL, Rodriguez-Ruiz ME, Jure-Kunkel M, Melero I. Agonists of Co-stimulation in Cancer Immunotherapy Directed Against CD137, OX40, GITR, CD27, CD28, and ICOS. Semin Oncol. 2015;42(4):640-655.
120. Darvin P, Toor SM, Sasidharan Nair V, Elkord E. Immune checkpoint inhibitors: recent progress and potential biomarkers. Exp Mol Med. 2018;50(12):1-11.
121. Kwok G, Yau TC, Chiu JW, Tse E, Kwong YL. Pembrolizumab (Keytruda). Hum Vaccin Immunother. 2016;12(11):2777-2789.
122. Gupta AK, Macleod MA, Abramovits W. OPDIVO (Nivolumab). Skinmed. 2015;13(6):471-474.
123. Markham A, Duggan S. Cemiplimab: First Global Approval. Drugs. 2018;78(17):1841-1846.
124. Markham A. Atezolizumab: First Global Approval. Drugs. 2016;76(12):1227-1232.
125. Alvarez-Argote J, Dasanu CA. Durvalumab in cancer medicine: a comprehensive review. Expert Opin Biol Ther. 2019;19(9):927-935.
126. Gupta AK, Versteeg SG, Abramovits W, Vincent KD. Bavencio((R)) (Avelumab)-A Newly Approved Anti-PD-L1 IgG1 Antibody. Skinmed. 2018;16(3):183-187.
127. Cameron F, Whiteside G, Perry C. Ipilimumab: first global approval. Drugs. 2011;71(8):1093-1104.
128. Haslam A, Prasad V. Estimation of the Percentage of US Patients With Cancer Who Are Eligible for and Respond to Checkpoint Inhibitor Immunotherapy Drugs. JAMA Netw Open. 2019;2(5):e192535.

129. Postow MA, Chesney J, Pavlick AC, Robert C, Grossmann K, McDermott D, Linette GP, Meyer N, Giguere JK, Agarwala SS, Shaheen M, Ernstoff MS, Minor D, Salama AK, Taylor M, Ott PA, Rollin LM, Horak C, Gagnier P, Wolchok JD, Hodi FS. Nivolumab and ipilimumab versus ipilimumab in untreated melanoma. N Engl J Med. 2015;372(21):2006-2017.
130. Melero I, Berman DM, Aznar MA, Korman AJ, Perez Gracia JL, Haanen J. Evolving synergistic combinations of targeted immunotherapies to combat cancer. Nat Rev Cancer. 2015;15(8):457-472.
131. Larkin J, Chiarion-Sileni V, Gonzalez R, Grob JJ, Cowey CL, Lao CD, Schadendorf D, Dummer R, Smylie M, Rutkowski P, Ferrucci PF, Hill A, Wagstaff J, Carlino MS, Haanen JB, Maio M, Marquez-Rodas I, McArthur GA, Ascierto PA, Long GV, Callahan MK, Postow MA, Grossmann K, Sznol M, Dreno B, Bastholt L, Yang A, Rollin LM, Horak C, Hodi FS, Wolchok JD. Combined Nivolumab and Ipilimumab or Monotherapy in Untreated Melanoma. N Engl J Med. 2015;373(1):23-34.

국문 요약

PART I

HER2 표적 치료를 위한 위암 환자 암조직 유래 이식 모델 구축 및 HER2 항체-약물 결합체의 정교한 링커 시스템에 의한 난치성 HER2 양성 암에 대한 치료효과 증진

암 세포주 및 이종이식 모델에서 표적 항암제의 개발은 유망한 효능을 나타냄에도 불구하고 임상 시험 중에 실패되는 경우가 자주 있다. 본 연구자는 HER2+ GC에 대한 표적 치료법의 성공적인 개발을 목표로 HER2 양성 위암 (HER2+ GC) 환자를 반영하는 환자 유래 이종이식 (PDX) 모델을 생성하고 특성화 하였다. 위암 환자의 수술에서 암 조직을 면역 결핍 마우스에 이식하고 환자의 조직 병리학 진단에 따라 HER2+ PDX를 선택하였다. HER2+ PDX는 면역조직화학(IHC)에 의해 발현되는 환자-유사 HER2에 대해 검증되었고, 상용화된 치료제인 Herceptin과 개발 중인 신규 HER2 항체 치료제로 테스트하여 확립한 HER2+ PDX 모델의 타당성을 검증하였다. 새로운 HER2 항체는 Herceptin과 함께 향상된 항암 효능을 보였고, 이를 통해 구축한 HER2+ PDX 모델은 정밀 치료를 위한 개인 맞춤형 도구의 이상적인 플랫폼으로서 HER2 표적 약물 및 위암 치료를 위한 복합 요법의 전임상 평가에 활용될 수 있도록 성공적으로 확립되었다.

HER2는 유방암과 위암에서 증폭 및 과발현되어 있으며 이는 좋지 않은 임상 결과를 초래한다. T-DM1과 Enhertu는 모두 HER2 표적 항체 약물 접합체 (antibody drug conjugate; ADC)로 승인되었지만, 이들 약물의 효과는 HER2를 발현하는 다양한 종양을 근절하기에는 여전히 만족스럽지 않다. HER2 표적 치료제의 이러한 단점을 해결하기 위해 정교하게 절단 가능한 링커를 만들고 trastuzumab과 MMAF로 구성된 새로운 HER2 표적 ADC를 제조하고, 이는 임상 1상 시험에서 조사 중이며 본 연구에서는 LCB-ADC라고 명명하였다. 세포 실험 결과에서, LCB-ADC는 T-DM1보다 더 높은 세포독성 효능을 보였고, 용량 의존적으로 더 높은 G2/M arrest를 보였다. 또한, 동물 실험에서 LCB-ADC는 HER2 과발현 N87 이종이식 종양에서 trastuzumab 또는 T-DM1과 비교하여 현저한 종양 성장 억제를 나타냈다. 특히 LCB-ADC는 HER2 양성 위암의 환자유래 이종이식편(PDX) 모델뿐만 아니라 HER2 저발현 JIMT-1 및 PDX 모델과 같은 T-DM1 내성 모델에서도 종양 성장 억제 측면에서 우수한 효능을 보였다. 종합적으로, 본 연구의 결과는 정교하게 절단 가능한 링커를 포함하는 LCB-ADC가 더 높은 항암 효능과 더 우수한 생체 안정성을 가지며 이전 치료법에 반응하지 않는 암 환자에서도 성공적인 치료 전략이 될 수 있음을 보여준다.

국문 요약

PART II

방사선치료 효능을 극대화하는 면역기전 규명과 이를 응용한 신규 방사선치료 기술 개발

방사선치료 기전의 기본적 이해 방식은 DNA 손상에 의한 세포사가 주류였으나, 최근에는 방사선에 의해 면역체계가 활성화되며 면역치료와 방사선치료 병행에 의한 시너지 효과가 속속 보고되고 있어 면역기전에 의한 방사선치료 효과에 많은 관심이 집중되고 있다. 방사선치료는 약 50%의 암 환자가 받는 주요 치료법이며 면역체계는 누구에게나 있는 인체 본연의 특성이므로, 방사선치료 관련 면역기전을 규명하고 이를 응용한 신규 방사선치료 효능 극대화 기술 개발은 암치료의 획기적 전환점이 될 것으로 기대되고 있다. 방사선은 면역에 다양한 방면으로 영향을 주는 것으로 알려져 있으며, 이에 해당되는 것으로 1) MHC class I의 세포 표면 발현, calreticulin 발현, HMGB1 분비 증가, 2) FAS의 표면 발현 증가, 3) 수지상세포(dendritic cell) 활성화 및 종양의 antigen cross-presentation을 증가, 4) tumor-infiltrating lymphocyte (TIL) 밀도 증가, 5) immune checkpoint 물질의 발현에 영향, 6) regulatory T cell (Treg)의 수를 조절 등이 있다. 또한, 임상에서 방사선치료와 immune checkpoint blockage (ICB)를 병행치료한 환자에서 abscopal effect를 관찰한 보고가 있지만 매우 드물게 일어나는 것으로 알려져 있다. 따라서 본 연구에서는 면역반응을 활성화시킬 수 있는 방사선 치료법과 면역 관문 억제제를 병용하는 요법을 통해 면역 세포의 변화를 관찰하고 abscopal effect를 증진시킬 수 있는 치료 전략을 개발하고자 하였다.

본 연구자는 방사선과 anti-PD-L1 병용 처리를 통해 MC-38 동종 이식 모델에서 종양의 성장이 단독 처리 그룹보다 억제되는 것을 관찰하였고, 방사선 선량과 약물의 농도를 증가하였을 때 그 효과는 더 극대화되었다. 병용 처리한 그룹에서 완전 관해를 보인 동물에 MC-38 세포주를 재이식하였을 때, 종양을 형성하지 못하는 것을 통해 병용 처리에 의해 전신 면역체계가 활성화된 것을 알 수 있었다. 더욱이, 양쪽 종양 이식 모델에서 방사선 선량과 약물의 농도를 증가하여 병용 효능을 평가에 의해서도 방사선 조사를 한 종양에서는 모든 개체에서 완전 관해를 보였고, 방사선 조사를 하지 않은 반대쪽 종양에서도 완전 관해를 관찰할 수 있었다. Abscopal effect를 관찰한 동물에서 면역세포 분포를 확인하였을 때, 방사선에 의해 종양 내 CD8+ T cell의 비율이 증가되며 일정시간이 흐른 후에는 전신의 CD8+ effector memory T cell이 증가함을 확인하였다. 본 연구의 결과를 통해 고선량의 방사선과 면역관문 역제제의 병용 처리가 abscopal effect를 증진시킬 수 있고,

이러한 효과는 전신 면역체계를 수반하여 발생하는 것을 검증하였다. 따라서 본 연구자는 방사선과 면역관문 억제제의 병용처리가 abscopal effect를 유도할 수 있는 새로운 치료 전략으로 제시할 수 있을 것으로 기대한다.